THE DYNAMICS OF MOVING FILAMENTS AND TAPES

BY

WILLARD W. ANDERSON

B.S. Northeastern University

(1962)

M.S. Massachusetts Institute of Technology

(1964)

SUBMITTED IN PARTIAL FULFILLMENT OF

THE REQUIREMENTS FOR THE

DEGREE OF DOCTOR OF SCIENCE

at the

MASSACHUSETTS INSTITUTE OF TECHNOLOGY

February, 1966

Signature of Author.....
Department of Mechanical Engineering
Fibers and Polymers Division, February 7, 1966

Certified by.....
Thesis Supervisor

Accepted by.....
Chairman, Departmental Committee
on Graduate Students

THE DYNAMICS OF MOVING FILAMENTS AND TAPES

by

Willard W. Anderson

Submitted to the Department of Mechanical Engineering on February 7, 1966 in partial fulfillment of the requirements for the degree of Doctor of Science.

ABSTRACT

The dynamics of filaments and tapes moving at constant velocity has been studied for two-dimensional and three-dimensional boundary conditions. The equations of motion solved are linear and include effects of tension, Coriolis' acceleration, relative logitudinal air motion, centrifugal acceleration, relative lateral air motion, and gravity. The solutions to these equations have been experimentally validated where necessary.

The additional effects of longitudinal accelerations and dynamic buckling have been studied. The effect of a surrounding matrix on these additional motions has also been studied. A set of twenty distinguishing parameters is included which are helpful in catagorizing the above motions.

Thesis Supervisor: Stanley Backer

Professor of
Mechanical Engineering

ACKNOWLEDGEMENTS

I wish to express gratitude and thanks to Professors Stanley Backer, A. B. McNamara and Dean Karnopp for their guidance and encouragement in this work.

In addition, to Draper Corporation, Hopedale, Massachusetts, goes my appreciation for their support for the initial phase of this work and to Cohoon and Heasley, Inc., Cambridge, Massachusetts, for their support of the final phase of this work.

I would like to thank Professor Eggerton for his assistance in photographing the extremely rapid phenomena of nylon filament snapback or dynamic buckling.

I would also like to thank Professor J. P. Den Hartog for a most important suggestion, namely to non-dimensionalize all of the parameters of this thesis.

Finally, I wish to thank my wife, Jane Anderson, for her diligence in typing this thesis.

TABLE OF CONTENTS

TABLE OF CONTENTS (continued)

LIST OF FIGURES

LIST OF FIGURES (continued)

NOMENCLATURE

a	Filament Acceleration in $\vec{i}$-direction
a_n	Infinite Series Coefficient
a_s	Material Sonic Velocity
b	Distinguishing Parameter Symbol (See Section VIII)
c	Lateral Wave Phase Velocity
c^*	Arbitrary Constant
$\vec{d}$	Unit Vector in Direction of Air Drag Force
f	Frequency
$f(s,t)$	Overall Filament Motion Function
$f(w)$	Initial Condition Displacement Function
g	Gravity Constant
$g(w)$	Initial Condition Velocity Function
$g(x)$	Amplitude Function (See Equation V-6)
h_o	Maximum Lateral Filament Displacement
$\vec{i}$	Unit Vector in the x-direction
$\vec{j}$	Unit Vector in the y-direction
k	Wave Number
$\vec{k}$	Unit Vector in the z-direction
ℓ	System Length
ℓ_o	Static Release Penetration Distance
ℓ_c	Cone Length
ℓ_e	Modified System Length
m,n	Integers
$\vec{n}$	Filament Principal Unit Normal Vector
p	Radial Interface Pressure
p_o	Stagnation Pressure of Fluid Stream

NOMENCLATURE (continued)

r	Instantaneous Filament Radius of Curvature
r_D	Linear Air Drag Coefficient
r_o	Amplitude of Oscillatory Boundary Conditions at $x = \ell$
r_o^*	Amplitude of Oscillatory Boundary Conditions at $x = 0$
s	Lagrangian Coordinate
t	Time
u	Unit Step Function
$\vec{u}$	Unit Vector in Filament Direction
$\vec{u}_r$	Unit Vector in Radial Direction
$\vec{u}_\theta$	Unit Vector in Tangential Direction
v	Filament Velocity
v_a	Longitudinal Air Velocity Relative to Filament
Δv_a	Longitudinal Air Velocity
w	Displacement Function
x	Coordinate
x_o	Strain Wave Penetration Length
y	Coordinate
z	Coordinate
A	Filament Cross Sectional Area
A_n	Arbitrary Constants
B_n	Arbitrary Constants
C_D	Pressure Drag Coefficient for Smooth Cylinders
D	Linear Operator
$\vec{D}_D$	Air Drag Force
D_f	Filament Diameter
D_ϵ	Forced Displacement Denominator (See Equation V-17)

NOMENCLATURE (continued)

E	Elastic Modulus
F_g	Gravity Force
I	Filament Cross Sectional Area Moment of Inertia
J_o	Bessel Function of Real Argument
K	Matrix Stiffness
M	Filament Bending Moment
N	Integer
P	Filament Longitudinal Impact Force
R	Distinguishing Parameter Function (See Equation V-2)
R_L	Limiting Ratio of Terms of Infinite Series
$\vec{R}$	Position Vector
Re	Real Part of Complex Function
T	Magnitude of Filament Tension
T_o	Constant Minimum Filament Tension
ΔT	Filament Tension Increase, $\Delta T = T - T_o$
$\vec{T}$	Filament Tension Vector
$\vec{V}_D$	Normal Component of Air Velocity Relative to the Filament
$\vec{V}_N$	Component of Filament Velocity Normal to Filament Direction
$\vec{V}_S$	Shear Force in Filament
Y_o	Bessel Function of Imaginary Argument
α_D	Linear Air Drag Parameter
α_n	Bessel Function Argument Coefficient
β	Acceleration Function
β^*	Deceleration Function
γ	Boundary Region Angle
γ_ϵ	Stiffness Function

δ	Boundary Region Length
$\delta_{1,2,3}$	Small Wave Number Corrections
δ_c	Displacement of Yarn Withdrawal Point From Cone Tip
δ_f	Broken Filament Extension
ϵ	Filament Stiffness Parameter = $EI/\rho_f A$
ϵ_f	Filament Strain
ξ	Displacement in the $\vec{u}_R$-direction
η	Displacement in the $\vec{j}$-direction
η_g	Gravity Deflection
η_o	General Lateral Maximum Amplitude
θ_R	Distinguishing Parameter Function (See Equation V-2)
θ	Filament Tangent Angle in x-y Plane
θ_o	Constant Inclination Angle of Filament at $x = \ell$
θ_o^*	Constant Inclination Angle of Filament at $x = 0$
θ_Y	Yarn Twist Angle
χ_c	Yarn Angle on Cone Surface
λ	Wave Length
λ_o	Euler Wave Length
μ	Coefficient of Friction Between Filament and Matrix
μ_c	Coefficient of Friction Between Filament and Cone
ν	Kinematic Viscosity of Air
ξ	Displacement in the $\vec{i}$-direction
ρ_a	Density of Air
ρ_f	Density of Filament
φ	Displacement in the $\vec{k}$-direction
ϕ	Phase Angle at $x = \ell$

NOMENCLATURE (continued)

ϕ^*	Phase Angle at x = 0
χ	Displacement in $\vec{u}_\theta$- direction
ψ_c	Cone Apex Angle
ψ_n	Special Modes (Hanging Chain Solution)
$\vec{\psi}$	Vector Displacement
ω	Frequency of Forced Oscillation Relative to Moving Filament
ω_n	Natural Frequency (Hanging Chain Solution)
ω_o	Frequency of Forced Oscillation at x = ℓ
ω_o^*	Frequency of Forced Oscillation at x = 0
Ω	System Natural Frequency for k_o Solution With Zero Air Drag
Ω'	System Natural Frequency for Boundary Region
Ω_ϵ	System Natural Frequency for Low Filament Stiffness
Ω_n	System Natural Frequency

I. INTRODUCTION

This thesis is intended to be primarily a general analytical approach and secondly an experimental approach, to the phenomena of moving filaments and tapes. The experimental approach is limited to the verification of only the fundamental results of the analytical approach. Extensive experimental validification of detailed analytical results is not intended.

The word filament is intended to imply a yarn, string, rope, wire, monofilament, etc.; a structure which is essentially thin, flexible and continuous with small, but not necessarily negligible, bending stiffness. Tapes are considered as two-dimensional filaments with primarily the same description. The phenomena of these moving filaments and tapes form a small related field within the subject matter of applied mechanics. Moving filaments and tapes can be characterized as mechanical systems and described with the concepts of mechanical engineering systems. The material in this thesis is intended to apply within the context of Textile Mechanical Processing.

If the path of a moving filament is separated into regions between guide points on a textile processing machine, these points can be considered as the boundaries of the mechanical system. Statements can be made concerning the conditions at these boundaries and equations developed to predict filament motion and tension within the boundaries. Examples of system boundaries are seen in machinery involved with the spinning,

the drafting, the winding, the twisting, etc., of both staple and continuous-filament yarn. In these cases the system includes both the region and the filament within the region. The spinning balloon, the overend unwinding balloon and the filament space curves associated with high frequency yarn traversing mechanisms are well known examples of yarn systems generated in the average textile mill.

The literature contains numerous reports related to the subject of moving filaments. However, in general, each of these reports has confined its attention to a specific phenomenon of filament motion within a specific textile machine, rather than to the overall phenomena of moving filaments within general system boundaries. The assumptions made in these previously published reports and papers have been too restrictive in the sense that the results cannot be applied to situations which are not completely similar. It is admitted, however, that there are published analyses which move further into the detailed mathematics of a single moving filament situation.

Hannah (11), Mack (23) and Crank (24) have studied in detail the nonlinear equations that apply to the cap and ring spinning systems, commonly employed in textile yarn processing. They have neglected filament stiffness, and tangential air drag and have considered the surrounding air as stationary. Their numerical results have been obtained from the direct numerical integration of their developed differential equations. Hannah (11) has dealt only with cap spinning and by making simplifying assumptions about air drag forces, she has expressed her

results as a function of a single cap spinning parameter. Mack (23) has made a more exact formulation of air drag and obtained results which apply to both cap spinning and ring spinning. His results are expressible as functions of two parameters, an air drag parameter and a tension parameter. Crank (24) has also investigated the equations which apply to cap and ring spinning systems. He has, however, included the effect of longitudinal yarn velocity, commonly called the " Coriolis Effect ". For zero longitudinal yarn velocity his results are also expressible as functions of a tension parameter and an air drag parameter, similar to those of Mack (23). DeBarr (3) has summarized previous theoretical and analytical findings for cotton ring spinning systems.

Padfield (4) has examined the specific equations of yarn motion for an overend unwinding yarn package. She has numerically integrated her derived differential equations and the results are presented as specific plots of yarn space curves. Padfield (10)(12) has discussed the boundary conditions at package surfaces, such as are used in this paper. Brunnschweiler (20)(21) has also dealt with overend unwinding yarn packages by measuring yarn tension and photographing yarn space curves. This study is unfortunately only experimental and does not try to validate a specific theory.

There are, of course, many linear solutions for oscillating strings and beams. But of these only Sack (19) has included longitudinal velocity in solving the differential equations of filament motion. A general approach to these systems is considered necessary.

A general analytical approach should begin with a general filament model. The equations which describe this general model must be complete in order to predict the behavior of an actual filament. Therefore, forces from filament tension, filament shear, gravity and air drag are included. A point on the filament is identified as an infinitesimal particle of constant mass. The above forces are then summed and equated to the rate of change of momentum of this infinitesimal mass. This summation leads to the general vector differential equation for a moving filament.

This general vector differential equation can be written in terms of a filament position vector, $\vec{R}(s,t)$. The position vector specifies the position in space of the filament particle, with respect to a fixed inertial reference frame. The coordinate, s, specifies the distance along the filament from a point on the filament, the position of which is known at some reference time. It is possible to choose a specific position vector in order to describe any type of filament motion desired. The position vector can contain a description of the net, or average motion, of the filament plus a statement of the perturbations or small deviations from this average motion. This makes it possible to derive governing differential equations for specific net motions and boundary conditions in a way such that the initial simplifications can be made from physical judgements.

The general vector differential equation has been examined extensively for the case of linear filament motion. The term

linear filament motion refers to filament motion which is essentially straight line travel between two boundary points with the addition of small perturbations in the two lateral directions. Linear filament motion is sufficient to describe the practical textile processing situations described above.

The results of this examination of the differential equations of linear filament motion are presented as simplified equations, which can be used to predict the paths through space of actual filaments. These equations are formulated in terms of dimensionless combinations of variables which refer to the relative magnitudes of filament stiffness, air drag, gravity, etc. These dimensionless parameters can also be used to predict identifying quantities such as the number of filament balloons (in an unwinding situation), the magnitude of the filament rotation angle in a given balloon, the length of the boundary "stiffness" region versus the flexible region in a given filament, etc. They are also logical correlation parameters for experimental or numerical data.

For moving filaments which have small, but not necessarily negligible stiffness, a concept of a boundary stiffness region is introduced. Equations are developed which allow a prediction of the length of this region. The equations describing the linear motion of flexible filaments are then modified using this length.

The linear equations assume constant overall filament velocity, v. There are practical situations, however, where the displacements and strains of accelerating or decelerating

filaments become important. These situations include the transient behavior of filament systems during the start up or shut down of processing equipment. They also include the dynamic buckling which occurs when a filament, moving at high speeds through a machine guide, is suddenly stopped at one point along its path. Equations have been developed to permit prediction of the time dependence and the mode shapes of both the stable oscillations corresponding to accelerating filaments, and the unstable deformations of decelerating or dynamically buckling filaments.

The effect that a surrounding matrix of solid material can have on the dynamics of filament rupture is also examined. The equations developed provide, to a limited extent, a quantitative picture of the internal dynamics of a breaking yarn. The internal dynamics of a breaking yarn is important in determining yarn strength and strength has an important effect on process efficiency.

It is felt that this thesis can be used as an aid to textile machinery designers, since it allows an accurate prediction to be made as to the actual filament motions and strains that take place as a result of machine-material interactions.

At the present time when one designs a piece of machinery through which a filament or a tape will pass, almost all of the design effort is involved with factors affecting machine life, cost, reliability, etc. Little consideration is given to the interaction between machine and filament. This can lead to situations where a filament is modified in some

undesirable manner as a result of passing through a machine. An example of this is the progressive drafting of cotton yarn that takes place as the yarn is being wound on a drum winder. It has been found that rewinding the same yarn package as few as five times on certain drum winders causes a sufficient amount of drafting that the yarn may break in several places (30). A second example is the package surface instability (shelloff) that occurs when yarn is drawn overend from a yarn cone at sufficient withdrawal speeds. Whole yarn loops slide down the cone surface leaving the package at one time and causing a disruption in smooth flow of yarn from the package. When one tries to use such a cone for the filling yarn on a shuttless loom the speed of the loom becomes limited by the speed at which this instability occurs (31).

It is suggested that the application of the solutions of this thesis toward specific problems such as those above is a logical initial step in the direction of reducing undesirable effects of machine-filament interaction.

II. GENERAL VECTOR DIFFERENTIAL EQUATION

A. Introduction

The first portion of this thesis is devoted to the examination of a general model of a moving filament. The equations which describe this general model must be complete in order to predict the behavior of an actual filament. Therefore, forces from filament tension, filament shear, gravity and air drag are included. A point on the filament is identified as an infinitesimal particle of constant mass. The above forces are then summed and equated to the rate of change of momentum of this infinitesimal mass. This results in an equation, called the general vector differential equation for a moving filament.

B. Definitions

In order to present the derivation of the general vector differential equation several definitions must first be established.

Filament Particle The filament particle is defined as the infinitesimal mass, $\rho_f A \Delta s$, which exists at a point on the filament defined by the coordinate, s.

Position Vector = $\vec{R}(s,t)$ The position vector specifies the position in space, with respect to a fixed inertial reference frame, of the filament particle. The coordinate, s, specifies the distance along the filament from a point on the filament, the position of which is known at some reference time. The derivatives of this vector have the

following properties.

$\frac{\partial \vec{R}}{\partial t}(s,t)$ = Velocity of particle s at time, t.

$\frac{\partial^2 \vec{R}}{\partial t^2}(s,t)$ = Acceleration of particle s at time, t.

$\frac{\partial \vec{R}}{\partial s}(s,t) = \vec{u}(s,t)$ = Unit Tangent Vector (in filament direction) at s.

$r\frac{\partial^2 \vec{R}}{\partial s^2}(s,t) = \vec{n}(s,t)$ = Unit Principal Normal Vector to the filament, where r is the instantaneous radius of curvature of the filament at s at time, t.

Tension Vector = $\vec{T}(s,t) = T\frac{\partial \vec{R}}{\partial s}(s,t)$ The tension in a filament acts in the direction of the filament axis and can be represented as the product of a scalar magnitude, T, and the unit vector, $\vec{u} = \frac{\partial \vec{R}}{\partial s}$.

Coordinate System

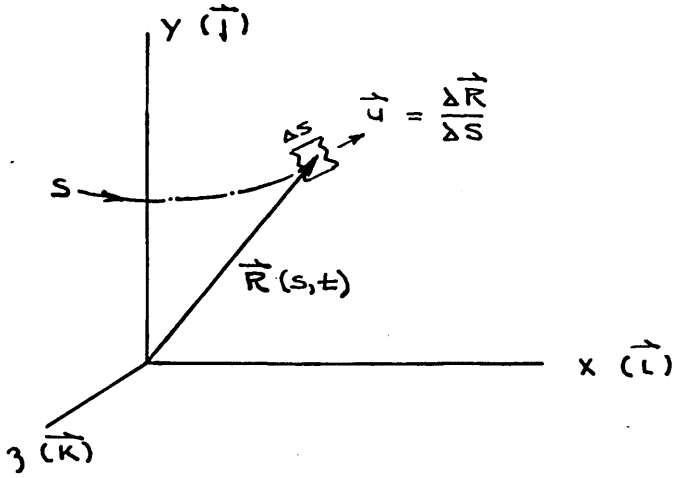

This right hand cartesian coordinate system will be used throughout unless noted. Gravity will be taken as acting in the negative $\vec{j}$-direction.

C. Forces Acting on an Identified Filament Particle.

Filament Tension, $\vec{T}$

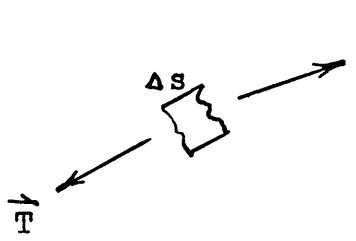

$$\Delta\vec{T} = \frac{\delta\vec{T}}{\delta s}\Delta s = \frac{\delta}{\delta s}\left(T\,\frac{\delta\vec{R}}{\delta s}\right)\Delta s$$

$$= \left(\frac{\delta T}{\delta s}\,\frac{\delta\vec{R}}{\delta s} + T\,\frac{\delta^2\vec{R}}{\delta s^2}\right)\Delta s$$

$$= \left(\frac{\delta T}{\delta s}\,\vec{u} + \frac{T}{r}\,\vec{n}\right)\Delta s$$

Filament Shear Force, $\vec{V}_s$

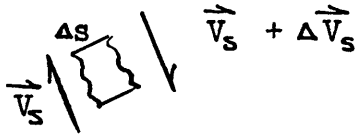

$$\Delta\vec{V}_s = \left(\frac{\delta\vec{V}_s}{\delta s}\right)\Delta s$$

This force is left in general form and will be considered in greater detail only in the specific cases where it is significant.

Gravity Force, $\vec{F}_g$

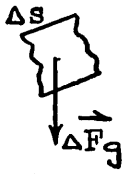

$$\Delta\vec{F}_g = -\rho_f g A\,\Delta s\,\vec{j}$$

Air Drag Force, $\vec{D}$

As a filament moves through the air or any viscous medium it feels a net drag force associated with the lack of pressure recovery behind it. This type of drag force is discussed for both continuous-filament yarns and staple fiber yarns in Chapter 3 of Reference 3. This reference

states that if the ratio of lateral yarn velocity to longitudinal yarn velocity is large then continuous-filament yarns behave substantially as smooth cylinders with the air drag force acting in a direction normal to the filament axis. However, for staple fiber yarns, the air drag is greater than would be expected on this basis - the effective yarn diameter being approximately 50% greater than the actual yarn diameter. This occurs because portions of fibers protrude from the yarn surface into the air stream, spoiling the flow.

If the ratio of lateral yarn velocity to longitudinal yarn velocity is not large then the air drag force has a component along the filament axis. This component does not influence lateral yarn motion directly, but affects tension - which in turn influences lateral motion.

The general filament model of this thesis considers that forces from air drag act normal to the filament axis and obey the standard equation for smooth cylinders. The normal component of air velocity relative to the filament is given the symbol, $\vec{V}_D$. The magnitude and direction of $\vec{V}_D$ is a function of the filament particle velocity, $\frac{\Delta \vec{R}}{\Delta t}$, and the unit vector in the filament direction, $\vec{u} = \frac{\Delta \vec{R}}{\Delta s}$. This can be shown as follows.

$(\frac{\Delta \vec{R}}{\Delta t} \cdot \frac{\Delta \vec{R}}{\Delta s}) \frac{\Delta \vec{R}}{\Delta s}$

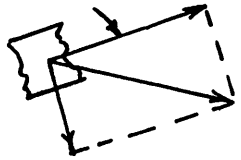

$\vec{u} = \frac{\Delta \vec{R}}{\Delta s}$ = Unit Tangent Vector (in Filament Direction)

$\frac{\Delta \vec{R}}{\Delta t}$ = Filament Particle Velocity

$\vec{V}_N$ = Component of Filament Velocity Normal to Filament Direction at s.

Since $$\vec{V}_N = \frac{\delta \vec{R}}{\delta t} - (\frac{\delta \vec{R}}{\delta t} \cdot \frac{\delta \vec{R}}{\delta s})(\frac{\delta \vec{R}}{\delta s}) = -\vec{V}_D$$

$$\therefore \vec{V}_D = (\frac{\delta \vec{R}}{\delta t} \cdot \frac{\delta \vec{R}}{\delta s})(\frac{\delta \vec{R}}{\delta s}) - \frac{\delta \vec{R}}{\delta t} \qquad \text{(II-1)}$$

The absolute value of $\vec{V}_D$ is most easily found by noticing that $(\frac{\delta \vec{R}}{\delta t} \cdot \frac{\delta \vec{R}}{\delta s})\frac{\delta \vec{R}}{\delta s}$, and $-\vec{V}_D$ are the two sides of a right triangle whose hypotenuse is $\frac{\delta \vec{R}}{\delta t}$. Therefore:

$$\frac{\delta \vec{R}}{\delta t} \cdot \frac{\delta \vec{R}}{\delta t} = (-\vec{V}_D) \cdot (-\vec{V}_D) + (\frac{\delta \vec{R}}{\delta t} \cdot \frac{\delta \vec{R}}{\delta s})\frac{\delta \vec{R}}{\delta s} \cdot (\frac{\delta \vec{R}}{\delta t} \cdot \frac{\delta \vec{R}}{\delta s})\frac{\delta \vec{R}}{\delta s}$$

$$\frac{\delta \vec{R}}{\delta t} \cdot \frac{\delta \vec{R}}{\delta t} = V_D^2 + (\frac{\delta \vec{R}}{\delta t} \cdot \frac{\delta \vec{R}}{\delta s})^2$$

$$\therefore V_D = |\vec{V}_D| = \left\{(\frac{\delta \vec{R}}{\delta t} \cdot \frac{\delta \vec{R}}{\delta t}) - (\frac{\delta \vec{R}}{\delta t} \cdot \frac{\delta \vec{R}}{\delta s})^2\right\}^{1/2}$$

The drag force can now be given the magnitude,

$$\Delta D = C_D \frac{\rho_a V_D^2}{2} D_f \Delta s$$

C_D is a function of Reynolds Number and is given in most standard fluid mechanics texts. Specifically, it is given in Reference 6. ρ_a is the density of air and D_f is the filament diameter.

The direction of the drag force is the same as the direction of $\vec{V}_D$. Therefore, if the unit vector in this direction is taken as $\vec{d} = \frac{\vec{V}_D}{V_D}$, the drag force vector can be expressed as:

$$\Delta \vec{D} = C_D \frac{\rho_a V_D^2}{2} D_f \Delta s \, \vec{d} \qquad \text{(II-2)}$$

Since C_D is a function of Reynolds Number, Rey$= \frac{V_D D_f}{\nu}$, where ν is the kinematic viscosity of air, it can be seen that for a given filament the magnitude of the drag force

is a function of V_D only. For low values of V_D the drag force is proportional to V_D, while for high values of V_D the drag force is proportional to V_D^2. This velocity dependence is shown in Figure 1 for a hypothetical 20 mil filament moving through air at standard temperature and pressure.

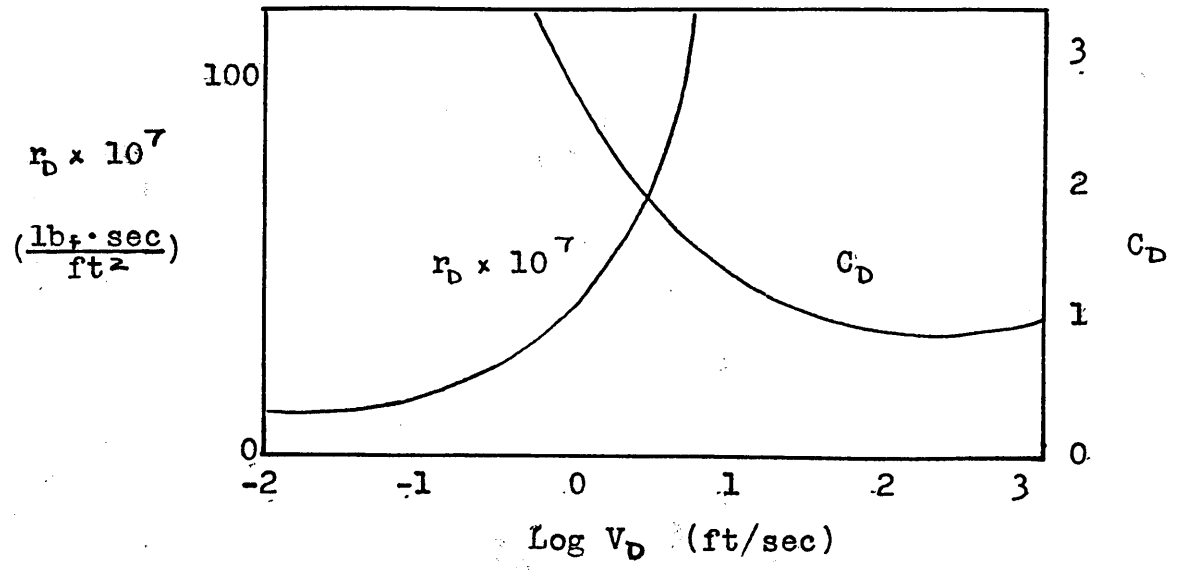

Drag Coefficients vs. Filament Lateral Velocity
FIG. 1

r_D is defined as the drag force per unit length of filament per unit of normal relative air velocity and is expressed by the equation,

$$r_D = \frac{\Delta D}{\Delta s} \frac{1}{V_D}$$

$$\therefore \vec{\Delta D} = r_D \vec{V_D} \Delta s \qquad \text{(II-3)}$$

Figure 1 illustrates that for a typical continuous-filament yarn the drag force is proportional to V_D(constant r_D) for values of $V_D < 0.1$ ft/sec. For values of $V_D > 100$ ft/sec the drag force is proportional to V_D^2 (constant C_D). It is

unfortunate that the range of practical interest lies between these two values of V_D and therefore, for most situations the drag force cannot be accurately modeled by a constant r_D or a constant C_D. However, when considering air drag in connection with the linear equations to be discussed later in this thesis, the air drag force will be assumed proportional to V_D. It is therefore, necessary to use an average value for r_D. The average value of r_D should be chosen so that it yields the actual energy loss per cycle. If the drag force is actually proportional to V_D^2 the correct average value for harmonic oscillation is:

$$r_D = .85 \frac{\text{Maximum Drag Force per Unit Filament Length}}{\text{Maximum Filament Normal Air Velocity}}$$

This value is calculated in Appendix 1.

D. General Vector Differential Equation

Since the filament particle has been defined to have a constant mass, $\rho_f A \Delta s$, then the resultant of all the forces acting on it must be equal to the product of its mass and acceleration.

$$\frac{\delta T}{\delta s}\frac{\delta \vec{R}}{\delta s} + T\frac{\delta^2 \vec{R}}{\delta s^2} + \frac{\delta \vec{V_s}}{\delta s} - \rho_f g A \vec{j} + C_D \frac{\rho_a V_D^2}{2} D_f \vec{d} = \rho_f A \frac{\delta^2 \vec{R}}{\delta t^2} \quad \text{(II-4)}$$

The terms in this equation refer to forces from variable tension, filament curvature, bending stiffness, gravity, air drag and rate of change of filament particle momentum (mass times acceleration). If the tension is considered constant and shear forces are negligible then the equation becomes:

$$T\frac{\partial^2\vec{R}}{\partial s^2} - \rho_f g A\vec{j} + C_D\frac{\rho_a V_D^2}{2} D_f\vec{d} = \rho_f A\frac{\partial^2\vec{R}}{\partial t^2} \qquad \text{(II-5)}$$

If forces from gravity and air drag are also negligible the equation is further reduced to:

$$\frac{\partial^2\vec{R}}{\partial s^2} = \frac{1}{c^2}\frac{\partial^2\vec{R}}{\partial t^2}, \qquad c^2 = \frac{T}{\rho_f A} \qquad \text{(II-6)}$$

where c is the well known phase velocity, a most important variable in any discussion of filament motion.

The general vector differential equation has been derived in terms of the general position vector, $\vec{R}$. It is therefore possible to choose any specific position vector in order to describe any type of filament motion desired. The position vector can contain a description of the net, or average motion, of the filament plus a statement of the perturbations or small deviations from this average motion. This makes it possible to derive governing differential equations for specific net motions and boundary conditions in a way such that the initial simplifications are made from physical judgments. As an example, consider the perturbations of an idealized horizontal lasso from an essentially circular path. The position vector is given as:

$$\vec{R}(s,t) = \left\{(vt + s) + \chi\right\}\vec{u}_\theta + \xi\vec{u}_r + \eta\vec{j}$$

Where χ, ξ and η are "small" displacements in the tangential, radial and vertical directions respectively; v is the net filament velocity and $\vec{u}_\theta$, $\vec{u}_r$ and $\vec{j}$ are unit vectors in the tangential, radial and vertical directions respectively.

If these small displacements are taken as zero the overall stability condition for this filament configuration can be found. Considering Equation II-6 to be applicable for this simple example and substituting the above position vector with the small displacements taken as zero, one finds that v must equal c for stability ($T = \rho_t A v^2$). This defines the net or average motion of the filament and substitution of the complete position vector yields three equations which define the three "small" displacements from this stable configuration.

This is a simple and well known example and illustrates the use of the position vector. However, there are many other stable configurations from which there can be small perturbations worthy of investigation. The position vector which defines an essentially straight line motion is the one of most practical interest in industrial processing of filaments, and so the rest of the thesis will be devoted to its examination.

III. GENERAL EQUATION REDUCTION FOR LINEAR MOTION

The practical aim of this thesis is to define quantitatively, and to a large degree qualitatively, a number of flowing yarn, wire, and tape situations. This can be accomplished by examining the solution to the general vector differential equation for a position vector where the net or overall motion is essentially straight line motion. This position vector can be defined as follows:

$$\vec{R}(s,t) = (f(s,t) + \xi)\vec{i} + \eta\vec{j} + \varphi\vec{k} \qquad \text{(III-1)}$$

In this equation η and φ are the "small" displacements in the y and z directions of a filament particle moving in the positive x direction with an overall motion defined by f(s,t) and an additional "small" displacement defined by ξ. This case is considered as linear motion since the filament deviates from an essentially straight line path in the $\vec{i}$-direction. The ratio of dx to ds is therefore taken as 1. The function f(s,t) will be given the value vt + s, in this section, where v is constant. This further limits the motion to essentially constant average velocity in the $\vec{i}$-direction.

In order to understand fully the phenomena of moving filaments, it has been found necessary to include the effects that air drag, filament stiffness, filament momentum and gravity have on the motions involved. Tension remains the predominant filament control force for the cases considered in this section. But situations, either caused by extreme boundary conditions or by extreme material properties

require the inclusion of stiffness, air drag and gravity to explain deviations from the predicted results of the simpler models. The winding of glass or metals or large polymer monofilaments represent the case of extreme material properties, while the unusual characteristics of filament motion near guides at high speeds are examples of extreme boundary conditions.

The general vector equation as defined in Section II is:

$$\frac{\partial T}{\partial s}\frac{\partial \vec{R}}{\partial s} + T\frac{\partial^2 \vec{R}}{\partial s^2} + \frac{\partial \vec{V_s}}{\partial s} - \rho_f g A\vec{j} + C_D\frac{\rho_a V_b^2}{2}D_f\vec{d} = \rho_f A\frac{\partial^2 \vec{R}}{\partial t^2} \quad \text{(II-4)}$$

Substitution for the $\vec{i}$ direction motion yields a one dimensional wave equation for the deflection, ξ, as measured from the moving reference frame.

$$\frac{\partial^2 \xi}{\partial s^2} = \frac{1}{a_s^2}\frac{\partial^2 \xi}{\partial t^2}, \qquad a_s^2 = E/\rho_f \quad \text{(III-2)}$$

This equation refers to the actual propagation along the filament of the strain $(\frac{\partial \xi}{\partial s})$ or tension $(EA\frac{\partial \xi}{\partial s})$. This propagation takes place at the sonic velocity of the material, a_s. The ratio of a_s to the transverse wave velocity, c, is:

$$\frac{a_s}{c} = \left(\frac{E/\rho_f}{T/\rho_f A}\right)^{\frac{1}{2}} = \left(\frac{1}{\epsilon_f}\right)^{\frac{1}{2}}$$

Therefore, if the average filament strain, ϵ_f, is small, the propagation of tension waves can be neglected in solving for the lateral displacements, η and φ. Therefore Equation III-1 can be simplified to:

$$\vec{R}(s,t) = (vt+s)\vec{i} + \eta\vec{j} + \varphi\vec{k} \quad \text{(III-3)}$$

The normal component of air velocity relative to the filament can be expressed as follows:

$$\vec{V}_D = V_{D_x}\vec{i} + V_{D_y}\vec{j} + V_{D_3}\vec{k}$$

The components V_{D_X}, V_{D_Y}, and V_{D_3}, are found by referring to Section II, Equation II-1, where it was shown that:

$$\vec{V}_D = \left(\frac{\Delta\vec{R}}{\Delta t}\cdot\frac{\Delta\vec{R}}{\Delta s}\right)\left(\frac{\Delta\vec{R}}{\Delta s}\right) - \frac{\Delta\vec{R}}{\Delta t} \qquad \text{(II-1)}$$

Substitution of the position vector, $\vec{R}(s,t)$, into this equation yields (neglecting second order small terms):

$$\vec{V}_D = \left(v\frac{\Delta\eta}{\Delta s} - \frac{\Delta\eta}{\Delta t}\right)\vec{j} + \left(v\frac{\Delta\varphi}{\Delta s} - \frac{\Delta\varphi}{\Delta t}\right)\vec{k}$$

The velocity, v, in the above equation refers to the velocity of the filament relative to the reference frame. If the air is at rest with respect to the reference frame, then the above equation is correct. However, the movement of the filament can develop a flow of air in the direction of net or overall filament motion, which in this case is the $\vec{i}$-direction. Therefore, using the average filament velocity, v, in the above equation causes an error.

By introducing the term, v_a, which is equal to the actual net filament velocity less the induced $\vec{i}$-direction air flow velocity, the above equation can be written more correctly as:

$$\vec{V}_D = \left(v_a\frac{\Delta\eta}{\Delta s} - \frac{\Delta\eta}{\Delta t}\right)\vec{j} + \left(v_a\frac{\Delta\varphi}{\Delta s} - \frac{\Delta\varphi}{\Delta t}\right)\vec{k} \qquad \text{(III-4)}$$

It is now necessary to express the air drag term in Equation II-4 in a linear form. This is done by using the

linear air drag parameter r_D, previously discussed. Referring to Equations II-2 and II-3:

$$\frac{\vec{\Delta D_D}}{\Delta s} = C_D \frac{\rho_a V_D^2}{2} D_f \vec{d} = r_D \vec{V_D}$$

Therefore, Equation II-4 can be rewritten as (noting that the tension is considered constant):

$$T\frac{\delta^2 \vec{R}}{\delta s^2} + \frac{\delta \vec{V_s}}{\delta s} - \rho_f g A \vec{j} + r_D \vec{V_D} = \rho_f A \frac{\delta^2 \vec{R}}{\delta t^2} \qquad \text{(III-5)}$$

The filament shear force, V_s, can be considered as the variation in bending moment along s. Since the bending moment is directly related to the local filament curvature it is possible to say:

$$M = \left|\frac{\vec{n}}{r} EI\right| = EI\left|\frac{\delta^2 \vec{R}}{\delta s^2}\right|$$

$$\therefore V_s = -\frac{\delta M}{\delta s} = -EI\frac{\delta}{\delta s}\left|\frac{\delta^2 \vec{R}}{\delta s^2}\right|$$

$$\frac{\delta V_s}{\delta s} = -EI\frac{\delta^2}{\delta s^2}\left|\frac{\delta^2 \vec{R}}{\delta s^2}\right|$$

This holds true for all magnitudes of position vector, $\vec{R}$, for a linear elastic material. Now substituting the position vector under consideration (Equation III-3):

$$\frac{\delta V_s}{\delta s} = -EI\ \frac{\delta^2}{\delta s^2}\left|\frac{\delta^2 \eta}{\delta s^2}\vec{j} + \frac{\delta^2 \varphi}{\delta s^2}\vec{k}\right|$$

For small curvatures superposition holds.

$$\therefore \frac{\delta \vec{V_s}}{\delta s} = -EI\ \frac{\delta^4 \eta}{\delta s^4}\vec{j} - EI\ \frac{\delta^4 \varphi}{\delta s^4}\vec{k} \qquad \text{(III-6)}$$

Having simplified filament tension, filament air drag force and filament shear force, it is now possible to

substitute for $\vec{R}$ (Equation III-3) in Equation III-5, separate it into two equations and rewrite in simple form.

For the $\vec{j}$-direction:

$$EI\frac{\partial^4\eta}{\partial s^4} - T\frac{\partial^2\eta}{\partial s^2} + \rho_f A\frac{\partial^2\eta}{\partial t^2} + r_D\left(\frac{\partial\eta}{\partial t} - v_a\frac{\partial\eta}{\partial s}\right) + \rho_f A g = 0 \qquad \text{(III-7)}$$

For the $\vec{k}$-direction:

$$EI\frac{\partial^4\varphi}{\partial s^4} - T\frac{\partial^2\varphi}{\partial s^2} + \rho_f A\frac{\partial^2\varphi}{\partial t^2} + r_D\left(\frac{\partial\varphi}{\partial t} - v_a\frac{\partial\varphi}{\partial s}\right) = 0 \qquad \text{(III-8)}$$

For the boundary conditions considered in the following sections, the lateral velocity of the filament varies harmonically with time. Thus in order to linearize the velocity dependence of air drag the constant value for r_D must be chosen as shown in Appendix I so that the energy loss to the air for actual air drag is the same as in the model. This is not a good approximation, but it will do no real harm to the solution since it is only an error in a second order effect. The linearized equations are therefore:

For the $\vec{j}$-direction

$$\epsilon\frac{\partial^4\eta}{\partial s^4} - c^2\frac{\partial^2\eta}{\partial s^2} + \frac{\partial^2\eta}{\partial t^2} + \alpha_D\left(\frac{\partial\eta}{\partial t} - v_a\frac{\partial\eta}{\partial s}\right) + g = 0 \qquad \text{(III-9)}$$

For the $\vec{k}$-direction:

$$\epsilon\frac{\partial^4\varphi}{\partial s^4} - c^2\frac{\partial^2\varphi}{\partial s^2} + \frac{\partial^2\varphi}{\partial t^2} + \alpha_D\left(\frac{\partial\varphi}{\partial t} - v_a\frac{\partial\varphi}{\partial s}\right) = 0 \qquad \text{(III-10)}$$

where

$$\epsilon = \frac{EI}{\rho_f A} = \frac{\text{Filament Flexural Rigidity}}{\text{Filament Mass per Unit Length}}$$

(Note: The choice of ϵ is to point out that this parameter is considered small.)

$$c = \sqrt{\frac{T}{\rho_f A}} = \text{Lateral Wave Velocity}$$

$$\alpha_D = \frac{r_D}{\rho_f A} = \text{Linear Air Drag Parameter}$$

The boundary conditions to be considered occur at points which generally move with respect to the filament. If the filament is considered to move toward positive x then points of fixed x - where some boundary conditions of forced vibration may be taking place - move toward negative s. This is simply expressed as:

$$s = x - vt$$

Therefore, a wave solution for η, for fixed x boundary conditions would have the form:

$$\begin{aligned} \eta &= \eta_o e^{\pm i(\omega_o t + kx)} + \eta_g(x) \\ &= \eta_o e^{\pm i(\omega t + ks)} + \eta_g(s + vt) \end{aligned} \qquad \text{(III-11)}$$

where $\omega = \omega_o + kv$

Substitution of this wave solution into Equation III-9 yields two equations:

$$\epsilon k^4 + k^2(c^2 - v^2) + k(-2\omega_o v + i\alpha_D(v - v_a)) + (-\omega_o^2 + i\alpha_D\omega_o) = 0 \qquad \text{(III-12)}$$

$$\epsilon \frac{\partial^4 \eta_g}{\partial x^4} - (c^2 - v^2)\frac{\partial^2 \eta_g}{\partial x^2} + \alpha_D(v - v_a)\frac{\partial \eta_g}{\partial x} + g = 0 \qquad \text{(III-13)}$$

Equation III-13 is reduced to derivatives with respect to the argument, s + vt = x. It is also possible to derive an equation similar to Equation III-12 for the displacement in the $\vec{k}$-direction, φ. But this is not considered necessary

since the equation would be identical to Equation III-12.

Equation III-12 can be further simplified by introducing five dimensionless parameters. These parameters are:

$$b_1 = \frac{\epsilon}{(c^2-v^2)\ell^2} = \frac{EI}{(T-\rho_f A v^2)\ell^2} \qquad \text{(Stiffness Parameter)}$$

$$b_2 = -\frac{2\omega_0 v\ell}{c^2-v^2} = -\frac{2\omega_0 v \rho_f A \ell}{T-\rho_f A v^2} \qquad \text{(Coriolis Parameter)}$$

$$b_3 = \frac{\alpha_D(v-v_a)\ell}{c^2-v^2} = \frac{r_D(v-v_a)\ell}{T-\rho_f A v^2} \qquad \text{(Longitudinal Air Motion Parameter)}$$

$$b_4 = -\frac{\omega_0^2\ell^2}{c^2-v^2} = -\frac{\rho_f A \omega_0^2 \ell^2}{T-\rho_f A v^2} \qquad \text{(Centrifugal Force Parameter)}$$

$$b_5 = \frac{\alpha_D \omega_0 \ell^2}{c^2-v^2} = \frac{r_D \omega_0 \ell^2}{T-\rho_f A v^2} \qquad \text{(Lateral Air Drag Parameter)}$$

The physical meaning of these parameters is discussed throughout the text and summarized in Section VIII. They refer, in order, to the effect that filament stiffness, Coriolis' acceleration, relative longitudinal air motion, centrifugal acceleration and relative lateral air motion have relative to net filament tension, $(T-\rho_F A v^2)$, on the motions of the filament. The system length, ℓ, is introduced as a convenient way to non-dimensionalize these parameters.

Equation III-12 becomes:

$$b_1(k\ell)^4+(k\ell)^2+(b_2+ib_3)(k\ell)+(b_4+ib_5) = 0 \qquad \text{(III-14)}$$

A good physical interpretation for $k\ell$ is that it is the number of waves that exist within the system boundaries, multiplied by the constant, 2π.

Equation III-13 can be rewritten by introducing:

$$b_6 = \frac{g\ell}{c^2-v^2} = \frac{\rho_f A g \ell}{T-\rho_f A v^2} \qquad \text{(Gravity Parameter)}$$

Equation III-13 becomes:

$$b_1 \left(\frac{\eta_3}{\ell}\right)^{IV} - \left(\frac{\eta_3}{\ell}\right)^{II} + b_3 \left(\frac{\eta_3}{\ell}\right)^{I} + b_6 = 0 \qquad \text{(III-15)}$$

Where the Roman numerals refer to differentiation with respect to the argument, $\frac{x}{\ell} = (s+vt)/\ell$.

In the following two sections Equations III-14 and III-15 are investigated for specific boundary conditions and for varying magnitudes of the parameters, $b_1 \rightarrow b_6$.

IV. SOLUTION FOR NON - OSCILLATORY BOUNDARY CONDITIONS

When a filament is moving horizontally at high speed (hundreds of feet per second) between two guides it might at first appear that the effect of gravity on the motion of the filament in the region between the guides, would be considerably reduced from that at lower speed. However, exactly the opposite occurs.

It will be shown that the " effective tension " or the value of tension which acts as a controlling and limiting variable with regard to filament motion can be expressed as $T - \rho_f A v^2$. When this " effective tension " becomes small, bending stiffness and air drag forces become important in controlling gravity deflections.* For relatively flexible filaments (yarns, thin tapes) the control forces come predominantly from surrounding air motion, while for relatively rigid filaments (monofilaments, metal wires) the control forces are caused by the bending stiffness of the filament itself. But, in either case, some mechanism other than tension must take over in controlling the motion between guides and it is the aim of this section to find out what this mechanism is.

Refer to Equation III-15:

$$b_1 \left(\frac{\eta_3}{\ell}\right)^{IV} - \left(\frac{\eta_3}{\ell}\right)^{II} + b_3 \left(\frac{\eta_3}{\ell}\right)^{I} + b_6 = 0 \qquad \text{(III-15)}$$

* These are, however, the predictions of a linear theory and do not hold for appreciable displacements.

This is the governing equation for $\frac{\eta_g}{\ell}$, for boundary conditions, at fixed points in space ($\frac{x}{\ell} = 0$, $\frac{x}{\ell} = 1$), which do not vary with time. The input force is, of course, gravity (b_6). The boundary conditions are stated simply as*:

$$\frac{\eta}{\ell}(0) = \frac{\eta}{\ell}^{x}(0) = \frac{\eta}{\ell}(1) = \frac{\eta}{\ell}^{x}(1) = 0 \qquad \text{(IV-1)}$$

Now assuming:

$$\frac{\eta}{\ell} = \frac{\eta_1}{\ell} - \frac{b_6}{b_3}\frac{x}{\ell} + c^* \qquad \text{(IV-2)}$$

it is possible to reduce Equation III-15 to:

$$(b_1 D^3 - D + b_3)\frac{\eta_1}{\ell} = 0 \qquad \text{(IV-3)}$$

where the D refers to a dimensionless operator. The equation for D is actually the reduced form of the general cubic equation and D can therefore be stated as:

$$D_1 = A + B$$

$$D_2 = -\frac{A+B}{2} + \frac{A-B}{2}\sqrt{-3}$$

$$D_3 = -\frac{A+B}{2} - \frac{A-B}{2}\sqrt{-3}$$

where $$A = \left(-\frac{b_3}{2b_1} + \frac{1}{b_1}\left(\frac{b_3^2}{4} - \frac{1}{27b_1}\right)^{\frac{1}{2}}\right)^{\frac{1}{3}}$$

and $$B = \left(-\frac{b_3}{2b_1} - \frac{1}{b_1}\left(\frac{b_3^2}{4} - \frac{1}{27b_1}\right)^{\frac{1}{2}}\right)^{\frac{1}{3}}$$

For the case where $b_1 b_3^2 > \frac{4}{27}$, one obtains one real and two conjugate imaginary roots. For the case where $b_1 b_3^2 < \frac{4}{27}$, one obtains three real, unequal roots.

Thus it is seen that superimposed on the linear term of

* The subscript g will not be carried further.

Equation IV-2, $-\frac{b_6}{b_3}\frac{x}{\ell}$, there is an additional displacement, $\frac{\eta_1}{\ell}$. The nature of $\frac{\eta_1}{\ell}$ varies with the magnitude of $b_1 b_3^2$. When $b_1 b_3^2 > \frac{4}{27}$, $\frac{\eta_1}{\ell}$ changes in nature from exponential to harmonic. This corresponds to a physical situation where the effects of forces arising from stiffness and air drag exceed those arising from effective tension.

It is possible to go ahead and solve for the boundary conditions as stated and then reduce the equation mathematically to examine each effect. But this requires extensive algebra and is impractical. The problem is more logically examined from physical considerations.

By letting $b_1 \to 0$, the fourth order dependence drops out of Equation III-15, thus making it simple to see what happens at high speeds for flexible filaments under the influence of gravity. The differential equation becomes:

$$\left(\frac{\eta}{\ell}\right)^{II} - b_3\left(\frac{\eta}{\ell}\right)^{I} - b_6 = 0 \qquad \text{(IV-4)}$$

where $$\frac{\eta}{\ell}(0) = \frac{\eta}{\ell}(1) = 0$$

This equation and these boundary conditions yield:

$$\frac{\eta}{\ell} = -\frac{b_6}{b_3}\left\{\frac{x}{\ell} - \frac{e^{\left(\frac{b_3 x}{\ell}\right)} - 1}{e^{b_3} - 1}\right\} \qquad \text{(IV-5)}$$

where $$\frac{\eta_{max}}{\ell} = -\frac{b_6}{b_3^2}\left\{\ln\left(\frac{e^{b_3}-1}{b_3}\right) + \frac{b_3}{e^{b_3}-1} - 1\right\}$$

For $b_3 << b_6$: $$\frac{\eta}{\ell} = \frac{\eta_{max}}{\ell}\left\{\frac{4x}{\ell}\left(1 - \frac{x}{\ell}\right)\right\} \qquad \text{(IV-6)}$$

where $$\frac{\eta_{max}}{\ell} = -\frac{b_6}{8} = \frac{-\rho_f A g \ell}{8(T - \rho_f A v^2)}$$

For $b_3 \gg b_6$:

$$\frac{\eta}{\ell} = \frac{\eta_{max}}{\ell}\left(\frac{x}{\ell}\right) \qquad \text{(IV-7)}$$

where

$$\frac{\eta_{max}}{\ell} = -\frac{b_6}{b_3} = -\frac{g}{\alpha_b(v-v_a)}$$

Equations IV-5, IV-6 and IV-7 are plotted in Figure 2. The initial low velocity configuration is a parabola, with the point of maximum deflection occurring at $\frac{x}{\ell} = \frac{1}{2}$. As the velocity is increased, the point of maximum deflection moves toward the downstream end, $(\frac{x}{\ell} = 1)$. When the filament velocity, v, reaches the lateral wave velocity, c, the point of maximum deflection has moved all the way to the downstream end, $\frac{x}{\ell} = 1$.

As seen in Figure 2, as the filament velocity approaches its maximum value the curvature of the filament at $\frac{x}{\ell} = 1$, becomes quite large and filament stiffness can no longer be neglected. It also cannot be neglected when the value of b_1 is high (metal wire, heavy monofilaments). It is thus necessary to examine Equation III-15 when $b_3 \to 0$. The differential equation becomes:

$$b_1\left(\frac{\eta}{\ell}\right)^{IV} - \left(\frac{\eta}{\ell}\right)^{II} + b_6 = 0 \qquad \text{(IV-8)}$$

where

$$\frac{\eta}{\ell}(0) = \frac{\eta}{\ell}^{I}(0) = \frac{\eta}{\ell}(1) = \frac{\eta}{\ell}^{I}(1) = 0$$

This equation and these boundary conditions yield:

$$\frac{\eta}{\ell} = -\frac{b_6}{2}\left\{\frac{\sinh\frac{x}{\delta} - \frac{x}{\delta}}{\frac{\ell}{\delta}} + \frac{\cosh\frac{x}{\delta} - 1}{\frac{\ell}{\delta}}\,\frac{\frac{2\delta}{\ell}\sinh\frac{\ell}{\delta} - (\cosh\frac{\ell}{\delta} + 1)}{\sinh\frac{\ell}{\delta} - \frac{2\delta}{\ell}(\cosh\frac{\ell}{\delta} - 1)} + \left(\frac{x}{\ell}\right)^2\right\} \qquad \text{(IV-9)}$$

where $\delta = b_1^{1/2}\ell$ = Boundary Region Length (to be discussed in Section V-C)

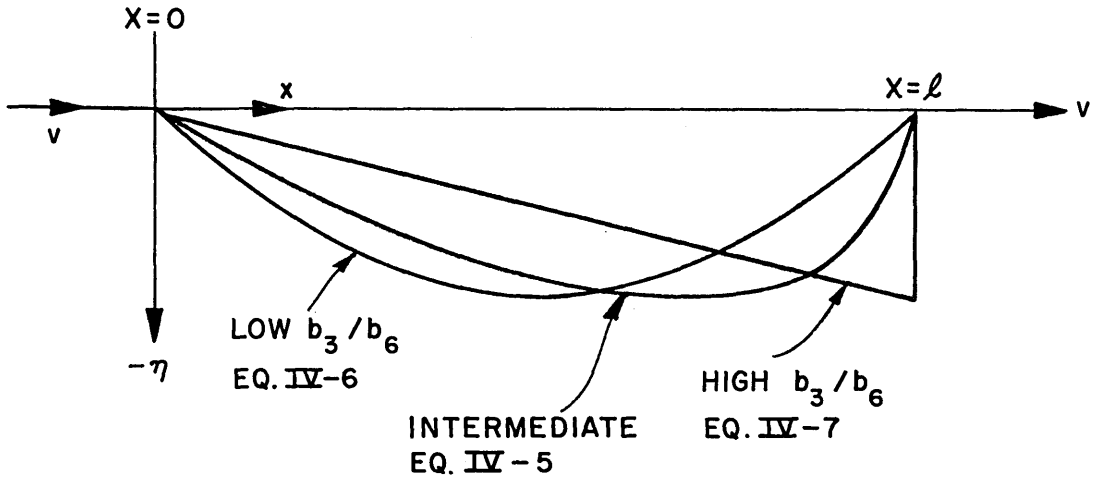

FIG. 2

GRAVITY EFFECTS, $b_1 \sim 0$

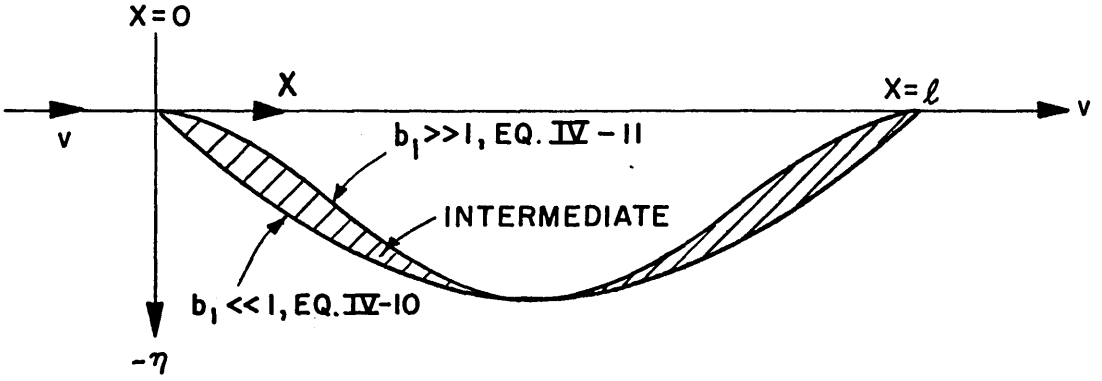

FIG. 3

GRAVITY EFFECTS, $b_3 \sim 0$

For $b_1 << 1$:

$$\frac{\eta}{\ell} = \frac{\eta_{max}}{\ell}\left\{\frac{4x}{\ell}\left(1 - \frac{x}{\ell}\right)\right\} \qquad \text{(IV-10)}$$

where

$$\frac{\eta_{max}}{\ell} = -\frac{b_6}{8} = \frac{-\rho_f A g \ell}{8(T - \rho_f A v^2)}$$

For $b_1 >> 1$:

$$\frac{\eta}{\ell} = \frac{\eta_{max}}{\ell}\left\{\left(\frac{x}{\ell}\right)^2\left(1 - \frac{x}{\ell}\right)^2 16\right\} \qquad \text{(IV-11)}$$

where

$$\frac{\eta_{max}}{\ell} = -\frac{b_6}{384 b_1} = \frac{-\rho_f A g \ell^3}{384 EI}$$

The filament is thus seen to move from a parabolic shape at low velocity ($b_1 << 1$) into a complicated exponential and parabolic curve and then become the " second order parabola " or regular beam shape at high velocity ($b_1 >> 1$). See Figure 3 which plots Equations IV-10 and IV-11.

The variable, δ, introduced above as the boundary region length, is derived and fully discussed in Section V-C. It is necessary, however, to explain here, that it refers to the length of filament, modeled as a massless beam, that extends from the system boundary to a point where the remaining filament can be considered as completely flexible, but of correct mass per unit length. Thus, for $\delta << \ell$ ($b_1 << 1$) the filament behaves as a flexible string. However, for $\delta >> \ell$ ($b_1 >> 1$) the filament behaves as a stiff beam.

Having the deflection curves for stiffness with zero air drag and for air drag with zero stiffness it is possible to compare the two and determine for what size filament the two effects are the same. This has been done for reasonable values of all parameters (See Appendix 2) and it was found that for monofilaments of 10 mil diameter the two effects are comparable. This diameter is considered typical.

It is unfortunately not possible within the scope of this thesis to investigate these solutions for values of overall filament velocity, v, approaching the limiting values of lateral wave velocity, c, since these limiting values can be two or three thousand ft/sec. It is expected, however, that textile processing machinery will begin to approach these values at some future date.

The last comment made in connection with this section is concerned with the notion of the overall filament velocity, v, being greater than c. If the parameter, $b_7 = \frac{v}{c}$=" Equivalent Mach Number " is introduced, this notion is expressed as the Equivalent Mach Number being greater than one. Physically this means that the tension is lower than the momentum flux of the filament, $\rho_t A v^2$, and therefore does not control filament motion. Figure 4 is a photograph of a cotton yarn forced to " flow " at approximately 150 ft/sec by a driven set of gears. The yarn is pushed out to the right away from the gears. The photograph was taken in a semi-dark room with the aid of one flash from a Strobotac. The overall motion is evidenced in the envelope of multiple yarn configurations, while one specific configuration is in focus. The behavior of the yarn is similar to a fluid stream, as evidenced by the deflection of the yarn at the plexiglass plate. Reference is made to Figure 29 of Section IX which contains other examples of this type of yarn motion.

Thus, filament speeds greater than c are certainly possible - but what happens is that downstream control is

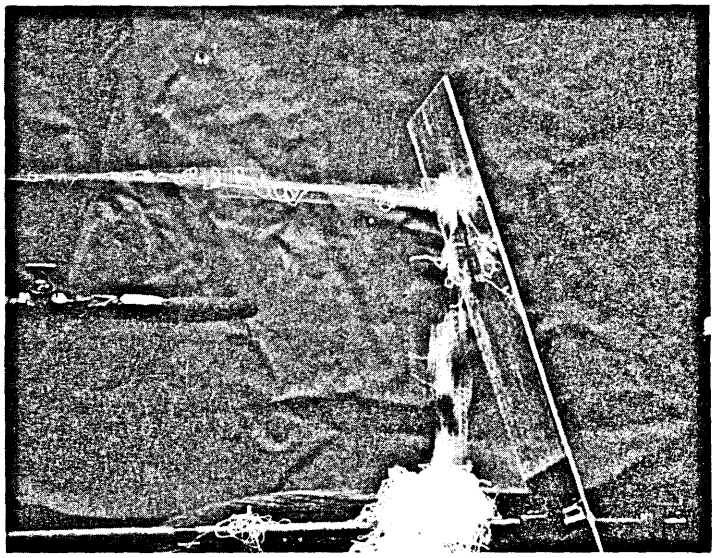

FIG. 4

FLUID STREAM BEHAVIOR OF HIGH SPEED YARN $b_7 > 1$

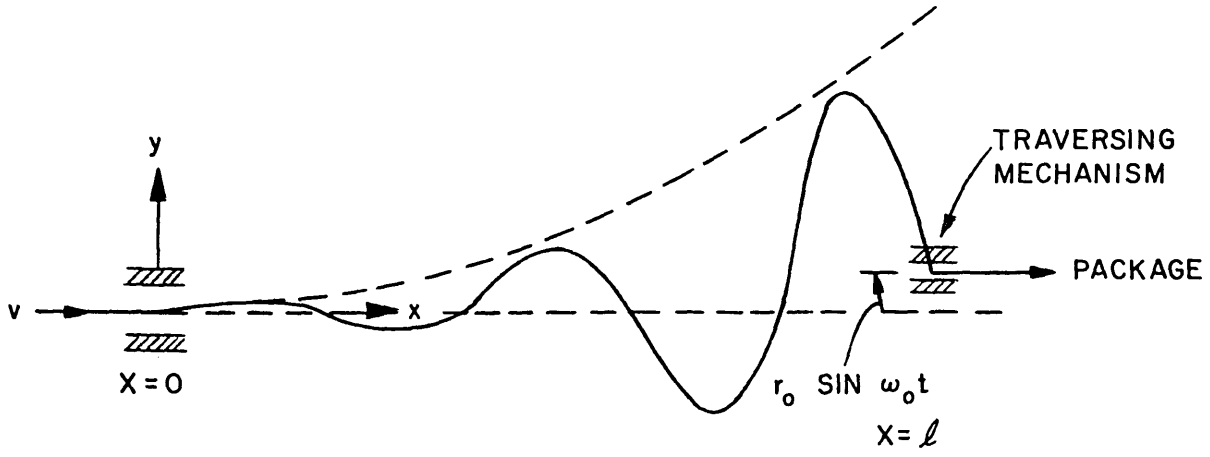

FIG. 5

BOUNDARY CONDITIONS FOR YARN WINDING MACHINERY

lost. If v is forced to be greater than c it must occur by some upstream mechanism - such as pushing the filament with an air jet or high speed rollers as was done in the experimental setup of Figure 4. Then the filament behaves as a fluid stream, and if the stiffness is low (yarn) it will deflect from boundaries and create stagnation pressures as is shown in Figure 4. This cannot occur if the yarn is " pulled downstream " as in most practical situations of textile processing.

V. SOLUTION FOR OSCILLATORY BOUNDARY CONDITIONS

A. . Two Dimensions

The lateral motions ($\vec{j}$ and $\vec{k}$-directions) of moving filaments are usually much more complex than the simple gravity deflections just discussed. The additional complexity is usually caused by periodic displacements or forces acting on the filament at points along its path. In order to examine these additional lateral motions the path of a moving filament must be broken down into regions between any two such points. These points can then be considered as system boundaries and statements can be made concerning conditions at these boundaries.

The boundary conditions for a situation of linear motion usually include harmonic oscillation. And if the oscillation is not harmonic, but periodic, the boundary conditions can usually be represented as an infinite number of harmonic oscillations summed in a Fourier Series. Examples of harmonic motion would be the spinning balloon or the overend unwinding balloon, while a typical periodic motion would be represented by the filament path of the many traversing mechanisms that exist in winding machinery. Another common periodic force is that caused by friction chattering induced by stationary guides.

In order to cover as many of these examples as possible, the boundary conditions for this section have therefore been chosen as general as possible.

The boundary conditions for harmonic displacement are:

$$\frac{\eta}{\ell}(0,t) = \frac{r_o^*}{\ell}\sin(\omega_o^* t + \phi), \quad \frac{\eta}{\ell}(1,t) = \frac{r_o}{\ell}\sin\omega_o t$$
$$\frac{\partial\eta}{\partial x}(0,t) = \theta_o^* \cos(\omega_o^* t + \phi), \quad \frac{\partial\eta}{\partial x}(\ell,t) = \theta_o \cos\omega_o t \qquad \text{(V-1)}$$

The boundary conditions for the $\vec{k}$-direction will be given later in this section, when three-dimensional motion is discussed. We shall limit the discussion here to displacements in the $\vec{j}$-direction because the equations of motion for the two lateral directions (y and z) are uncoupled and can be solved independently.

Two-dimensional considerations are enough to describe the dynamics of moving tapes since tapes usually have stiffness ratios, for the cross directions, of many tens of thousands. However, it must be mentioned that the " virtual mass per unit length " of a tape is greater than its actual mass. This effect is a consequence of the relatively large local mass of air that moves with the filament.

In order to investigate the lateral motions of flowing filaments forced by the periodic boundary conditions of Equations V-1 - it is necessary to solve the wave number equation (Equation III-14) for the traveling wave discussed in Section III, i.e.,

$$b_1(k\ell)^4 + (k\ell)^2 + (b_2 + ib_3)(k\ell) + (b_4 + ib_5) = 0 \qquad \text{(III-14)}$$

The general quartic equation, can be solved using Ferrari's method. But this method involves finding the three roots of a cubic equation; then, with each of these roots, reducing the quartic to a quadratic, and solving the quadratic. Since the

coefficients in the above formula are complex and the method itself is extremely lengthly (even for real coefficients), no attempt was made to use it. Instead two approximate solutions are examined.

The first approximate solution is for filaments which have very little bending stiffness (b_1 is small). This solution was not carried through to completion because of the extreme amount of algebra involved and because, as will be shown later in this section, it is possible to use a " boundary layer " or in this case boundary region concept for moving filaments possessing small bending stiffness. This first solution is outlined as follows:

Let k_o be a root of the wave number equation (Equation III-14) for zero filament stiffness ($b_1 = 0$).

Therefore $$(k_o\ell)^2 + (k_o\ell)(b_2 + ib_3) + (b_4 + ib_5) = 0 \qquad (V\text{-}2)$$

$$k_o\ell = -\frac{b_2+ib_3}{2}\left(1 \pm \left(1 - \frac{4(b_4+ib_5)}{(b_2+ib_3)^2}\right)^{\frac{1}{2}}\right)$$

$$= \frac{-b_2+R\cos\theta_R}{2} + i\,\frac{-b_3+R\sin\theta_R}{2}$$

where $$R = \pm\left((b_2^2 - 4b_4 - b_3^2)^2 + 4(b_2b_3 - 2b_5)^2\right)^{\frac{1}{4}}$$

$$\theta_R = \tfrac{1}{2}\tan^{-1}\frac{2b_2b_3 - 4b_5}{b_2^2 - b_3^2 - 4b_4}$$

Now let there be one solution of the form:

$$k_1\ell = k_o\ell\,(1 + \delta_1)^{\frac{1}{2}}, \qquad \text{where} \quad \delta_1 \ll 1$$

and one solution of the form:

$$k_2\ell = k_o\ell\left(\frac{1}{\delta_2}\right), \qquad \text{where} \quad \delta_2 \ll 1$$

Substitution into Equation III-14 yields:

$$k_1 \ell = k_0 \ell \left(1 - \frac{b_1 (k_0 \ell)^4}{(k_0 \ell)^2 + (b_2 + i b_3)(k_0 \ell / 2)}\right)^{\frac{1}{2}} \qquad \text{(V-3)}$$

$$k_2 \ell = \pm i b_1^{-\frac{1}{2}} = \pm i \frac{\ell}{\delta} \qquad \text{(V-4)}$$

These are the four required wave numbers for Equation III-14 when filament stiffness can be considered small (small b_1).

The first wave number, k_1 , is a correction of k_0. The correction is obviously related to the magnitude of b_1 (filament stiffness) and is zero when b_1 is zero. It can be considered an increase in the " system wave length " (or a " stiffening " of the system) since, by definition, a decrease in wave number represents an increase in wave length. This is a minor correction, however, since k_1 is only slightly decreased from k_0.

The second wave number, k_2, is more interesting since it represents an additional exponential displacement of the filament, with which it is possible to correct the k_0 solution for boundary conditions of slope. The magnitude of k_2 is the reciprocal of δ, mentioned earlier as the boundary region length. Thus the amplitude of the stiffness correction varies directly with the size of the boundary region. As mentioned, this concept is fully discussed in Section V-C.

The k_0 solution will be carried through to completion, however, because the model for this solution represents the majority of moving flexible filament situations. The boundary conditions for slope at $x/\ell = 0$ and $x/\ell = 1$ are ignored, since filament stiffness is neglected. The procedure for

this is as follows:

First, solve for the boundary conditions (Equations V-1) with $r_o^* = 0$. An example of these boundary conditions would be the yarn winding machinery depicted in Figure 5. Here the yarn enters through a field guide at the left ($x = 0$), then moves through a traversing mechanism at the right ($x = \ell$). The displacements in this figure are exagerated to illustrate typical deviations from straight line flow. The solution is undertaken by separating the complex exponential representation of η into two functions, one representing the usual spacial mode (or a wave function traveling relative to the filament at velocity, -v) and the other considered as a correction function to make the product of the two a solution of the differential equation.

Let:
$$\frac{\eta}{\ell} = \left\{ c_1 e^{i(\omega_o t - \frac{b_2}{2}\frac{x}{\ell})} + c_2 e^{-i(\omega_o t - \frac{b_2}{2}\frac{x}{\ell})} \right\} \left\{ e^{(i\frac{R\cos\theta_R}{2} - \frac{R\sin\theta_R}{2})\frac{x}{\ell}} - e^{-(i\frac{R\cos\theta_R}{2} - \frac{R\sin\theta_R}{2})\frac{x}{\ell}} \right\} \left\{ e^{\frac{b_3}{2}\frac{x}{\ell}} \right\} \qquad (V\text{-}5)$$

This function fits the boundary condition at $\frac{x}{\ell} = 0$ (or $s=-vt$) namely $\frac{\eta}{\ell}(0,t) = 0$. In order that it fit the boundary condition at $\frac{x}{\ell} = 1$ (or $s= \ell -vt$) let:

$$c_1 = \frac{-c_3 i}{2} e^{i\frac{b_2}{2}}, \qquad c_2 = \frac{c_3 i}{2} e^{-i\frac{b_2}{2}}$$

where
$$c_3 = \frac{r_o}{\ell} e^{-\frac{b_3}{2}} c_4$$

Equation V-5 can now be more simply expressed:

$$\frac{\eta}{\ell} = g(x) \left\{ \frac{r_o}{\ell} \sin(\omega_o t - b_{11}(1 - \frac{x}{\ell})) \right\} \left\{ e^{\frac{b_3}{2}(\frac{x}{\ell} - 1)} \right\} \qquad (V\text{-}6)$$

(Note: The amplitude function, $g(x)$, is found by taking the

real part of the product of c_4 and the amplitude function of Equation V-5.)

where $$g(x) = \frac{\sin b_{15} x/\ell \sin b_{15} \cosh b_{16} x/\ell \cosh b_{16}}{\sin^2 b_{15} \cosh^2 b_{16} + \cos^2 b_{15} \sinh^2 b_{16}}$$

$$+ \frac{\cos b_{15} x/\ell \cos b_{15} \sinh b_{16} x/\ell \sinh b_{16}}{\sin^2 b_{15} \cosh^2 b_{16} + \cos^2 b_{15} \sinh^2 b_{16}}$$

$$b_{15} = R\frac{\cos\theta_R}{2}, \qquad b_{16} = R\frac{\sin\theta_R}{2}, \qquad b_{17} = \frac{-b_2}{2}$$

For $b_3 = b_5 = 0$ (zero air drag) the solution reduces to:

$$\frac{y}{\ell} = \frac{r_0}{\ell} \frac{\sin b_{18} x/\ell}{\sin b_{18}} \sin(\omega_0 t - b_{17}(1 - \frac{x}{\ell})), \quad b_{18} = \frac{\omega_0 \ell/c}{1 - v^2/c^2} \qquad (V\text{-}7)$$

Equation V-7 has been published previously by Sack (19).

It is easier to understand this solution by rewriting b_{17} and b_{18} in terms of the natural frequency of the system, Ω. This concept was discussed by Skutsch (28), however its derivation is included here for sake of completeness. It is written as:

$$\Omega = \frac{\pi c}{\ell}(1 - \frac{v^2}{c^2}). \qquad (V\text{-}8)$$

Physically, Ω can be interpreted as follows. Consider the case of a flexible filament moving through two fixed guides a distance ℓ apart. If a positive lateral disturbance is initiated midpoint between the guides it will propagate in both directions. The disturbance will then be reflected at the guides and return towards the midpoint but with negative sense. It will pass through the midpoint and be reflected at the opposite guides and again return to the midpoint, but this time with the initial positive sense. This is seen in

the following figure where only the initially upstream wave is considered.

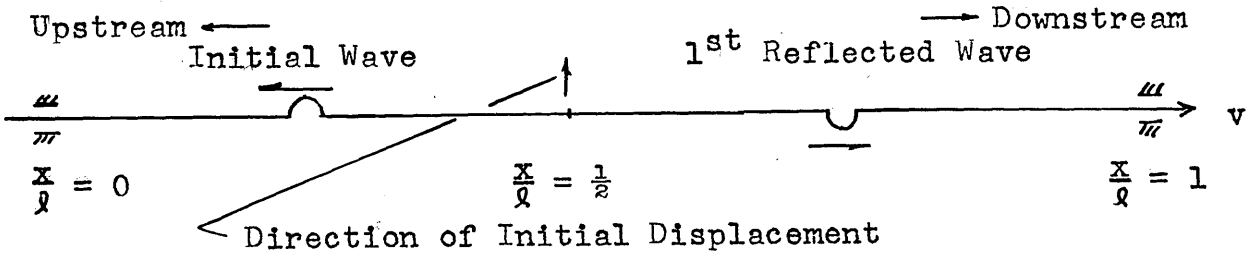

$$\text{From } \frac{x}{\ell} = \tfrac{1}{2} \rightarrow 0, \qquad \Delta t = \frac{\ell/2}{c-v}$$

$$\text{From } \frac{x}{\ell} = 0 \rightarrow 1, \qquad \Delta t = \frac{\ell}{c+v}$$

$$\text{From } \frac{x}{\ell} = 1 \rightarrow \tfrac{1}{2}, \qquad \Delta t = \frac{\ell/2}{c-v}$$

$$\therefore \Delta t_T = \frac{\ell}{c-v} + \frac{\ell}{c+v} = \frac{2\ell c}{c^2-v^2}$$

$$\Omega = 2\pi f = 2\pi \frac{1}{\Delta t_T} = \frac{\pi c}{\ell}\left(1 - \frac{v^2}{c^2}\right)$$

The important point to be noticed here is that the natural frequency of the system decreases as $v \rightarrow c$. This is obviously caused by the increase in the time required for disturbances to be propagated upstream.

Introducing $b_{19} = 2\frac{\omega_0}{\Omega}$ it is possible to simplify b_{17} and b_{18} of Equations V-6 and V-7.

$$b_{17} = \frac{\pi}{2} b_1 b_{19}, \qquad b_{18} = b_{19}\frac{\pi}{2}$$

The equation for $\frac{\eta}{\ell}$ can now be rewritten:

$$\frac{\eta}{\ell} = \frac{r_0}{\ell} \frac{\sin b_{16}\frac{\pi x}{2\ell}}{\sin b_{16}\frac{\pi}{2}} \sin(\omega_0 t - b_{17}(1 - \frac{x}{\ell})) \qquad \text{(V-9)}$$

The first term represents the amplitude or limiting shape of the mode. The second term is the time variation

containing a correction for the phase at different x. This phase correction will be discussed when three-dimensional shapes are considered because b_{17} is actually the angle in the y-z plane through which the filament path rotates from $\frac{x}{\ell} = 0$ to $\frac{x}{\ell} = 1$. The time variation is such that at each $\frac{x}{\ell}$ between $\frac{x}{\ell} = 0$ and $\frac{x}{\ell} = 1$, the point through which the filament passes, oscillates laterally at frequency, ω_o. For b_{19} equal to odd integral values, the amplitude function is a minimum and the shape becomes b_{19} quarter sine waves with an amplitude of h_o. This is shown in Figure 6, where h_o is introduced as the maximum amplitude of lateral displacement, which for this case is $h_o = r_o$.

If the value of b_{19} is not an odd integer, the magnitude of h_o increases from its minimum value, r_o. This is shown in Figure 7, a typical resonance diagram. For zero air drag ($b_3 = b_5 = 0$) the predicted amplitudes can become very large. This is, however, a result of the assumption of linearity. Figure 7 is more realistic when the energy loss caused by air drag is considered ($b_3 \neq 0$, $b_5 \neq 0$). Under these conditions the maximum amplitude of the system, h_o, is considerably reduced.

The final correction to the k_o solution for $b_3 = b_5 = 0$, relates to the exponential amplitude. Since positive values of b_3 mean an air flow of positive velocity (toward increasing $\frac{x}{\ell}$) this correction is seen to be a decrease in the amplitude of oscillation at each $\frac{x}{\ell}$. The magnitude of this correction decreases for increasing $\frac{x}{\ell}$, until for $\frac{x}{\ell} = 1$, there is no correction.

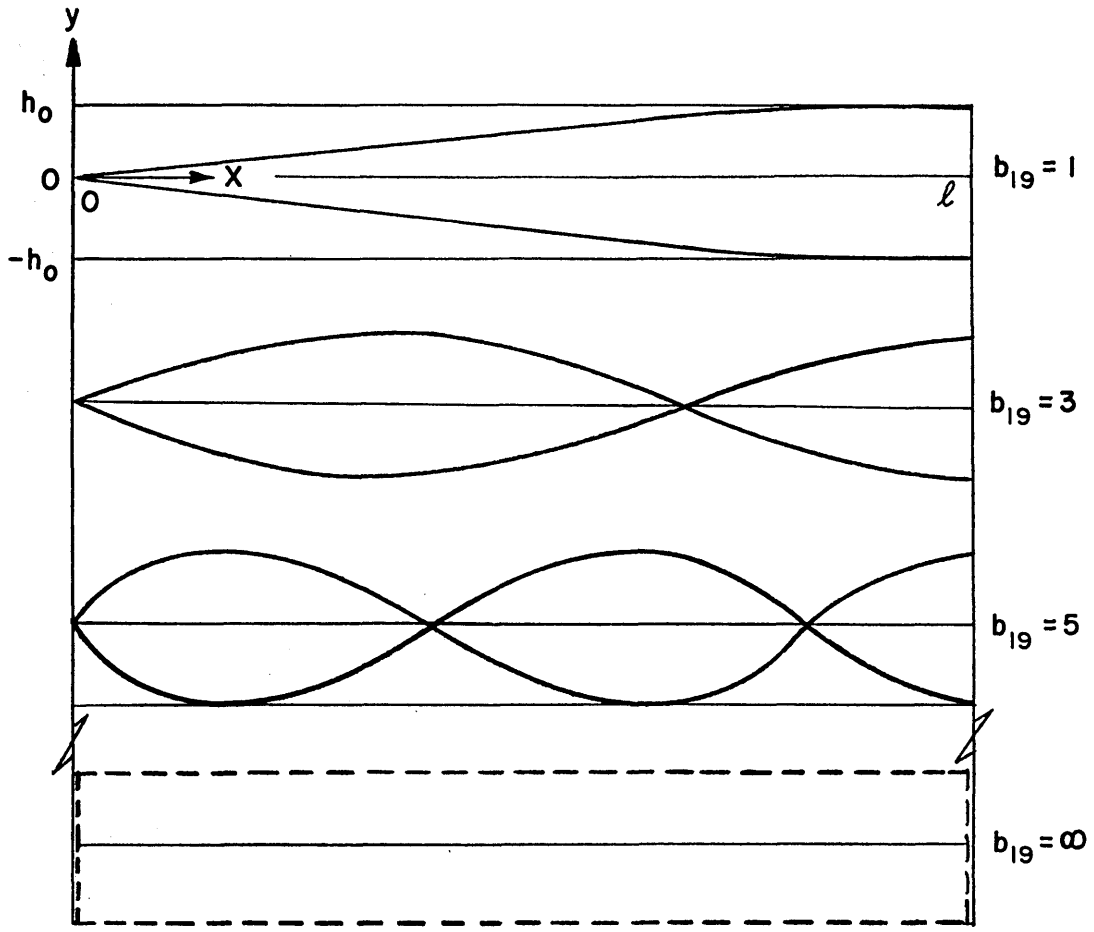

FIG. 6

AMPLITUDE FUNCTION vs X, $b_3 = b_5 = 0$

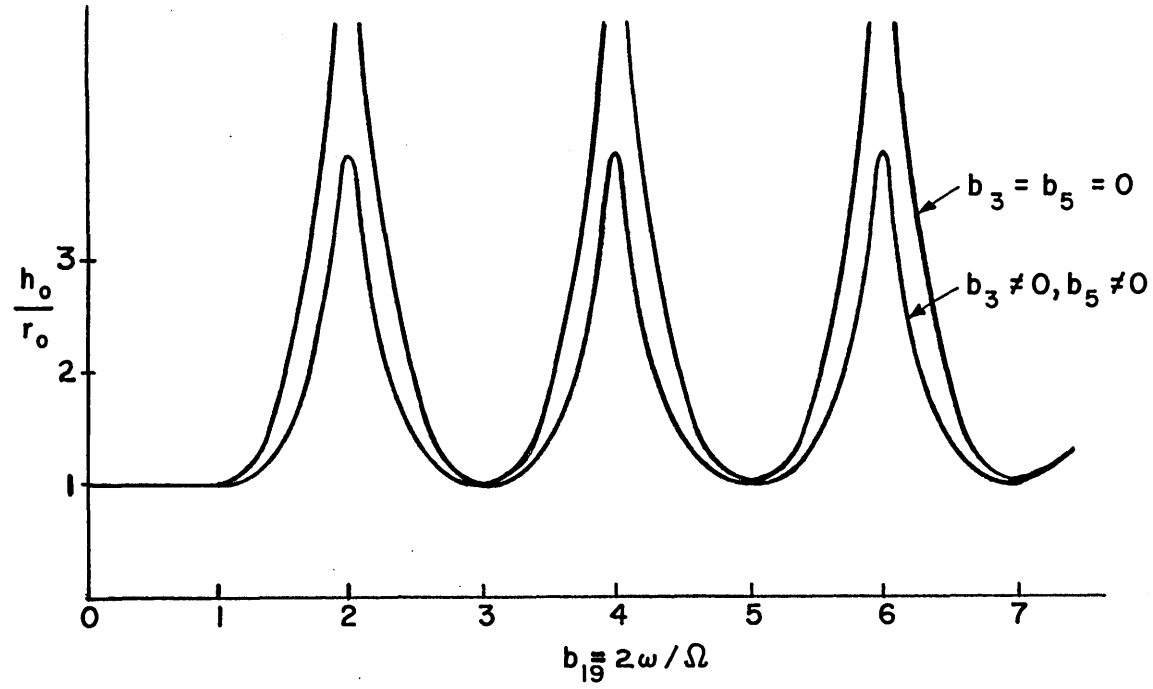

FIG. 7

AMPLITUDE FUNCTION vs b_{19}, MAXIMUM VALUE

For $r_o^* \neq 0$, the boundary conditions include harmonic oscillation at $\frac{x}{\ell} = 0$, of frequency, ω_o^*, and phase angle, ϕ. The solution for $\frac{\eta}{\ell}$ now becomes:

$$\frac{\eta}{\ell} = g(\tfrac{x}{\ell}) \left\{ \frac{r_o}{\ell} \sin(\omega_o t - b_{17}(1 - \tfrac{x}{\ell})) \right\} \left\{ e^{\frac{b_3}{2}(\frac{x}{\ell} - 1)} \right\} + g^*(1 - \tfrac{x}{\ell}) \left\{ \frac{r_o^*}{\ell} \sin(\omega_o^* t + \phi + b_{17}^* \tfrac{x}{\ell}) \right\} \left\{ e^{\frac{b_3^*}{2} \frac{x}{\ell}} \right\} \quad \text{(V-10)}$$

A simple illustration of the above boundary conditions would be a flexible filament which moves at velocity, v, between two guides which move harmonically and are in phase. This represents the type of oscillatory input that a vibrating machine gives to a flexible filament as the filament moves through guides attached to the machine. To simplify the interpretation, let $b_3 = b_5 = 0$, $r_o = r_o^* = 1$, and $\omega_o = \omega_o^*$. Equation V-10 becomes:

$$\frac{\eta}{\ell} = \frac{\sin(\omega_o t - b_{17}(1 - \tfrac{x}{\ell}))\sin b_{19}\frac{\pi x}{2\ell} + \sin(\omega_o t + \phi + b_{17}\tfrac{x}{\ell})\sin(b_{19}\frac{\pi}{2}(1 - \tfrac{x}{\ell}))}{\sin b_{19}\frac{\pi}{2}} \quad \text{(V-11)}$$

For $\phi = 0$, an oscillatory translation of the machine is represented, while for $\phi = 180^\circ$, an oscillatory rotation of the machine is represented. The two plots in Figure 8 show the upper half of the amplitude envelope of the space curves (Equation V-11) for $\phi = 0$ and $\phi = 180^\circ$, and for three odd integral values of b_{19}. Again it is mentioned that odd integral values of b_{19} yield minimum filament amplitude, while for b_{19} equal to even integers, maximum amplitude occurs, limited by air drag (and energy loss in the filament itself).

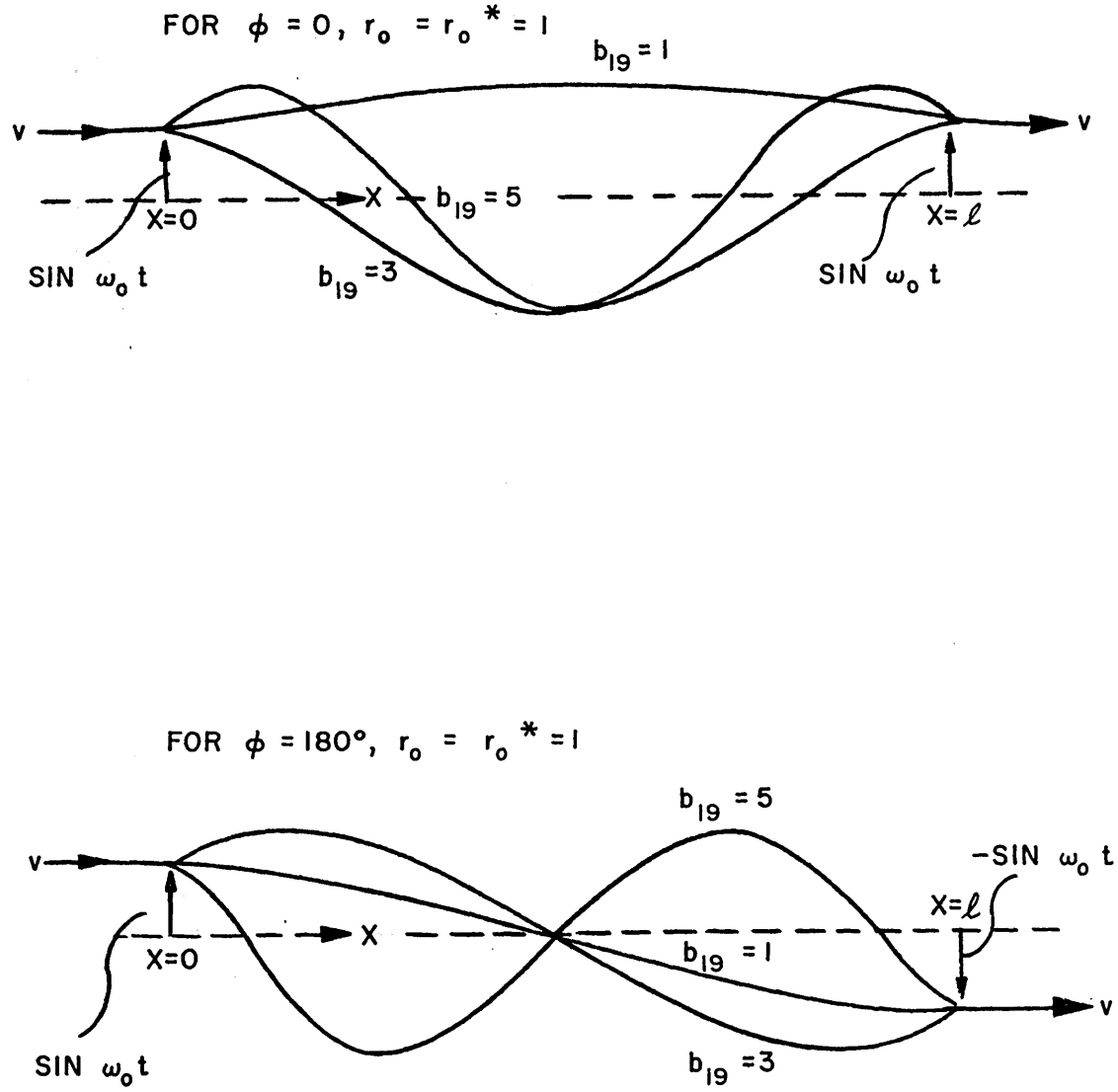

FIG. 8
TYPICAL MACHINE OSCILLATIONS

The linear solution of this thesis is for constant filament tension. The tension is not constant, however, but is a function of filament shape. The first order change in tension can be found by considering the constant tension solution as being approximately correct and calculating the variation in tension necessary to satisfy conservation of momentum. This can be done as follows:

From conservation of momentum in the $\vec{i}$-direction:

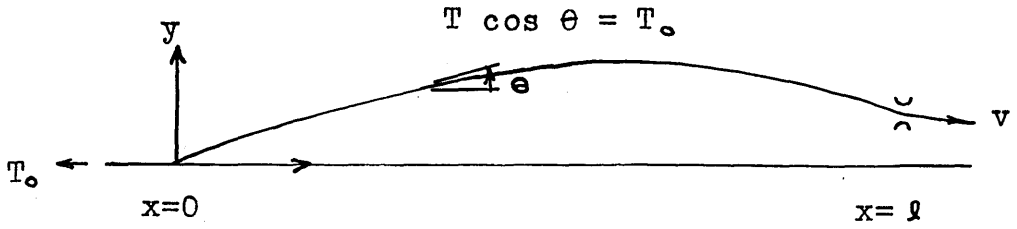

if guide friction and $\rho_f A \frac{\partial^2 \eta}{\partial t^2}$ are neglected.

By letting $T_{max} = T_o + \Delta T$, then for small θ,

$$\frac{\Delta T}{T_o} = \frac{\theta^2_{max}}{2} \qquad \text{(V-12)}$$

Since it is also true that for small θ , $\theta = \partial\eta/\partial x$, then it is possible to differentiate the expression for η (for zero air drag) and solve for $\Delta T/T_o$. This yields:

$$\left(\frac{\partial \eta}{\partial x}\right)_{max} = \frac{\omega_o r_o}{c\left(1 - \frac{v^2}{c^2}\right)\left(\sin b_{19}\frac{\pi}{2}\right)} = \theta_{max}$$

Substituting this expression into Equation V-12 gives:

$$\frac{\Delta T}{T_o} = \frac{1}{2}\left\{\frac{\omega_o r_o}{c\left(1 - \frac{v^2}{c^2}\right)\left(\sin b_{19}\frac{\pi}{2}\right)}\right\}^2 \quad \text{(a)} \qquad \text{(V-13)}$$

i.e.

$$\frac{\Delta T}{A} = \frac{1}{2}\rho_f\left\{\frac{\omega_o r_o}{\left(1 - \frac{v^2}{c^2}\right)\left(\sin b_{19}\frac{\pi}{2}\right)}\right\}^2 \quad \text{(b)}$$

Equation V-13a is of practical importance since it allows the increase in tension to be predicted as a function of the system design variables. It also serves to estimate how good the constant tension assumption is. If the parameter b_{20} is introduced into Equation V-13a, where b_{20} is defined as;

$$b_{20} = \frac{\Delta T}{T_0} = \frac{1}{2}\left(\frac{r_0}{\ell}\right)^2 \left(\frac{b_2}{2b_7 \sin b_{19}\frac{\pi}{2}}\right)^2$$

then it is possible to estimate the limit of the linear solution, since for $b_{20} \ll 1$, the solution is correct.

Considering again the wave number equation, Equation III-14, a second approximate solution can be obtained. This solution refers to filaments with large bending stiffness, but with small Coriolis' and longitudinal air velocity effects (small b_2 and b_3). This second solution is outlined as follows.

Note: In fluid mechanics, pressure rises or pressure drops are expressed as functions of the free stream stagnation pressure, $p_0 = "\frac{\rho V_\infty^2}{2}"$. An analogy can be made between this concept and the parameters of Equation V-13b. In this equation the filament stress, $\frac{\Delta T}{A}$, is analogous to the stagnation pressure p_0; the filament density is analogous to the fluid density; and the corrected maximum lateral velocity $\omega_0 r_0 / (1 - \frac{V^2}{c^2})(\sin b_{19}\frac{\pi}{2})$ is analogous to the free stream velocity, V_∞. Analogies such as this are helpful in appreciating the physical significance of filament parameters.

Let k_3 be a root of the wave number equation (Equation III-14) for $b_2 = b_3 = 0$.

Therefore: $$b_1 (k_3\ell)^4 + (k_3\ell)^2 + (b_4 + ib_5) = 0 \qquad \text{(V-14)}$$

$$k_3\ell = \pm \left\{ \frac{1}{2b_1} \right\}^{\frac{1}{2}} \left\{ \pm (1 - 4b_1 (b_4 + ib_5))^{\frac{1}{2}} - 1 \right\}^{\frac{1}{2}}$$

Now let there be one solution of the form:

$$k_4\ell = k_3\ell (1 + \delta_3), \quad \text{where} \quad \delta_3 \ll 1$$

Substitution into Equation III-14 yields:

$$k_4\ell = k_3\ell \left\{ 1 - \frac{(b_2 + ib_3) k_3\ell}{4b_1 (k_3\ell)^4 + 2(k_3\ell)^2} \right\} \qquad \text{(V-15)}$$

These four wave numbers are those required for Equation III-14 for small b_2 and b_3. They can be written in a more convenient notation as:

$$k_4\ell = \pm k_5\ell, \quad \pm k_6\ell$$

Where k_5 refers to Equation V-15, with $k_3\ell$ chosen to have the positive sign under the radical and where k_6 refers to Equation V-15 with $k_3\ell$ chosen to have the negative sign under the radical.

Using these four wave numbers, $\pm k_5$ and $\pm k_6$, a solution can be found which satisfies the boundary conditions of Equations V-1. These conditions (for $r_o^* = \theta_o^* = 0$) are:

$$\frac{\eta}{\ell}(1,t) = \frac{r_o}{\ell} \sin \omega_o t, \quad \frac{\partial \eta}{\partial x}(\ell,t) = \theta_o \cos \omega_o t$$

$$\frac{\eta}{\ell}(0,t) = \frac{\partial \eta}{\partial x}(0,t) = 0$$

The solution is:

$$\frac{\eta}{\ell} = \frac{r_o}{\ell}\eta_1\left(\frac{x}{\ell}\right)\sin\omega_o t + \theta_o \eta_2'\left(\frac{x}{\ell}\right)\cos\omega_o t \qquad \text{(V-16)}$$

where

$$\eta_1\left(\frac{x}{\ell}\right) = \mathrm{Re}\left\{\frac{(-k_5\sin k_5\ell + k_6\sin k_6\ell)(\sin k_5\ell\frac{x}{\ell} - \frac{k_5}{k_6}\sin k_6\ell\frac{x}{\ell})}{D_\epsilon} + \frac{(-k_5\cos k_5\ell + k_5\cos k_6\ell)(\cos k_5\ell\frac{x}{\ell} - \cos k_6\ell\frac{x}{\ell})}{D_\epsilon}\right\}$$

$$\eta_2'\left(\frac{x}{\ell}\right) = \frac{1}{\ell}\mathrm{Re}\left\{\frac{(-\cos k_5\ell + \cos k_6\ell)(\sin k_5\ell\frac{x}{\ell} - \frac{k_5}{k_6}\sin k_6\ell\frac{x}{\ell})}{D_\epsilon} + \frac{(\sin k_5\ell - \frac{k_5}{k_6}\sin k_6\ell)(\cos k_5\ell\frac{x}{\ell} - \cos k_6\ell\frac{x}{\ell})}{D_\epsilon}\right\} \qquad \text{(V-17)}$$

$$D_\epsilon = -2k_5 + 2k_5(\cos k_5\ell\cos k_6\ell) + \frac{k_5^2 + k_6^2}{k_6}(\sin k_5\ell\sin k_6\ell)$$

The functions $\eta_1\left(\frac{x}{\ell}\right)$ and $\eta_2'\left(\frac{x}{\ell}\right)$ require excessive algebraic manipulation to be written in any other form. However, Equations V-16 and V-17 are a complete answer and can be simplified for cases where some of the parameters are zero. For example, let $b_2 = b_3 = b_5 = 0$ (i.e. negligible air drag and Coriolis' acceleration), then Equation V-15 is reduced to:

$$k_4\ell = k_3\ell = \pm\left\{\frac{1}{2b_1}\right\}^{\frac{1}{2}}\left\{\pm(1-4b_1b_4)^{\frac{1}{2}} - 1\right\}^{\frac{1}{2}} \qquad \text{(V-18)}$$

For small b_1 :

$$k_4\ell = \pm(-b_4)^{\frac{1}{2}}, \quad \pm i(b_4)^{\frac{1}{2}}$$

This solution is the same as the $k_{1,2}$ solution for $b_2 = b_3 = b_5 = 0$ and will not be discussed further.

For large b_1 :

$$k_4\ell = \pm\left(\frac{b_4}{b_1}\right)^{\frac{1}{4}}, \quad \pm i\left(\frac{b_4}{b_1}\right)^{\frac{1}{4}}$$

Therefore, $k_5 \ell = (\frac{b_4}{b_1})^{\frac{1}{4}}$ and $k_6 \ell = ik_5 \ell$ are the wave numbers to be used in Equation V-17 to determine the amplitude of the forced response predicted by Equation V-16. This forced response of filaments of large bending stiffness (with respect to beams) is a well known phenomenon and will not be treated further.

This second approximate solution to Equation III-14 can be used to obtain an equation to predict the natural frequency of a moving filament, Ω_n. This is done as follows for boundary conditions of zero slope and zero displacement at the guides. These conditions are:

$$\frac{\eta}{\ell}(0,t) = \frac{\eta'}{\ell}(0,t) = \frac{\eta}{\ell}(1,t) = \frac{\eta'}{\ell}(1,t)$$

The original form of η was chosen as:

$$\frac{\eta}{\eta_0} = e^{\pm i(\omega_0 t + kx)}$$

Equation V-15, with $b_2 = b_3 = b_5 = 0$, is:

$$k_4 \ell = \pm \left\{\frac{1}{2b_1}\right\}^{\frac{1}{2}} \left\{\pm(1-4b_1 b_4)^{\frac{1}{2}} - 1\right\}^{\frac{1}{2}}$$

$$k_4 \ell = \pm k_5 \ell, \quad \pm k_6 \ell$$

Therefore η can be expressed as:

$$\frac{\eta}{\eta_0} = \cos \omega_0 t \left\{c_1 \sin k_5 x + c_2 \cos k_5 x + c_3 \sin k_6 x + c_4 \cos k_6 x\right\}$$

To fit the above boundary conditions the following equation must be satisfied. (or $D_6 = 0$).

$$\cos k_5 \ell \cosh k_5 \ell \gamma_\epsilon + \tfrac{1}{2}(\frac{1}{\gamma_\epsilon} - \gamma_\epsilon) \sin k_5 \ell \sinh k_5 \ell \gamma_\epsilon = 1 \quad \text{(V-19)}$$

where $$\chi_\epsilon = \left\{ 1 + \frac{1}{b_1 k_5^2 \ell^2} \right\}^{\frac{1}{2}}$$

The roots of this equation can be assigned the values:

$$k_5\ell)_n = k_5\ell)_1 , k_5\ell)_2 , k_5\ell)_3 \ldots$$

Specific values of $k_5\ell)_n$ have not been calculated for this example, although it is possible to define their range on the basis of known solutions to Equation V-19. For example, for a filament with zero longitudinal velocity (v = 0) and under zero tension (c = 0) the value of parameter b_1 becomes infinite. Therefore, χ_ϵ, becomes equal to one and Equation V-19 becomes:

$$\cos k_5\ell \cosh k_5\ell = 1$$

The roots of this equation are well known and are given by Lord Rayleigh (5). They are:

$$k_5\ell)_1 = 4.730$$
$$k_5\ell)_2 = 7.853$$
$$k_5\ell)_3 = 10.996$$
$$k_5\ell)_4 = 14.137$$
$$k_5\ell)_n \doteq (\frac{2n+1}{2})\pi$$

For a filament with zero bending stiffness the value of parameter b_1 becomes zero. Therefore, χ_ϵ becomes infinite and Equation V-19 becomes:

$$\sin k_5\ell = 0, \quad \therefore k_5\ell)_n = n\pi$$

These roots illustrate the effect of filament stiffness

on $k\ell$. The effect of filament motion on $k\ell$ can be estimated by referring back to the k_o solution. These two effects, filament stiffness and filament motion can be combined in an equation which provides an estimation of the natural frequency of a moving filament, neglecting air drag. This is done as follows:

Equation III-14 for zero air drag becomes:

$$b_1 (k\ell)^4 + (k\ell)^2 + b_2 (k\ell) + b_4 = 0 \qquad \text{(V-20)}$$

Rewritten in terms of the natural frequency, Ω_n, this equation is:

$$\Omega_n = k\ell \frac{c}{\ell} \left\{ (1+b_1 (k\ell)^2 - b_7^2 \, b_1 (k\ell)^2)^{\frac{1}{2}} - b_7 \right\} \qquad \text{(V-21)}$$

The natural frequency of the k_o solution (for zero air drag), Ω, can now be equated with Equation V-21 with $b_1 = 0$.

$$\Omega = \frac{\pi c}{\ell}(1-b_7^2) = k\ell \frac{c}{\ell}(1-b_7)$$

This gives the initial value of $k\ell$ for the k_o solution as:

$$k\ell)_{k_o \text{ sol.}} = \pi(1+b_7)$$

Therefore, the correction to $k\ell$ for filament velocity has the form, $1+b_7$. This correction is now made to Equation V-21, which becomes:

$$\Omega_n = k_5\ell \, \frac{c}{\ell} \left\{ 1+b_7 \right\} \left\{ (1+b_1 (k_5\ell)^2 (1+b_7)^2 (1-b_7^2))^{\frac{1}{2}} - b_7 \right\} \qquad \text{(V-22)}$$

where the values of $k_5\ell$ are calculated from Equation V-19.

Equation V-22 is, therefore, taken to be correct for

values of b_1 and b_{-1} which are not necessarily small with respect to one. In a later section, Section V-C, a boundary region is discussed for moving filaments where b_1 is taken to be small and a much simpler approach is used.

The equations developed thus far are for two-dimensions only. It is possible, however, to use the principle of superposition and develop three-dimensional equations. This is done in the next part of this section.

B. . Three Dimensions

The majority of moving filament situations involve boundary conditions in three dimensions. Examples are the spinning balloon or the overend unwinding balloon which are typical textile systems. Of these, the most common are produced by boundary conditions of forced circular motion in the y-z plane. An example would be the package of yarn shown in Figure 9, from which yarn is being withdrawn " overend ". The boundary conditions for circular y-z motion are given ($r_o^* = \theta_o^* = 0$) as:

$$\frac{\eta}{\ell}(0,t) = \frac{\partial \eta}{\partial x}(0,t) = \frac{\varphi}{\ell}(0,t) = \frac{\partial \varphi}{\partial x}(0,t) = 0$$

$$\frac{\eta}{\ell}(1,t) = \frac{r_o}{\ell} \sin \omega_o t, \quad \frac{\partial \eta}{\partial x}(1,t) = \theta_o \cos \omega_o t \qquad \text{(V-23)}$$

$$\frac{\varphi}{\ell}(1,t) = \frac{r_o}{\ell} \cos \omega_o t, \quad \frac{\partial \varphi}{\partial x}(1,t) = -\theta_o \sin \omega_o t$$

where η and φ are displacements in the $\vec{i}$ and $\vec{j}$-directions. As seen in Figure 9 these conditions correspond to a circular filament path at $\frac{x}{\ell} = 1$ (the withdrawal point), of constant radius, r_o, and constant inclination angle, θ_o, revolving at angular frequency, ω_o.

As previously mentioned it is possible to use superposition in order to solve for the equations of motion for filaments subjected to three-dimensional boundary conditions. This is done as follows, by first writing the boundary conditions for $\frac{\varphi}{\ell}$ in terms of the boundary conditions for $\frac{\eta}{\ell}$.

$$\frac{\varphi}{\ell}(1,t) = \frac{r_o}{\ell} \cos \omega_o t = \frac{r_o}{\ell} \sin(\omega_o t + \pi/2) = \frac{\eta}{\ell}(1, t + \pi/2\omega_o)$$

$$\frac{\partial \varphi}{\partial x}(1,t) = -\theta_o \sin \omega_o t = \theta_o \cos(\omega_o t + \pi/2) = \frac{\partial \eta}{\partial x}(1, t + \pi/2\omega_o) \qquad \text{(V-24)}$$

OVER-END UNWINDING OF YARN PACKAGE

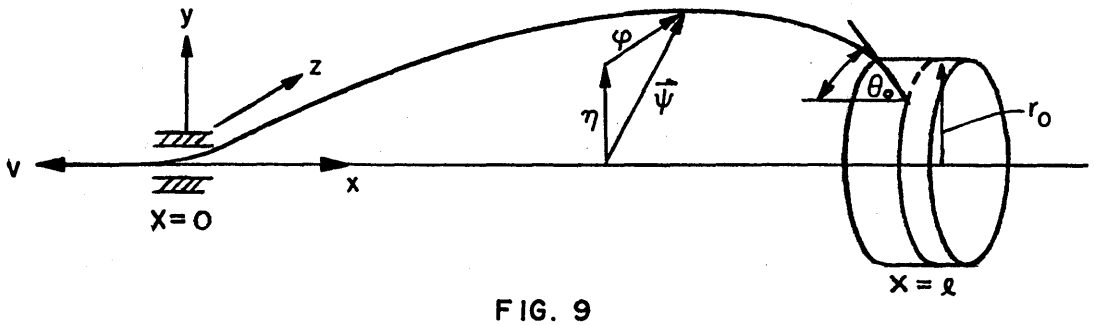

FIG. 9

EXAMPLE OF CIRCULAR Y-z BOUNDARY CONDITIONS

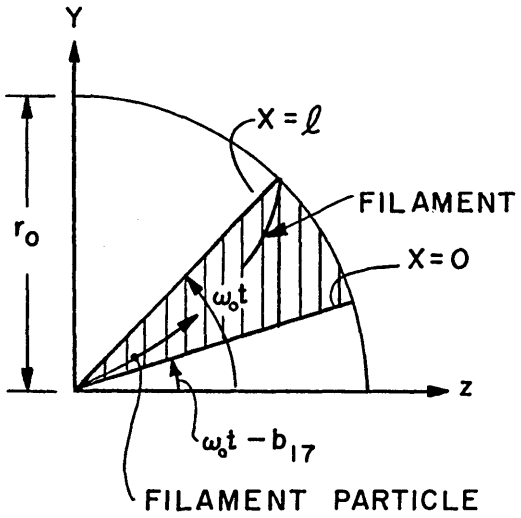

FIG. 10

FILAMENT ROTATION

Therefore, $\frac{\varphi}{\ell}(x,t) = \frac{\eta}{\ell}(x, t+ \pi/2\omega_o)$. This means that the three-dimensional solutions can be written directly in terms of the two-dimensional solutions, provided the time increment, $\pi/2\omega_o$, is properly considered. It must be pointed out that this is not a right hand coordinate system, being chosen to represent the more familiar counterclockwise rotation, at the loss of consistency.

The k_o solution for three-dimensions becomes:

$$\frac{\vec{\Psi}}{\ell} = \frac{r_o}{\ell}\, g(\tfrac{x}{\ell}) \left\{ \vec{j} \sin(\omega_o t - b_{17}(1 - \tfrac{x}{\ell})) + \vec{k} \cos(\omega_o t - b_{17}(1 - \tfrac{x}{\ell})) \right\} \left\{ e^{\frac{b_3}{2b_1}(\frac{x}{\ell} - 1)} \right\}$$

The central bracketed term in the above expression is a vector of unit length, at an angle, $\omega_o t - b_{17}(1 - \frac{x}{\ell})$, referred to the z-axis. $\frac{\vec{\Psi}}{\ell}$ can therefore be more simply expressed as:

$$\frac{\vec{\Psi}}{\ell} = \frac{r_o}{\ell}\, g(\tfrac{x}{\ell}) \left\{ \vec{u}_z (\omega_o t - b_{17}(1 - \tfrac{x}{\ell})) \right\} \left\{ e^{\frac{b_3}{2b_1}(\frac{x}{\ell} - 1)} \right\} \qquad \text{(V-25)}$$

The magnitude of this vector equals the amplitude of the sinusoidal time and space dependence for the two-dimensional case formulated in Equation V-6, and plotted in Figures 6 and 7. It is therefore not necessary to discuss this magnitude further. The argument of the unit vector, however, shows clearly the physics behind the phase angle, b_{17}. Figure 10 is a plot of Equation V-25, where the magnitude of $g(\frac{x}{\ell})$ and the magnitude of $\exp(\frac{b_3}{2b_1}(\frac{x}{\ell} - 1))$ are equal to one. The shaded region containing the filament " end view " projection is seen to rotate at angular velocity, ω_o. Within this shaded region the filament projection rotates about the x-axis through the angle, b_{17}. The projection is fixed relative to the shaded region.

For $b_3 = b_5 = 0$ (the case for zero air drag) the solution simplifies. In Figure 11 there are plotted two projections of the filament for several odd integral values of b_{19}(Relative Frequency Parameter = $2\frac{\omega_o}{\Omega}$). This has been done for two values of b_7("Mach Number"). The parameter b_{17} is clearly seen to be the amount of rotation about the x-axis of the filament at a given instant of time, between $x = 0$ and $x = \ell$. The dotted lines are the envelope of filament motion while the solid lines represent an actual space curve. Since the envelope of the end views are circles they are omitted for clarity. Also the side views in the bottom plots of Figures 11a and 11b are omitted since the end view is intended as that for all the curves given for b_{19} greater than a minimum value.

The rotation angle, b_{17}, has been measured by the author from Figures 2-11 of Reference 4. These figures represent the results of numerical integrations by Padfield of the non-linear differential equations of filament motion. Padfield's equations were not linearized as they have been in this thesis. Padfield's experimental data and photographs validify her numerical integrations. This same rotation angle, b_{17}, has also been calculated, by the author, from the definition of b_{17}, namely:

$$b_{17} = \frac{\pi}{2} b_7 b_{19},$$

where b_7 and b_{19} are calculated from Padfield's original data.

Figure 12 is a cross plot of b_{17} measured from Padfield's figures versus b_{17} as calculated by the above equation developed

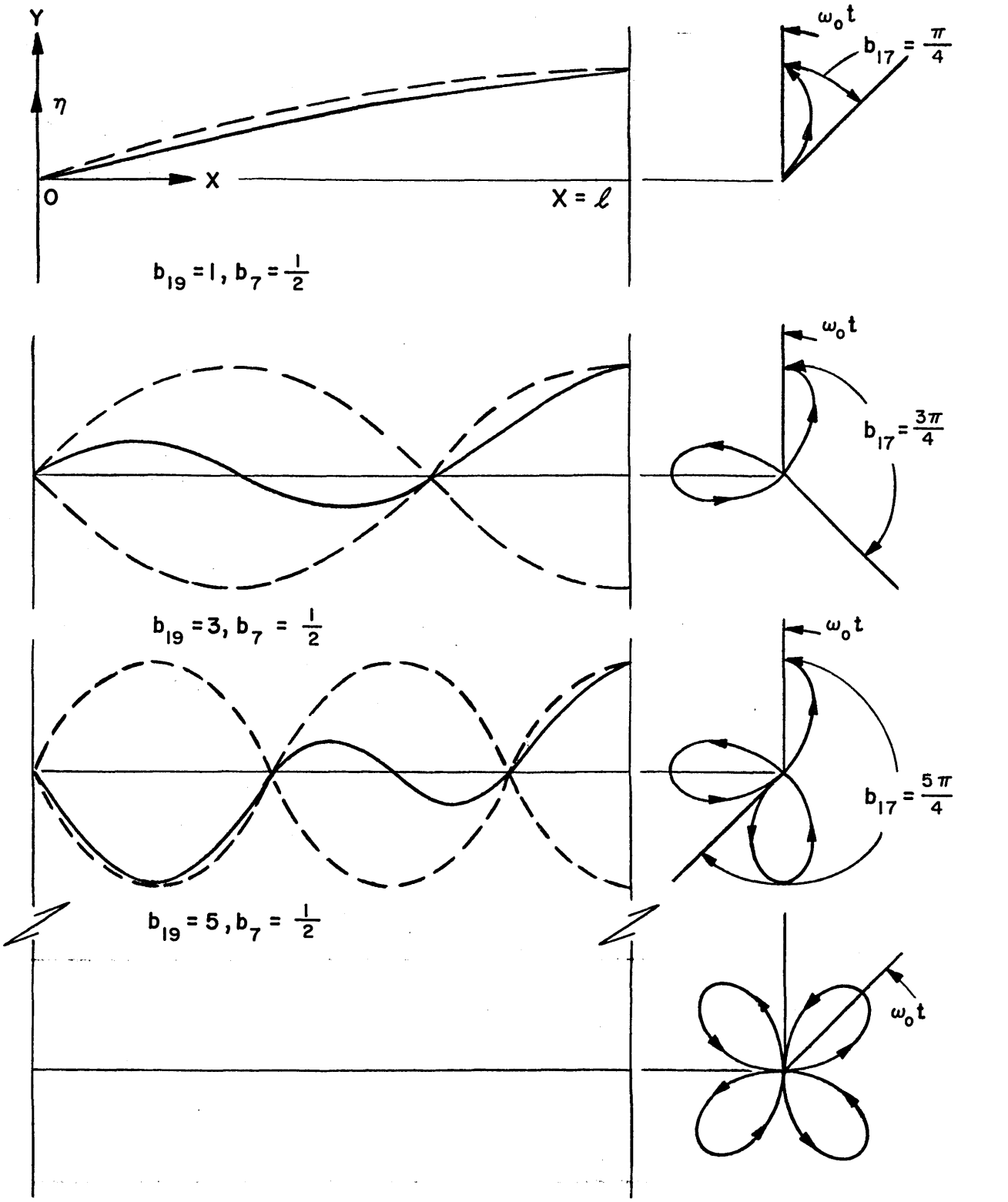

CONSTANT "MACH NUMBER", b_7

VARIABLE RELATIVE FREQUENCY, b_{19}

FIG. 11(a)

THREE DIMENSIONAL k_0 SOLUTION, $b_7 = \frac{1}{2}$

ZERO AIR DRAG & STIFFNESS, $b_1 = b_3 = b_5 = 0$

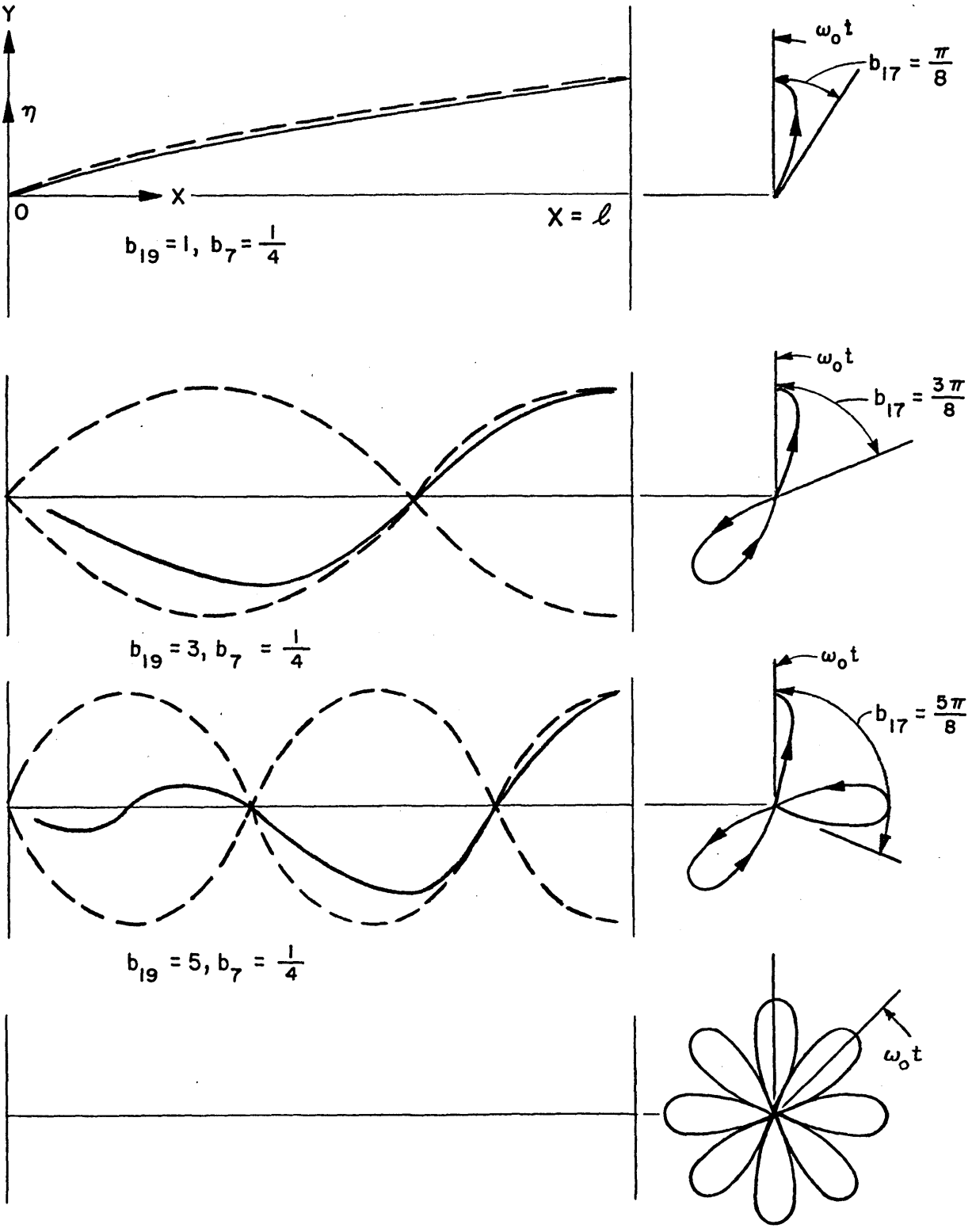

CONSTANT "MACH NUMBER", b_7

VARIABLE RELATIVE FREQUENCY, b_{19}

FIG. 11 (b)

THREE DIMENSIONAL k_0 SOLUTION, $b_7 = \frac{1}{4}$

ZERO AIR DRAG & STIFFNESS, $b_1 = b_3 = b_5 = 0$

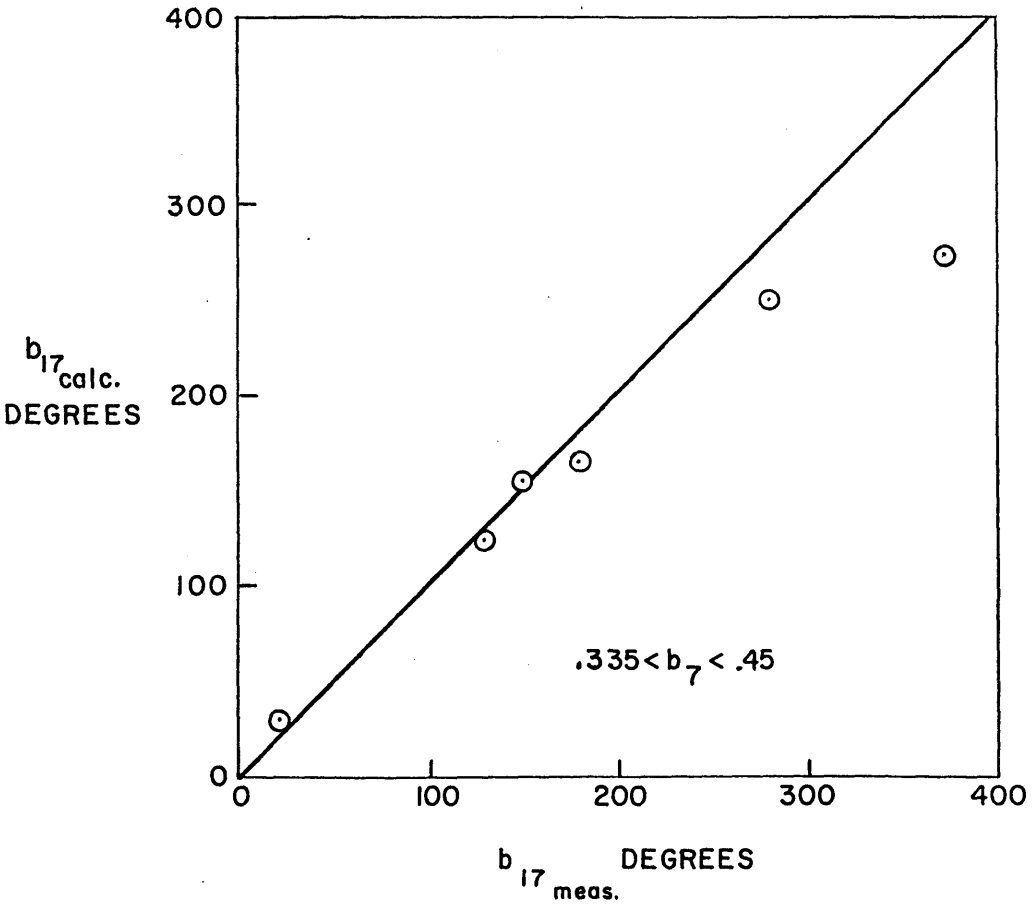

FIG. 12

FILAMENT ROTATION ANGLE

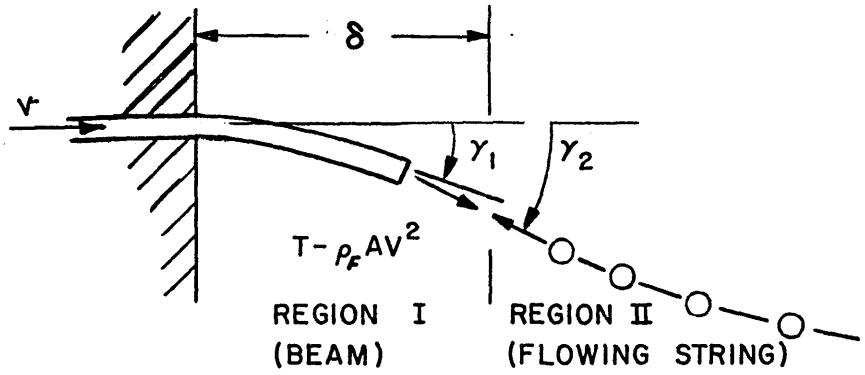

FIG. 13

BOUNDARY REGION

in this thesis, from Padfield's original data. The agreement is very good up to the point where the nonlinear air drag begins to cause a rotation of its own ($b_{17} > 200^o$), where it is seen that the " measured " b_{17} becomes much higher than the value calculated by the above equation. Thus the formulation of the parameter, b_{17}, is seen to have considerable validity over a wide range of practical situations.

For $\frac{r_o^*}{\ell} \neq 0$ the k_o solution becomes:

$$\frac{\vec{\Psi}}{\ell} = \frac{r_o}{\ell}\, g(\tfrac{x}{\ell}) \left\{ \vec{u}_R(\omega_o t - b_{17}(1-\tfrac{x}{\ell})) \right\} \left\{ e^{\frac{b_3}{2b_1}(\frac{x}{\ell}-1)} \right\} \qquad (V\text{-}26)$$
$$\frac{+r_o^*}{\ell}\, g(1-\tfrac{x}{\ell}) \left\{ \vec{u}_R(\omega_o t + \phi + b_{17}\tfrac{x}{\ell}) \right\} \left\{ e^{\frac{b_3}{2b_1}\frac{x}{\ell}} \right\}$$

Projections onto the x-y plane of the upper half of the amplitude envelope of this solution are the same as plotted for two dimensions in Figure 8. These curves illustrate the same ideas for three-dimensions as they did for two, namely that the shape is most significantly dependent on b_{19}, the ratio of input frequency to natural frequency. For further discussion of the three-dimensional k_o solution the reader is referred to Section V-D.

The second approximation of the solution of the wave number equation, Equation III-14, can also be extended to three-dimensions since $\frac{\varphi}{\ell}(x,t) = \frac{\eta}{\ell}(x, t + \pi/2\omega_o)$ as follows:

$$\begin{aligned}\frac{\vec{\Psi}}{\ell} &= \frac{\eta}{\ell}(\tfrac{x}{\ell},t)\vec{j} + \frac{\varphi}{\ell}(\tfrac{x}{\ell},t)\vec{k} \\ &= \frac{\eta}{\ell}(\tfrac{x}{\ell},t)\vec{j} + \frac{\eta}{\ell}(\tfrac{x}{\ell},t+\pi/2\omega_o)\vec{k} \qquad (V\text{-}27) \\ &= \frac{r_o}{\ell}\eta_1(\tfrac{x}{\ell})\vec{u}_R(\omega_o t) + \theta_o \eta_2'(\tfrac{x}{\ell})\vec{u}_R(\omega_o t)\end{aligned}$$

Where $\eta_1(\frac{x}{\ell})$ and $\eta_2'(\frac{x}{\ell})$ are given by Equation V-17.

This solution corresponds to the physical case of very stiff filaments, such as metal wire, metal cables, hose, metal tubing, etc., moving at moderate speeds. This case is not considered to be of interest within the context of textile processing but it is presented here because it is an approximate solution for three-dimensional filament motion which includes all the effects considered in the general vector equation, and because it fits the boundary conditions of Figure 9. These boundary conditions include the fact that the filament withdrawal angle, θ, is not zero but has the specific value, θ_o. The solution is not dealt with further because, as stated above, this thesis is primarily concerned with the motions of filaments that have only a small amount of bending stiffness. This concept can be investigated more easily by using the concept of a boundary region - to be discussed in the next section.

The above solution is applicable to an interesting problem known as the " garden hose problem " which considers the motion of a fluid moving with constant velocity through a stiff hose. The momentum flux of the fluid is analogous to the momentum flux of the filament; the stiffness of the hose analogous to the filament stiffness; and the axial stress caused by the fluid pressure and viscous drag, times the annular area of the hose cross-section, analogous to the filament tension. The results of this section can then be applied to this problem, once these analogies are made.

C. . Boundary Region

For filaments with low - but not negligible - stiffness (small b_1) it is possible to use the concept of a " boundary layer " or in this case, more specifically, a boundary region. This boundary region is defined as that portion of a moving filament near a system boundary for which the ratio of shear force to inertia force is large. Such a region exists because for fixed lateral oscillation frequency, ω_o, the inertia force near the boundary, which is proportional to the square of lateral displacement, becomes negligible. However, the boundary condition of fixed slope means a sudden increase in filament bending moment near the boundary and therefore large shear forces.

Thus the filament in Region I of Figure 13 behaves as a cantilever beam and can be described by the usual beam equations. Region II, on the other hand, is removed from the system boundaries and therefore, has large lateral displacement and inertial forces but small shear forces. It can be described by the equations for a moving flexible filament.

The hypothesis is made here that regions of high shear force within a moving flexible filament tend to exist near the boundaries only, in order that the elastic energy of the filament be a minimum. Therefore it is not considered possible to have more than two boundary regions as described above, each adjoining one of the two system boundaries.

These regions are shown in Figure 13 where δ is defined as the length of the boundary region and δ_1 and δ_2 refer respectively to the slopes of the beam and of the moving

flexible filament (or flowing string) at the edge of the boundary region. It is now possible to calculate δ from simple beam theory by assuming that the effective net tension, $T-\rho_f A v^2$, acts on the beam, and by matching beam displacement and, to a lesser degree, slope to that of the flexible filament, at the edge of the boundary region. This is done as follows.

From elementary beam theory:

$$\text{"}\frac{P\delta^2}{2EI}\text{"} = \frac{\delta^2(T-\rho_f A v^2)\sin\gamma_2}{2EI} = \gamma_1$$

Since for linear theory $\sin\gamma_2 \sim \gamma_2$,

$$\delta = \left(\frac{2\gamma_1}{\gamma_2}\right)^{\frac{1}{2}}\left(\frac{EI}{T-\rho_f A v^2}\right)^{\frac{1}{2}} = \left(\frac{2\gamma_1}{\gamma_2}\right)^{\frac{1}{2}}(b_1 \ell^2)^{\frac{1}{2}}$$

The boundary region length is now defined by the point where γ_1 is equal to one half of γ_2.

Therefore:
$$\frac{\delta}{\ell} = b_1^{\frac{1}{2}} \qquad \text{(V-28)}$$

Referring to the beginning of this section, the wave number $k_2\ell = \pm i b_1^{-\frac{1}{2}} = \pm i\,\frac{\ell}{\delta}$ clearly implies a correction to the k_o solution, near the boundaries, which varies exponentially with the number of the boundary region widths as:

$$\left(\frac{\eta}{\ell}\right)_{cor.} \sim e^{\pm\frac{x}{\delta}}$$

For systems where $\frac{\delta}{\ell}$ is small (small b_1) the suggestion is made that the parameters which describe the system (b_{17}, b_{19}, $\frac{h_o}{r_o}$) can be modified, from those predicted by the k_o solution, by changing the system length, ℓ, to a modified

system length, ℓ_ϵ, where:

$$\ell_\epsilon = \ell - 2\delta = \ell(1-2b_1^{\frac{1}{2}})$$

An estimate can now be made as to the change in the system natural frequency, Ω, by substituting ℓ_ϵ for ℓ.

$$\Omega' = \frac{\pi c}{\ell_\epsilon}\left(1-\frac{v^2}{c^2}\right) = \frac{\Omega}{1-2b_1^{\frac{1}{2}}} \qquad \text{(V-29)}$$

With this corrected system natural frequency, Ω', it is possible to estimate corrected values of b_{17} and b_{19}. These corrected values for b_{17} and b_{19} can then be used in the equations which describe filament motion. They are:

$$b_{17}' = b_{17}(1-2b_1^{\frac{1}{2}})$$
$$b_{19}' = b_{17}(1-2b_1^{\frac{1}{2}})$$

Therefore, the first order effect that stiffness has is to decrease the filament rotation angle and also to decrease the number of " balloons ".

The fundamental concept here is that the natural frequency of the system increases with the boundary region length. This is to be expected. However, the form of this increase caused by stiffness can be verified by comparing Equation V-29 with the filament velocity, v, taken as zero, to the more commonly known equation for the natural frequency of " slightly stiff " filaments, given by Lord Rayleigh (5) as:

$$f_1 = \frac{c}{2\ell}(1+2b_1^{\frac{1}{2}}) \qquad \text{(V-30)}$$

This equation has been rewritten in the nomenclature of this

thesis. f_1 is introduced as filament frequency expressed in cycles per unit time, rather than radians per unit time, as has been done previously.

Equation V-29 is also rewritten in terms of frequency expressed in cycles per unit time as:

$$f_2 = \frac{\Omega'}{2\pi} = \frac{c}{2\ell}\left(\frac{1}{1-2b_1\frac{1}{z}}\right) \qquad \text{(V-31)}$$

Figure 14 is a plot of f_1 and f_2 normalized with respect to the ratio $c/2\ell$ as functions of the boundary region length, δ, normalized with respect to the system length, ℓ. The agreement of the two plotted equations is within 4% at $\frac{\delta}{\ell} = 0.1$, which is considered adequate. Thus the physical conceptualization of a boundary region has been verified for the case when filament velocity is zero. It is also hypothesized as correct for the case when filament velocity is not zero. The simplicity of this concept and of its use is pointed out as its major merit.

Equation V-30 has been satisfactorily verified experimentally by Seebeck (5) for metal wires. For polymeric monofilaments, specifically nylon, a series of tests were conducted using the apparatus shown in Figure 15. This apparatus is discussed in Section IX. The natural frequency of the nylon specimins was measured as a function of b_1 and the experimental points are plotted in Figure 14 along with the theoretical curves. A single value for elastic modulus, E, was used in calculating the values of b_1 used in the data plotting. The one value of E was selected to give agreement between experiment and theory

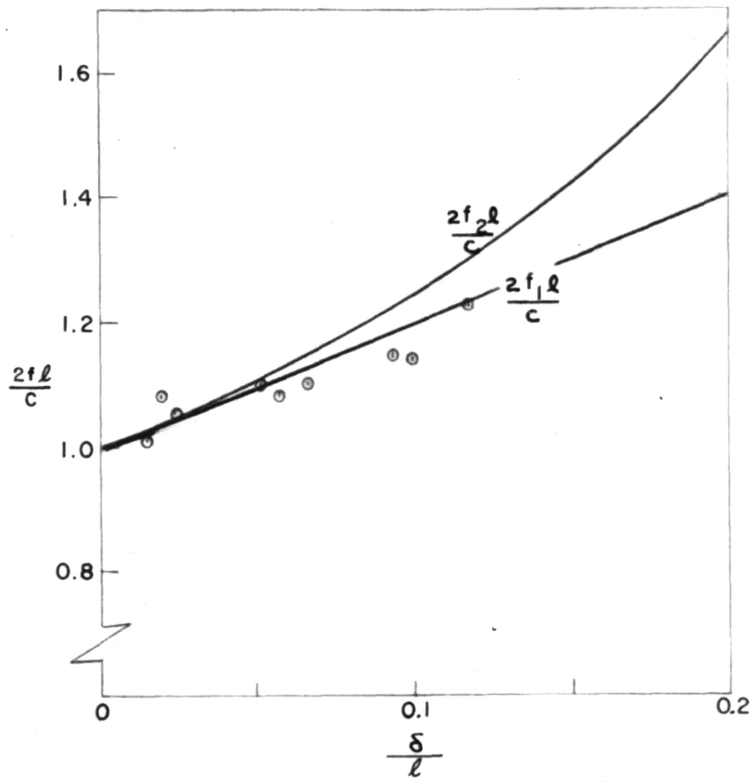

FIG. 14

COMPARISON OF BOUNDARY LAYER SOLUTION WITH CALCULATED AND WITH EXPERIMENTAL

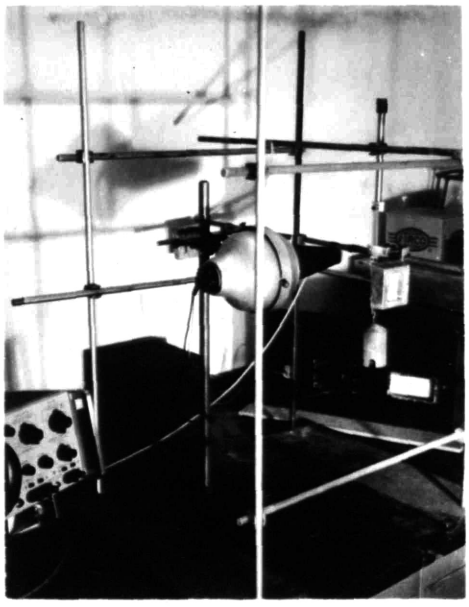

FIG. 15

FREQUENCY MEASUREMENT APPARATUS

at a single point. This indicates that despite the dependence of modulus, E, on load (which varied by a factor of 6), it is also possible to use a constant dynamic modulus in order to predict the frequency of a nylon monofilament. The particular dynamic modulus used was ~80% of the sonic modulus of the nylon, measured on a Pulse Propagation Meter.

Thus the concept of a boundary region seems adequate, not only as a qualitative concept, but also as a quantitative method (for small b_1) to obtain the first order effect that stiffness has on filament motion. Again the simplicity of this concept is emphasized. The first order effect of filament bending stiffness can be quickly estimated by calculating the boundary region length, $\delta = b_1^{\frac{1}{2}}\ell = (EI/T-\rho Av^2)^{\frac{1}{2}}$. The system length, ℓ, is then reduced by two boundary region lengths to $\ell_\epsilon = \ell - 2\delta = \ell(1-2b_1^{\frac{1}{2}})$. And this modified system length, ℓ_ϵ, is used in estimating filament rotation, b'_n, and the number of " balloons ", $b'_n/2$. These two parameters are then used in Equation V-9 to estimate the lateral amplitude of the filament space curve..

D. . Practical Example of an Unwinding Cone

In order to develop more fully the results of the preceding section, V. , we shall now examine the motion of an unwinding cone of yarn. This motion has been investigated experimentally on several prior occasions.(4, 7, 11, 17, 18, 21). Since the rotation of yarn about its axis has been well documented (Figure 12) this will not be discussed.

Referring to Figure 16a, we can express the eleven variables for this system as a minimum of eight dimensionless π groups; one dimensionless group expressed as a function of the other seven.

$$T/\rho_f A v^2 = f(r_o/\ell, \quad \delta_c/\ell, \quad \ell_c/\ell, \quad \psi_c, \quad \mu_c, \quad \theta_y, \quad \kappa_c) \qquad (V\text{-}32)$$

These variables are identified with the aid of Figure 16a. The cone geometry variables include r_o, the lesser cone radius; ℓ_c, the cone length; κ_c, the wind angle of the yarn on the cone; and ψ_c, the cone apex angle. The yarn variables include $\rho_f A$, the yarn mass per unit length; θ_y, the yarn twist; and μ_c, the coefficient of friction between the yarn and the cone surface. The system variables also include T, the yarn tension; v, the yarn withdrawal speed; ℓ, the system length; and δ_c, the longitudinal position on the cone surface of the yarn take off point.

For a given yarn; $\rho_f A$, θ_y and μ_c are constant. Therefore:

$$T/\rho_f A v^2 = f(r_o/\ell, \quad \delta_c/\ell, \quad \ell_c/\ell, \quad \psi_c, \quad \kappa_c) \qquad (V\text{-}33)$$

For a given yarn and a given cone: r_o, ℓ_c, ψ_c, $\rho_f A$, θ_y, κ_c and μ

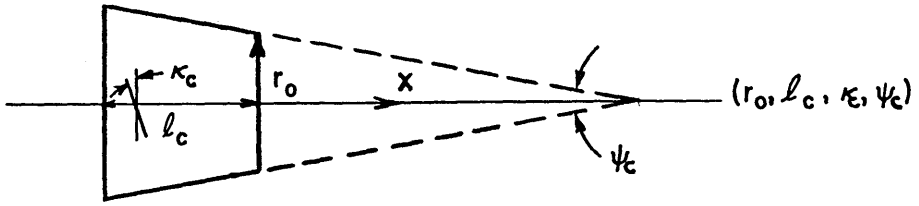

MINIMUM CONE GEOMETRY VARIABLES

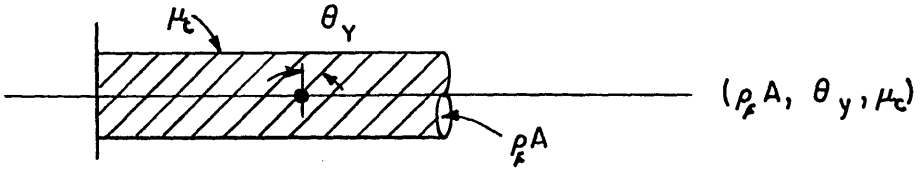

MINIMUM YARN VARIABLES

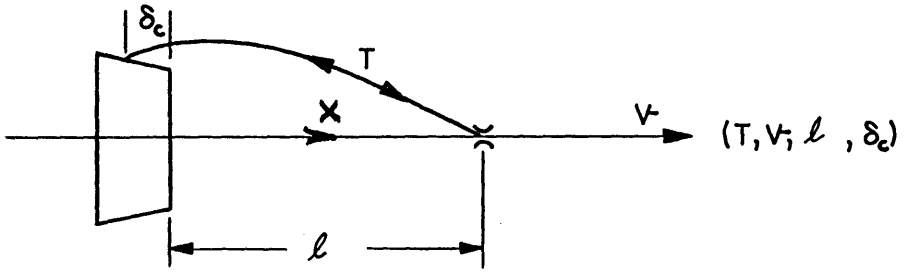

MINIMUM SYSTEM VARIABLES

FIG. 16 a

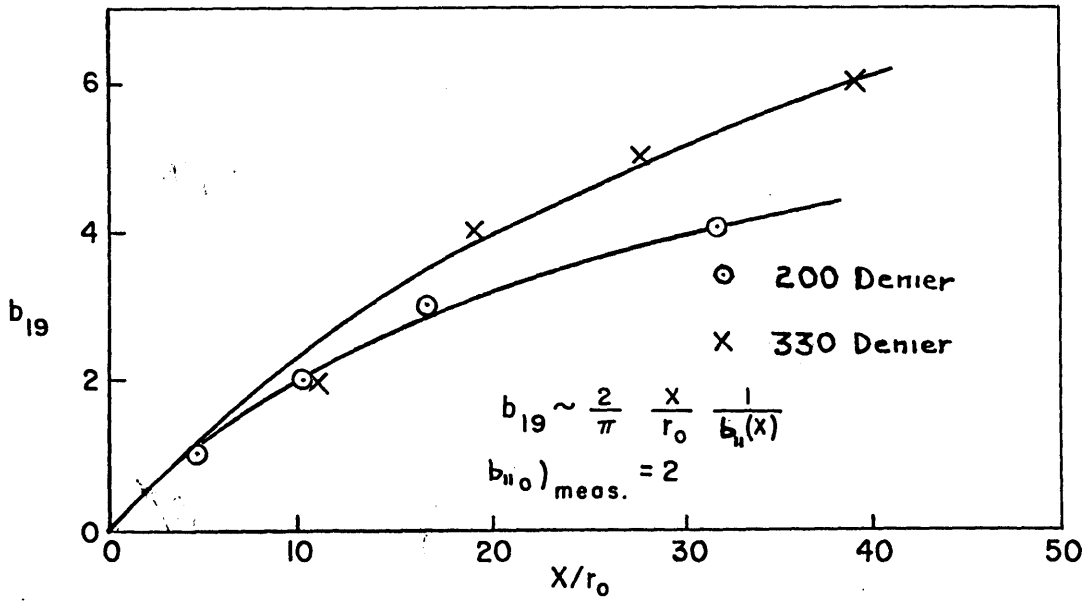

FIG. 16 b

b_{19} vs x/r_0 FOR TWO YARNS

are constant. Therefore:

$$T/\rho_f A v^2 = f(r_o/\ell,\ \delta_c/\ell) \qquad \text{(V-34)}$$

It is unfortunate that the system has eleven variables, even though one omits: the effect of variable tension along the yarn, of time derivatives, of yarn non-uniformity, of air resistance, and of all package variables except those describing the geometry. This is the primary reason why meaningful experimental data is difficult to obtain. Unwinding tension has, however, been measured as a function of velocity, guide distance, and package radius for a given yarn wound on a given package. The data are expressible in the form:

$$T/\rho_f A v^2 = f(r_o/\ell) \qquad \text{(V-35)}$$

Although this data always contains oscillations about some mean value which are caused by the δ_c/ℓ fluctuations, the fluctuations are not significant in most cases. References 12, 16, 17, and 21 report work that has been done to validate Equation V-35. They conclude that the tension varies linearly with yarn mass density, $\rho_f A$, and as the square of withdrawal velocity, v^2, for a given r_o/ℓ. Equation V-35 can be rewritten as the definition of a tension parameter as follows:

$$f\left(\frac{r_o}{\ell}\right) = b_{11}^2 = \frac{T}{\rho_f A v^2} = \frac{c^2}{v^2} = \left(\frac{1}{b_7}\right)^2$$

With this parameter the definition of b_{19} can be rewritten for an overend unwinding cone since $v = r_o \omega_o$.

$$b_{19} = \frac{2\omega_o}{\Omega} = \frac{2\ell}{\pi r_o}\left(\frac{1}{1-\frac{1}{b_{11}^2}}\right)\frac{1}{b_{11}} \qquad \text{(V-36)}$$

If b_7 is small (large b_{11}) Equation V-36 can be approximated as:

$$b_{19} = \frac{2\ell}{\pi r_o b_{11}} \qquad \text{(V-37)}$$

This expression means simply that the number of " half balloons ", b_{19}, increases with ℓ/r_o and decreases with the tension parameter, b_{11}. It must be pointed out again that b_{11} is a function of r_o/ℓ.

If the distance from the front of a yarn cone is defined (Figure 16a) as x and Equation V-37 is considered valid between the successive nodes of a multiple balloon filament space curve, then b_{19} can be written as a " function of x ".

$$b_{19} = \frac{2x}{\pi r_o b_{11}(x)} \qquad \text{(V-38)}$$

This means that the system boundaries are redefined within the yarn space curve at the two nodal points of each balloon.

The form of Equation V-38 has been experimentally verified by the author for two different cotton yarns ($\rho_f A$ = 200 and 330 denier). The experimental apparatus is described in Section IX. Figure 16b is a plot of b_{19} versus x. If b_{11} were constant the data would plot on a straight line, b_{11} being equal to b_{11_o}, which when measured from the plot turns out to have the value 2.0. However, as $\frac{x}{r_o}$ increases, two curves for the two different yarns are seen to deviate from the " constant b_{11} solution ". This deviation can be explained in terms of an increasing $b_{11}(x)$. Thus the form of Equation V-38 is seen to be consistent with experimental observations. It should be mentioned that values of x/r_o of such large magnitude are not

at all practical because the tension constant (and therefore also the tension) becomes too large. Thus Equation V-38 can be used with b_{11} taken as constant for most situations.

Data given by Padfield (4) also support the prediction of b_{19} of this thesis.

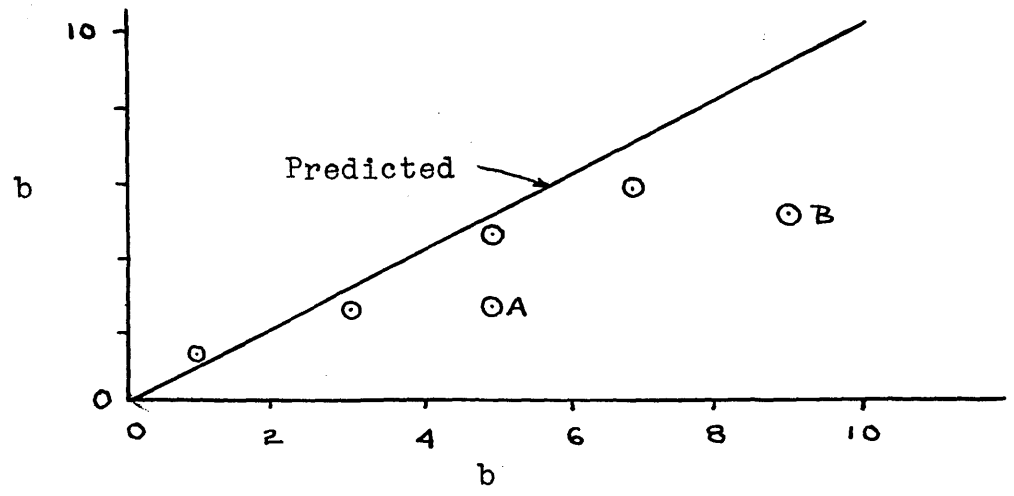

FIG. 16c

Comparison of Relative Frequency Parameter

Figure 16c is a cross plot of b_{19} measured from the figures of Reference 4, versus b_{19} as calculated from Equation V-37 using Padfield's original data. The method of measurement is explained in Section IX. The agreement between calculated and measured b_{19} is good except for the points A and B of Figure 16c. These two points are for systems with low filament tension where it is not possible to neglect air drag. The effect of air drag is seen to increase b_{19} for a given b_{11} which, of course, means an increase in the number of system balloons.

In this chapter the general vector differential equation has been examined extensively for the case of linear filament motion between two boundaries. The boundary conditions have

been taken as harmonic lateral oscillation at $x = 0$ and at $x = \ell$ for both the $\vec{j}$-direction and the $\vec{k}$-direction. The solutions of these equations are applicable to many practical problems of monofilament, multifilament and staple yarn processing situations such as the spinning balloon, the overend unwinding balloon and the yarn space curves near the traversing mechanisms of winding machinery. They can also be used to predict the space paths of thin tapes, where air drag becomes important, and heavy metal cable, where stiffness becomes important.

The concept of a stiffness boundary region was developed, which can be utilized to predict easily the extent that filament motion will be a function of stiffness. The parameters of the equations which describe filament motion for zero stiffness have been modified to include the length of this boundary region.

Finally, the case of an overend unwinding yarn cone was briefly discussed, as an example, in terms of the variables involved and the validity of the prediction of the number of balloons, $b_{19}/2$, within the yarn space curve. The verification of the rotation angle of the filament, b_{17}, was previously included in Section V-B.

The assumption of constant longitudinal filament velocity is not always valid as has been assumed thus far. The next section examines the initial effects of longitudinal acceleration and deceleration and the dynamic buckling that may take place.

VI. ACCELERATION EFFECTS

A. Introduction

The previous two sections dealt with steady state situations where filament accelerations in the x-direction were negligible and the tension was taken as constant. The purpose of this section is to examine this assumption by first reviewing the relatively straight forward phenomena of accelerating filaments and then by examining the equations of motion for decelerating filaments - and the dynamic buckling that invariably takes place.

B. Accelerating Filaments

When a straight filament at rest or at constant velocity is subjected to a sudden increase in velocity along its axis, of magnitude, Δv, at one end, a corresponding increase in filament strain, $\Delta\epsilon_f = \Delta v/a_s$ (where a_s = sonic velocity of material) will propagate down the filament from the point of impact. This is of course a well know situation of one-dimensional strain wave propagation. If at an arbitrary distance, ℓ, from the point of impact, a partial restriction (such as a " frictioned " guide) to filament motion is present, then the wave will be reflected. It will return toward the point of impact, where it will again be reflected. This repeated reflection continues, with each reflection increasing the strain level an amount $\Delta\epsilon_f$, until the total filament strain or tension is sufficient to overcome the partial restriction at ℓ. Then relative motion between the

filament and the guide will take place. This assumes that the level of strain at the moment when relative motion takes place is below the rupture strain.

The time increment between initial impact and relative motion at the partial restriction can be expressed as a function of the final strain, ϵ_f, the sudden increase in velocity, Δv, and the distance, ℓ. This time increment is found by equating the final filament strain, ϵ_f, to the ratio of filament extension to filament length.

$$\frac{\Delta v t}{\ell} = \epsilon_f \qquad \therefore t = \frac{\epsilon_f \ell}{\Delta v}$$

This time increment is short for practical textile situations. For an example let the impact velocity be $\Delta v = 50$ ft/sec; the length be $\ell = 2$ ft.; and the final strain level be $\epsilon_f = .01$. These values yield a time increment of $t = 0.4$ milisec.

If the filament is not initially aligned with the direction of the sudden increase in velocity, then lateral deformation will also take place. However, lateral deformation proceeds at a much slower rate and tension fluctuations can be neglected when considering lateral deformation. An example of this is the intermittent withdrawal of yarn from a yarn cone, such as is used in the external filling supply of the Draper Shuttleless Loom. High speed motion pictures of the yarn as it leaves the cone surface show that steady state as would be described by the equations of Section V, is established in one or two revolutions. This seems amazing since the yarn revolves at $\sim$1700 RPM, however, during these first two revolutions there are $\sim$140 complete longitudinal strain wave cycles which

allow an equilibrium tension to be reached. Thus the assumption of negligible longitudinal accelerations, $\frac{\partial^2 \xi}{\partial t^2}$, of Section V seems very reasonable.

When the filament axis is not initially aligned in the direction of acceleration, lateral as well as longitudinal displacement will take place. It is informative in the context of this section to look at these lateral deformations for a flexible filament ($b_1 = 0$) of finite length. The propagation of the strain (or tension) distribution will be taken as occurring at infinite velocity in light of the previous discussion.

The position vector, $\vec{R}$, is defined in Section III as:

$$\vec{R}(s,t) = (f(s,t) + \xi)\vec{i} + \eta\vec{j} + \varphi\vec{k}$$

The displacement function is chosen as $f(s,t) = s + \frac{1}{2} at^2$ which describes a filament essentially aligned in the $\vec{i}$-direction, and subjected to a constant acceleration of magnitude, a, and direction, $\vec{i}$. Neglecting the effects of air drag, gravity and filament stiffness, Equation II-4 reduces to:

$$\frac{\partial T}{\partial s}\frac{\partial \vec{R}}{\partial s} + T\frac{\partial^2 \vec{R}}{\partial s^2} = \rho_f A \frac{\partial^2 \vec{R}}{\partial t^2} \qquad \text{(VI-1)}$$

Substitution of the position vector, $\vec{R}$, yields three equations:

For the $\vec{i}$-direction:

$$\frac{\partial T}{\partial s}\frac{\partial \xi}{\partial s} + T\frac{\partial^2 \xi}{\partial s^2} = \rho_f A \frac{\partial^2 \xi}{\partial t^2} + \left(\rho_f Aa - \frac{\partial T}{\partial s}\right) \qquad \text{(VI-2)}$$

For the $\vec{j}$-direction:

$$\frac{\partial T}{\partial s}\frac{\partial \eta}{\partial s} + T\frac{\partial^2 \eta}{\partial s^2} = \rho_f A \frac{\partial^2 \eta}{\partial t^2} \qquad \text{(VI-3)}$$

For the $\vec{k}$-direction:

$$\frac{\partial T}{\partial s}\frac{\partial \varphi}{\partial s} + T\frac{\partial^2 \varphi}{\partial s^2} = \rho_f A \frac{\partial^2 \varphi}{\partial t^2} \qquad \text{(VI-4)}$$

As previously stated the variations in η can be considered small compared with the tension variation for time large compared with ℓ/a_s. Therefore Equation VI-2 reduces to:

$$\frac{\partial T}{\partial s} = \rho_f A a, \qquad T = T_o + \rho_f A a s$$

This value for tension can be substituted into Equations VI-3 and VI-4 which then become:

For the $\vec{j}$-direction: $$\frac{\partial \eta}{\partial s} + s\frac{\partial^2 \eta}{\partial s^2} = \frac{1}{a}\frac{\partial^2 \eta}{\partial t^2} \qquad \text{(VI-5)}$$

For the $\vec{k}$-direction: $$\frac{\partial \varphi}{\partial s} + s\frac{\partial^2 \varphi}{\partial s^2} = \frac{1}{a}\frac{\partial^2 \varphi}{\partial t^2} \qquad \text{(VI-6)}$$

where $s \equiv s + T/\rho_f A a$.

These differential equations are identical to the differential equations which describe the well known motion of a " hanging chain ". Bowman (8) includes their solution which is summarized below for the reader, for the $\vec{j}$-direction only. The solution is:

$$\frac{\eta}{\ell}(s,t) = \mathrm{Re}\left\{\sum_1^\infty \psi_n(s)\, e^{i\omega_n t}\right\}$$

where the spacial modes, ψ_n, are Bessel Functions:

$$\psi_n(s) = A_n J_o\left(2\sqrt{\frac{s\omega_n^2}{a}}\right) + B_n Y_o\left(2\sqrt{\frac{s\omega_n^2}{a}}\right)$$

The magnitudes of A_n and B_n are determined for the initial conditions, f(w) and g(w). f(w) is the initial condition for lateral displacement for the non-dimensional coordinate, $w = (\frac{s}{\ell})^{\frac{1}{2}}$. g(w) is the initial condition for velocity for the same coordinate. The Bessel function argument coefficient, α_n is also non-dimensional and of magnitude $2(\frac{\ell \omega_n^2}{a})^{\frac{1}{2}}$.

$$A_n = \frac{2}{J_1^2(\alpha_n)} \int_0^1 w f(w) J_0(w\alpha_n) dw, \qquad w = (\frac{s}{\ell})^{\frac{1}{2}}$$

$$B_n = \frac{2}{-\omega_n J_1^2(\alpha_n)} \int_0^1 w g(w) J_0(w\alpha_n) dw, \qquad w = (\frac{s}{\ell})^{\frac{1}{2}}$$

$$\alpha_n = 2\sqrt{\frac{\ell \omega_n^2}{a}}$$

For a straight flexible filament ($b_1 = 0$) of length, ℓ, initially at rest and aligned at a small angle, $\tan^{-1} \frac{h_o}{\ell}$, (See Figure 17a) with the direction of acceleration, ($\vec{i}$-direction) f(w) and g(w) become:

$$f(w) = \frac{h_o}{\ell}(1-w^2), \qquad g(w) = 0$$

The solution for $\frac{\eta}{h_o}$ is therefore:

$$\frac{\eta}{h_o}(s,t) = 8 \sum_1^\infty \frac{J_0(\alpha_n w)}{\alpha_n^3 J_1(\alpha_n)} \cos \alpha_n \beta t \qquad \text{(VI-7)}$$

where $\beta = (\frac{a}{4\ell})^{\frac{1}{2}}, \qquad J_0(\alpha_n) = 0$

The solution can now be written in simpler form as:

$$\begin{aligned} \frac{\eta}{h_o}(\frac{s}{\ell},t) = {} & 1.108\ J_0(2.405w) \cos 2.405\beta t \\ & - .140\ J_0(5.520w) \cos 5.520\beta t \\ & + .045\ J_0(8.654w) \cos 8.654\beta t + \cdots \end{aligned} \qquad \text{(VI-8)}$$

This solution is plotted in Figure 17a for various values of βt

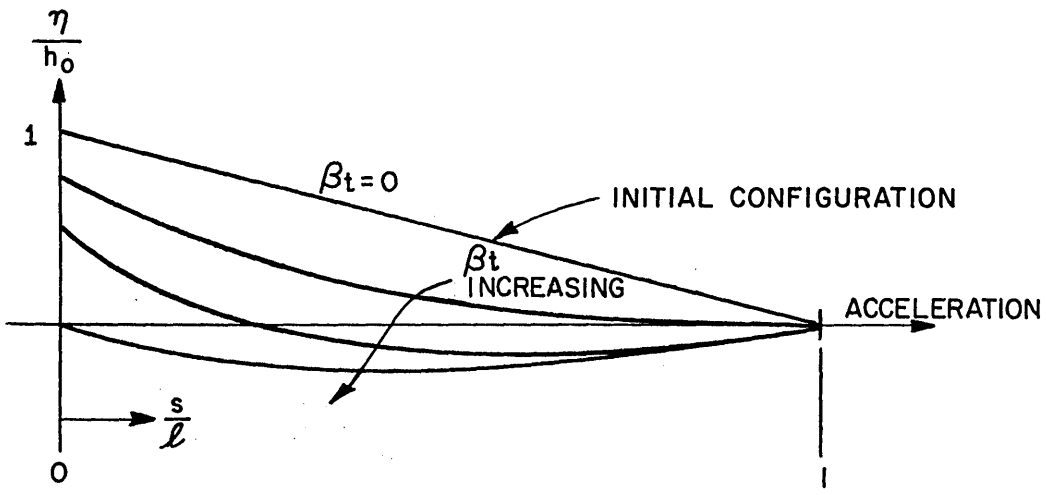

a.

ACCELERATING FLEXIBLE FILAMENT

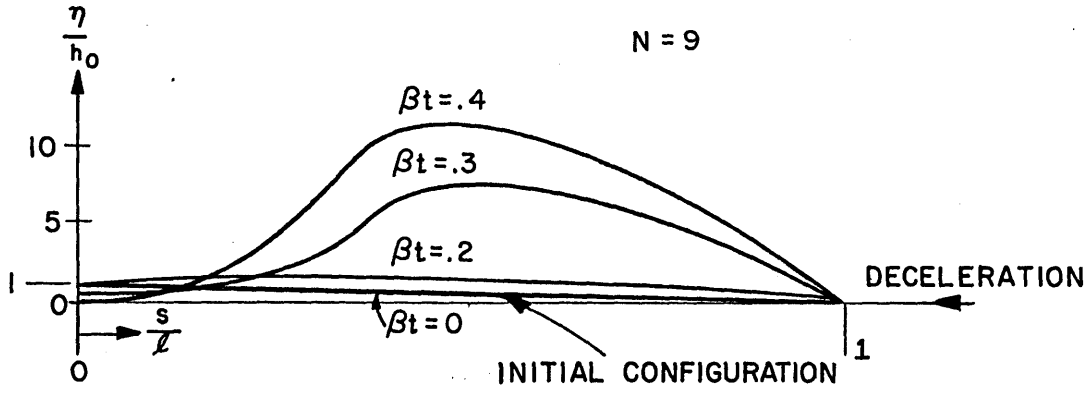

b.

FIG. 17

DECELERATING FLEXIBLE FILAMENT

increasing from zero. It must be remembered that the origin of the plot (s = 0) accelerates in the $\vec{i}$-direction with reference to the stationary coordinate system, with acceleration, a. It is helpful in picturing this to make the following observation.

The frequency of the first term in the above series expression for $\frac{\eta}{h_o}$ is:

$$\frac{2.405}{2\pi}\beta t = 1.087\left(\frac{a/g}{\ell}\right)^{\frac{1}{2}}$$

where g = 32.2 ft/sec^2 and ℓ is given in feet. Therefore, the origin moves a distance, x, in the time, $t = \frac{1}{4f_1}$ (the time required for the main portion of the filament to cross the x-axis) of:

$$x = \tfrac{1}{2}at^2 = .851\ell$$

This is a useful parameter of the system since for any acceleration this value remains constant. Filament rigidity also has very little effect, since for a completely rigid filament, the value of x only changes $\sim 3\%$, to $x = .832\ell$.

C. Decelerating Filaments

The discussion thus far has been for positive acceleration. If negative acceleration is considered, it is not possible to use Fourier or Bessel Series to model the initial conditions since for time, t, greater than zero the series do not converge. This is shown as follows by letting a = -a. Equation VI-5 then becomes:

$$\frac{\Delta\eta}{\Delta s} + s\frac{\Delta^2\eta}{\Delta s^2} = -\frac{1}{a}\frac{\Delta^2\eta}{\Delta t^2}, \qquad \text{where } s = s - T_o/\rho_f Aa \quad \text{(VI-9)}$$

The solution to this equation is identical to the previous solution, for the spacial modes, ψ_n. And for time, t = 0, the initial conditions give identical values for the constants, A_n and B_n. However, the time variation is now in terms of hyperbolic cosines instead of cosines. Referring to the series expression for $\frac{\eta}{h_o}$, the ratio of the n + 1 term to the n term becomes, in the limit, for t positive:

$$R_L = \lim_{n\to\infty} \left| \frac{\eta_{n+1}}{\eta_n} \right| = e^{\pi\beta t}$$

This value is certainly greater than 1 and the series is therefore not convergent. What is possible, however, is to look at the first few terms of the series which means that the only error involved is that the initial condition becomes slightly different than the actual one chosen. There is nothing else mathematically wrong however, since the boundary conditions at $\frac{s}{\ell} = 0$ and $\frac{s}{\ell} = 1$ are still satisfied. See Figure 17b.

For the purpose of numerical calculation the series expression can be divided by a number which approaches the large amplitude that the series yields for finite n. Denoting this number as M;

where:
$$M = \sum_{n=1}^{N} (e^{\pi})^{n\beta t}$$

$$\frac{\eta}{h_o}(s,t) = \frac{8}{M} \lim_{N\to\infty} \sum_{1}^{N} \frac{J_o(\alpha_n W)}{\alpha_n^3 J_1(\alpha_n)} \cosh \alpha_n \beta t \qquad \text{(VI-10)}$$

Figure 17b is a plot of Equation VI-10 for increasing values

of βt. The value of such a plot is that one can predict the extent of lateral deformation as a function of the increment of time under which the filament is subjected to a deceleration. For example, if the limit of maximum lateral displacement is set at approximately fifteen units of initial lateral displacement, h_o, then from Figure 17b βt is seen to be approximately $\beta t = 0.5$. Therefore a limit of the " time under deceleration " would be, $t = 0.5/\beta = (\ell/a)^{\frac{1}{2}}$. For example a one foot filament can be subjected to a one g acceleration for only a little less than .2 seconds before the magnitude ratio becomes fifteen. This solution has been verified in the laboratory in a qualitative way only, by watching pieces of string fall from an initially vertical configuration. The observed shape is that of Figure 17b and the time increments have the correct order of magnitude. The most fascinating observation made during these experiments is that the top point of the piece of string falls vertically, as in Figure 17b. The suggestion is made to the reader to try this himself, since it is so easy and so interesting.

This solution considers time large compared with ℓ/a_s, and therefore deformation takes place at an observable rate (the falling string just discussed). This is not true for filaments under high deceleration, because the dynamic buckling that takes place becomes localized when the decelerating force approaches the same order of magnitude as the filament Euler buckling force, and when the deformation takes place in times with orders of magnitude of ℓ/a_s, or less.

If the Euler buckling force is expressed as $P = (\frac{\pi}{\ell})^2 EI$, and the time for deformation as $(\ell/a)^{\frac{1}{2}}$, the parameters b_s and b_q can be introduced as:

$$b_s = \frac{\rho_f A \ell^3 a}{\pi^2 EI}, \qquad b_q = (\frac{a_s^2}{a\ell})^{\frac{1}{2}} = (\frac{E}{\rho_f a \ell})^{\frac{1}{2}}$$

Equation VI-10 can be considered valid when b_s and b_q are much greater than one.

When b_s and b_q are small, the dynamic buckling becomes totally dependent on stiffness and the entire nature of the model must change. Figure 18 shows an 8.5 mil nylon monofilament, initially under tension. The filament is attached at one end to a clamp shown on the right side of the photographs of Figure 18. The other end is suddenly cut and a strain release wave propagates from the cut end to the clamped end, at velocity, a_s. See Figure 20. For an elastic filament, the strain is completely released - the strain energy becoming the kinetic energy of the portion of filament behind the strain wave. Therefore, when the strain wave reaches the right hand clamp, the entire filament is moving with velocity, $v = \epsilon_f a_s$. The situation is completely analogous to the upstream side of a moving filament which is suddenly stopped at one point. The reader is referred to Section IX where a complete description of the apparatus, loaned to the author by Professor Eggerton, of M. I. T., is presented. The one important point to be made concerning these photographs is that they are not successive photographs of the same filament, but photographs of identical filaments under

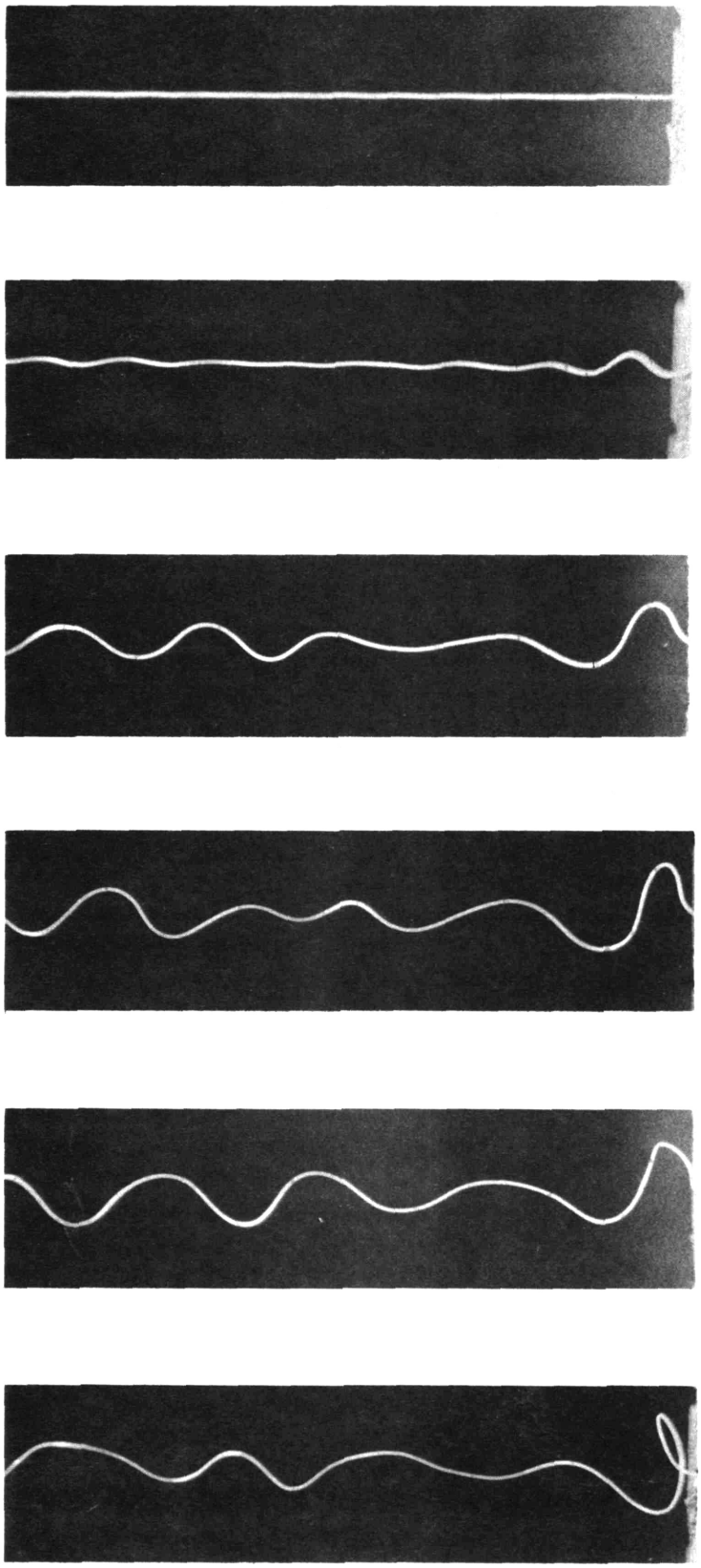

NYLON FILAMENT SNAP BACK

FIG. 18

identical test conditions, taken at successively longer time intervals from the moment of filament rupture. This points out the uniqueness of the phenomenon. The following treatment attempts to analytically describe this second type of dynamic buckling by examining the mathematics of a second model.

The second model will consider the filament impact force to be constant for initial deformation. This assumption is certainly verified by Figure 18, since the time between the first two figures is only ~50 microseconds, while the time for one complete strain wave cycle is ~450 microseconds. Therefore the initial deformation is caused by constant impact force and becomes large before the strain wave can return to the deforming region. This constant force model will first be examined for negligible filament stiffness with a non-zero initial displacement configuration and then will include filament stiffness and consider a zero initial displacement configuration. Only the $\vec{j}$-direction equation will be considered since the $\vec{k}$-equation is the same and the two are uncoupled.

Equation VI-3 for negligible filament stiffness and constant impact force, P = -T, reduces to:

$$\frac{P}{\rho_f A}\frac{\partial^2 \eta}{\partial s^2} + \frac{\partial^2 \eta}{\partial t^2} = 0 \qquad \text{(VI-11)}$$

The impact force, P, can be expressed in terms of the sudden velocity change, v, as $P = \frac{vEA}{a_s}$. Therefore, $\frac{P}{\rho_f A}$ can be rewritten as:

$$\frac{P}{\rho_f A} = \frac{vEA}{a_s \rho_f A} = va_s \quad \left(\text{Note: } a_s = \left(\frac{E}{\rho_f}\right)^{\frac{1}{2}}\right)$$

Equation VI-11 can be rewritten as:

$$va_s \frac{\partial^2 \eta}{\partial s^2} + \frac{\partial^2 \eta}{\partial t^2} = 0$$

The general solution of Equation VI-11 is:

$$\eta(\frac{s}{\ell},t) = f_1 (i(\frac{va_s}{\ell^2})^{\frac{1}{2}} t + \frac{s}{\ell}) + f_2 (i(\frac{va_s}{\ell^2})^{\frac{1}{2}} t - \frac{s}{\ell})$$

The boundary conditions will be taken as:

$$\frac{\eta}{h_o}(0,t) = \frac{\eta}{h_o}(1,t) = 0$$

The initial conditions will be taken as:

$$\frac{\eta}{h_o}(\frac{s}{\ell},0) = \frac{s}{b\ell} e^{1 - \frac{s}{b\ell}}, \qquad \frac{\partial \eta}{\partial t}(\frac{s}{\ell},0) = 0$$

The actual initial conditions to this problem are $\eta = \partial\eta/\partial t = 0$, but the mathematics demands initial conditions for a non-trivial solution. What usually occurs to an initially straight filament moving with velocity, v, when it is suddenly stopped at some point, is that it buckles with a predictable wave length as will be discussed later in this section. However, for flexible filaments with extremely small stiffness these waves can be smaller than the normal perturbations occurring from high speed motion through a piece of moving machinery. The above initial condition (See Figure 19) is chosen to represent such a perturbation. This initial condition will not be used for stiff filaments under similar impact.

The solution becomes:

$$\frac{\eta}{h_o}(\frac{s}{\ell},t) = \sum_1^\infty a_n e^{n\beta^* t} \sin \frac{n\pi s}{\ell}, \qquad \text{where } \beta^* = \pi(\frac{va_s}{\ell^2})^{\frac{1}{2}}$$

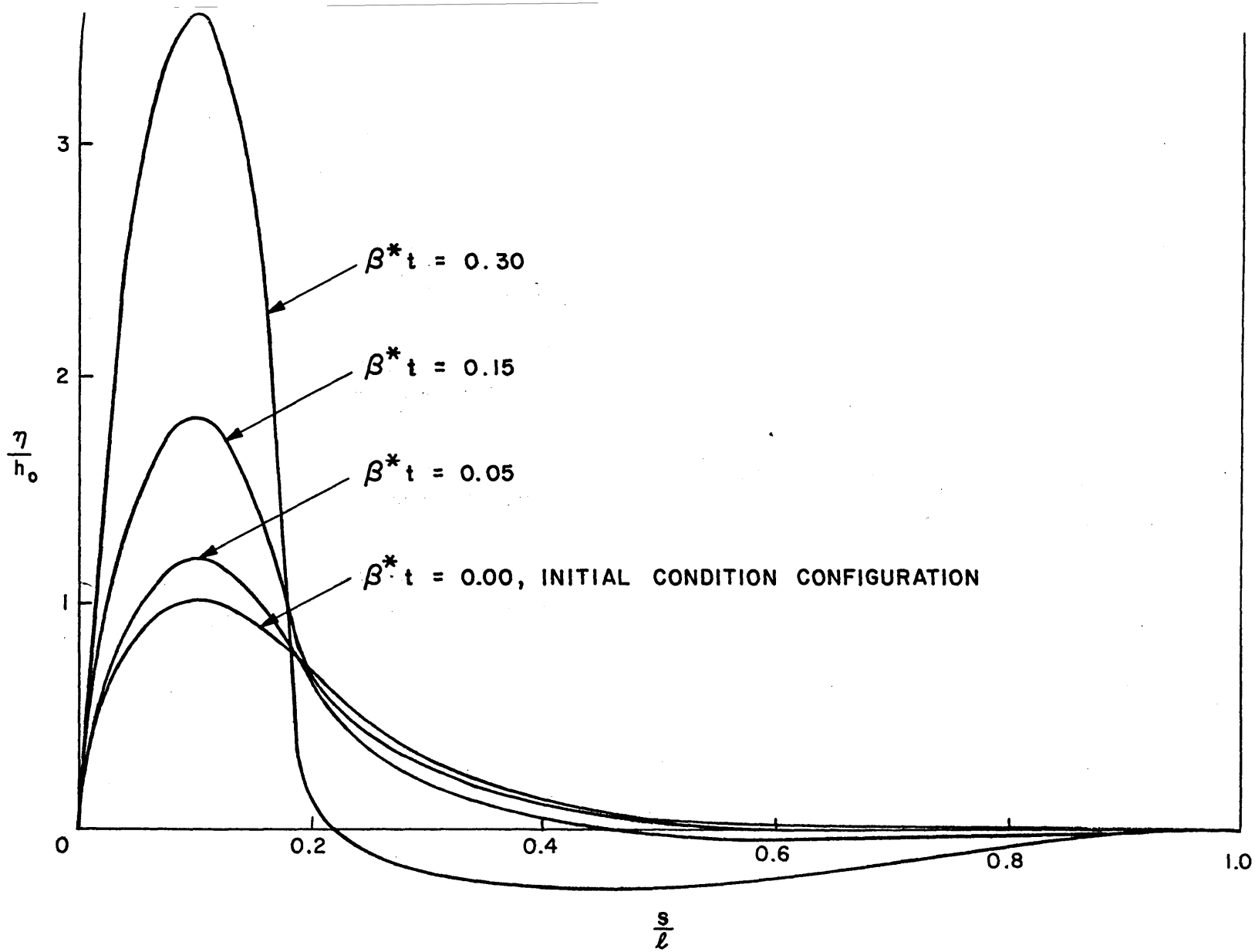

FIG. 19

BUCKLING FLEXIBLE FILAMENT

where: $$a_n = \frac{2n\pi e b^2}{((n\pi b)^2+1)^2}\left\{1-\frac{(-1)^n(1+2b+(n\pi b)^2)}{be^{1/b}}\right\}$$

As in the previous solution for buckling flexible filaments the series will not converge. Therefore only a finite number of series terms can be used. Again it is stated that this only means that the initial condition is slightly altered. If b (where $\frac{s}{\ell} = b$ is the position of maximum deflection) is chosen as 0.1 the second term in the expression for a_n is negligible for $n < 100$. Therefore, a_n can be written as:

$$a_n = \frac{(2n\pi e)(10^{-2})}{((\pi n/10)^2+1)^2}, \quad n < 100$$

This solution is plotted in Figure 19 as $\frac{\eta}{h_o}$ versus $\frac{s}{\ell}$ for increasing values of $\xi^* t$. It should be pointed out that for this solution the initial deflection at $\frac{s}{\ell} = 1$ is not zero but $\frac{\eta}{h_o} = \frac{10}{e^9}$. This is considered small enough.

In this figure, as was done before with Figure 17b, it is possible to estimate the magnitude of the ratio, $\frac{\eta_{max}}{h_o}$, as a function of time ($\xi^* t$). For example, for a one inch portion of filament ($\ell = \frac{1}{12}$), moving at 100 ft/sec ($v = 100$), with a strain wave velocity of 6500 ft/sec ($a_s = 6500$), it takes approximately 35 microseconds for the initial perturbation to increase by a factor of four. These numbers correspond very roughly to the situation shown in Figure 18. However, the initial configuration of this figure is not a random machine perturbation, but a unique and predictable phenomenon as will now be shown.

When filament stiffness is of a magnitude such that the

buckling wave length is larger than normal machine excited perturbations it is possible to pick initial conditions which are unique. The work reported in Reference 2 was concerned with the dynamic motions and buckling which take place when the strain in a filament is suddenly released. The work was done as a Masters Degree Thesis by the author. The equations developed are reviewed and elaborated on here because, as is shown as follows, the buckling that takes place is completely analogous to the buckling that takes place when a moving filament is suddenly decelerated.

This analogy is clearly seen from the well known solution to Equation III-2:

$$\frac{\partial^2 \xi}{\partial s^2} = \frac{1}{a_s^2} \frac{\partial^2 \xi}{\partial t^2}, \qquad a_s^2 = E/\rho_f \tag{III-2}$$

where: $\frac{\partial \xi}{\partial x}(0,t) = 0, \qquad \xi(\ell,t) = \epsilon_f \ell$

$$\xi(s,0) = \epsilon_f s, \qquad \frac{\partial \xi}{\partial t}(s,0) = 0$$

The solution is expressed in terms of strain and velocity as:

$$\frac{\partial \xi}{\partial s} = \epsilon_f(1-u(s-a_s t)), \qquad \frac{\partial \xi}{\partial t} = \epsilon_f a_s u(s-a_s t) \tag{VI-12}$$

where: $u(s-a_s t)=1 \quad (s < a_s t), \quad u(s-a_s t)=0 \quad (s > a_s t)$

Referring to Figure 20 (illustrating the situation dealt with in Reference 2), as the strain release wave proceeds from the suddenly free end (s = 0) the region behind the wave has zero strain but positive velocity, $\epsilon_f a_s$. This means that when the strain wave reaches $s = \ell$, the entire filament has

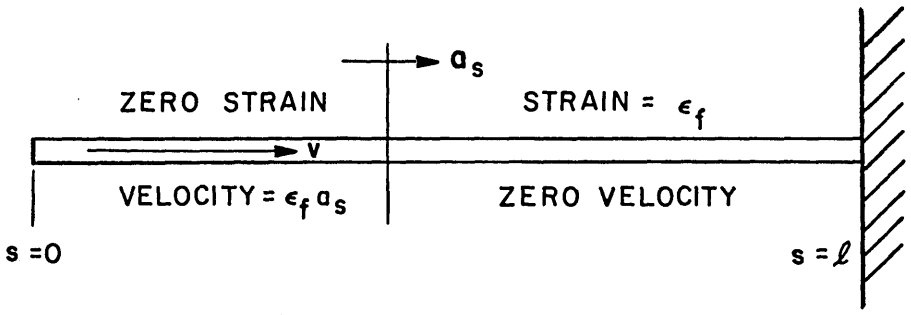

FIG. 20

STRAIN WAVE PROPAGATION

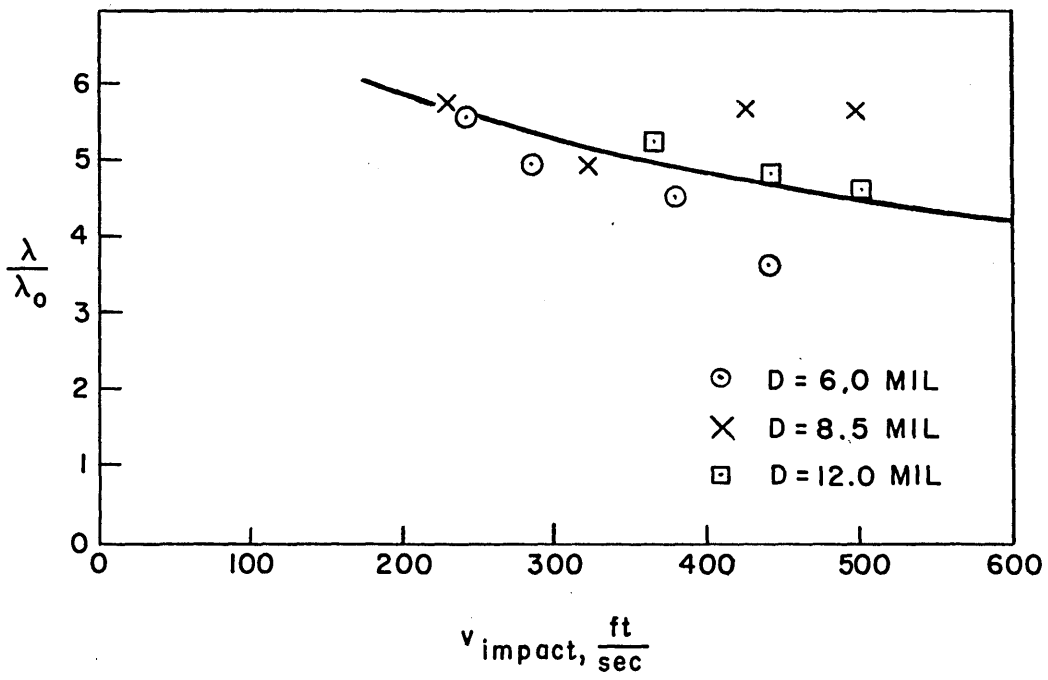

FIG. 21

WAVELENGTH RATIO vs IMPACT VELOCITY FOR NYLON MONOFILAMENT

zero strain and positive velocity, $\epsilon_f a_s$. Thus the filament is completely analogous to the upstream portion of a moving filament (of velocity, $v = \epsilon_f a_s$) which is suddenly stopped at one point.

The results of the Masters Thesis are reviewed as follows, beginning with the linear position vector:

$$\vec{R}(s,t) = (s + vt + \xi)\vec{i} + \eta\vec{j} + \varphi\vec{k}$$

For negligible air drag and gravity effects Equation II-4 reduces, after substitution of $\vec{R}$, (for the $\vec{j}$-direction only) to:

$$\epsilon \frac{\partial^4 \eta}{\partial s^4} + v a_s \frac{\partial^2 \eta}{\partial s^2} + \frac{\partial^2 \eta}{\partial t^2} = 0, \qquad \epsilon = \frac{EI}{\rho_f A} \tag{VI-13}$$

The boundary conditions are:

$$\eta(0,t) = \frac{\partial \eta}{\partial s}(0,t) = \eta(a_s t,t) = \frac{\partial \eta}{\partial s}(a_s t,t) = 0$$
$$\xi(0,t) = \frac{\partial \xi}{\partial s}(\infty,t) = 0 \tag{VI-14}$$

The actual initial conditions are:

$$\eta(s,0) = \frac{\partial \eta}{\partial t}(s,0) = 0$$
$$\xi(s,0) = 0, \qquad \frac{\partial \xi}{\partial t}(s,0) = -\epsilon_f a_s = -v \tag{VI-15}$$

(It must be pointed out that the coordinate system has been changed here for consistency of presentation. Positive s is now taken as beginning at the right hand clamp of Figure 18 and increasing towards the left, while time is referenced to the moment of impact.)

The unfortunate fact is that the answer to this problem is $\eta(s,t) = 0$. However, what really happens is that after the strain wave has passed a certain distance, the filaments lowest energy configuration suddenly changes from pure axial compression to lateral deformation. It then buckles and it is at this point that the above problem formulation becomes valid, with initial conditions given by this initial mode. The initial mode can be found by assuming that at some time, t_o (and corresponding distance to the strain wave front, $s_o = a_s t_o$) there will be a configuration which satisfies the above differential equation and boundary conditions. For a wave solution this initial strain wave front distance is found to be a multiple of " Euler Wave Lengths " (namely 5) where:

$$\eta_3(s,0) = \eta_o\left(\sin \frac{4}{5}\frac{2\pi}{\lambda_o} s - \frac{4}{3}\sin \frac{3}{5}\frac{2\pi}{\lambda_o} s\right), \quad 0 < s < 5\lambda_o \qquad \text{(VI-16)}$$

where: $$\lambda_o = 2\pi\sqrt{\frac{EI}{P}} = \text{"Euler Wave Length"}$$

Thus when the strain wave has moved a distance of $s_o = 5\lambda_o$ the filament has a deformation mode of lower energy than pure axial compression. This mode then becomes the initial condition for the above problem. Therefore the boundary conditions are:

$$\eta(0,t) = \frac{\partial \eta}{\partial s}(0,t) = \eta(\infty,t) = \frac{\partial \eta}{\partial s}(\infty,t) = 0$$

$$\xi(0,t) = \frac{\partial \xi}{\partial s}(\infty,t) = 0$$

And the simulated initial conditions are:

$$\eta(s,0) = \eta_o\left(\sin \frac{4}{5}\frac{2\pi s}{\lambda_o} - \frac{4}{3}\sin \frac{3}{5}\frac{2\pi s}{\lambda_o}\right), \quad 0 < s < 5\lambda_o$$

$$\eta(s,0) = 0, \quad 5\lambda_o < s < \ell$$

$$\frac{\partial \eta}{\partial s}(s,0) = -\frac{v}{a_s} \quad (0 < s < 5\lambda_o), \quad = 0 \quad (5\lambda_o < s < \infty)$$

The differential equation is no longer uncoupled and becomes:

$$\epsilon \frac{\partial^4 \eta}{\partial s^4} + u(s-a_s t)va_s \frac{\partial^2 \eta}{\partial s^2} + \frac{\partial^2 \eta}{\partial t^2} = 0 \qquad \text{(VI-17)}$$

where $u(s-a_s t)$ is as previously formulated.

This problem as formulated above was not solved previously and will not be solved here because of its inherent complexity. Also the buckling that takes place decreases longitudinal compressive strain and therefore the coefficient va_s. The problem can have a nonlinear formulation, which is discussed in Reference 2, but the equations are too complicated for this context.

It is possible to measure the deformations of filament samples which have been buckled in this manner. For copper wire (3.5 mil diameter) which yields at low strain - before the nonlinear deformation can take place - the wave lengths agree very well with those predicted by the initial condition function, $\eta_3(s,0)$. Figure 22 is a plot of the average measured wave length of a deformed sample as a function of the calculated impact velocity, v, where: $v = \epsilon_f a_s$. The value of a_s was calculated from the average material properties. ϵ_f is calculated from the measured load of a sample at rest just prior to being cut and allowed to buckle dynamically. This is a nice controlled variable experiment and as previously discussed it is analogous to a sudden velocity

decrease (of magnitude v) for a moving filament. The measured values are only slightly higher than those predicted.

For materials with higher yield strains (polymers such as nylon, dacron and saran) the wave lengths of the deformed samples are always several times higher than predicted by linear theory, a point substantiated by the nonlinear formulation of Reference 2. In Figure 21 the results of a series of tests of nylon monofilaments of varying diameter are plotted as λ, the average measured wave length of deformed sample, divided by λ_o, versus calculated impact velocity, v, where again, $v = \epsilon_f a_s$. The values of a_s were measured on a Pulse Propagation Meter for the samples in question. ϵ_f is again calculated from the measured load of a sample at rest just prior to being cut and allowed to buckle dynamically.

It is shown in Reference 2 that the value of the wave length ratio should be independent of load for a given sample, if the load is of sufficient magnitude. This is supported by Figure 21, the value of the ratio approaching 4. It is also seen from Figure 18 that, this is the correct order of magnitude increase in the final wave length from the initial wave length.

The buckling described thus far has been considered only two-dimensional. Referring to Figure 23, a 10 mil nylon monofilament, of two inch initial length, is shown as it buckles statically into the third dimension. This occurs, as is predicted by the solution of the equations for the model of Reference 2, when the maximum tangent angle reaches 90°.

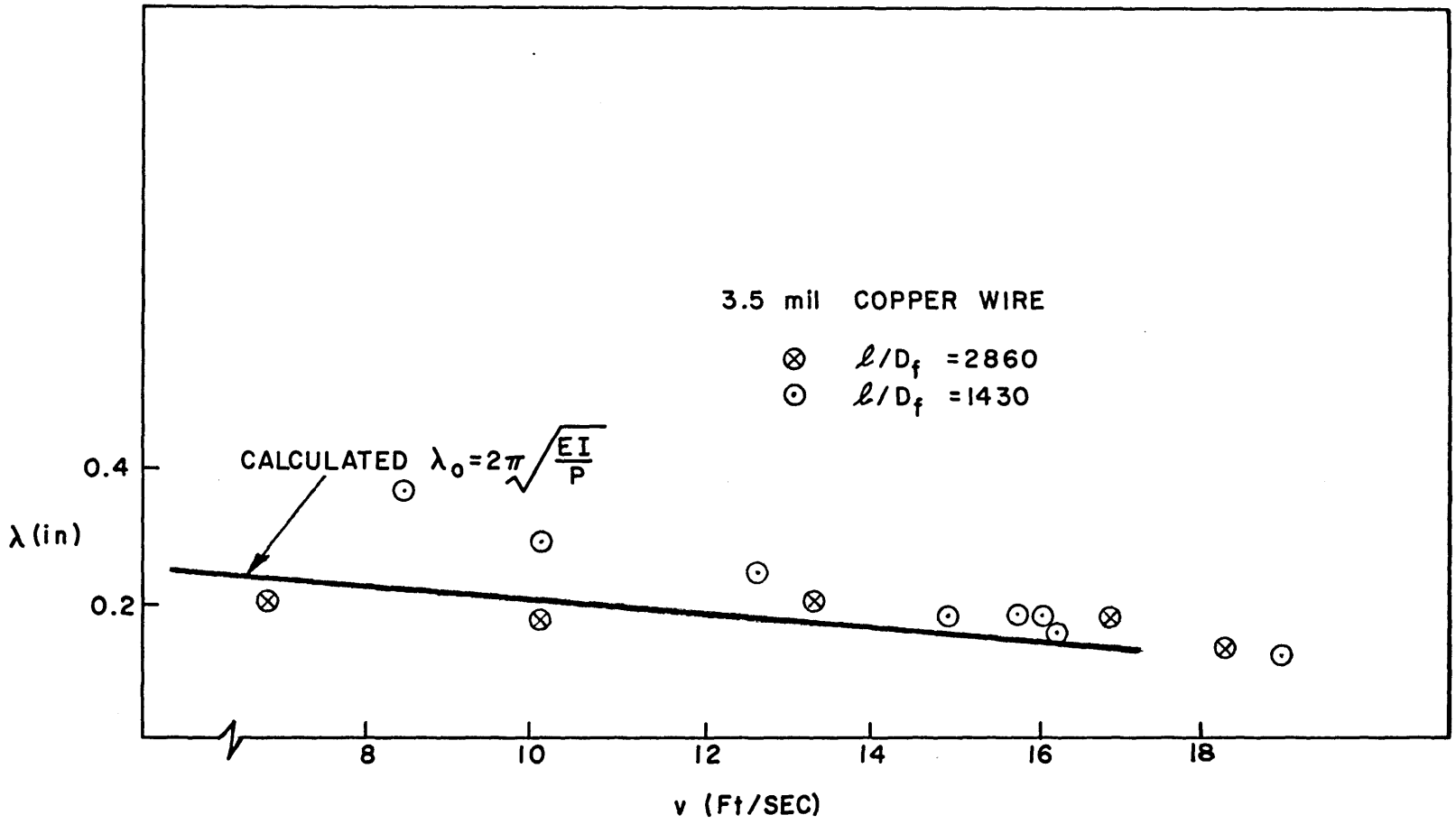

FIG. 22

FUNDAMENTAL WAVELENGTH vs. IMPACT VELOCITY

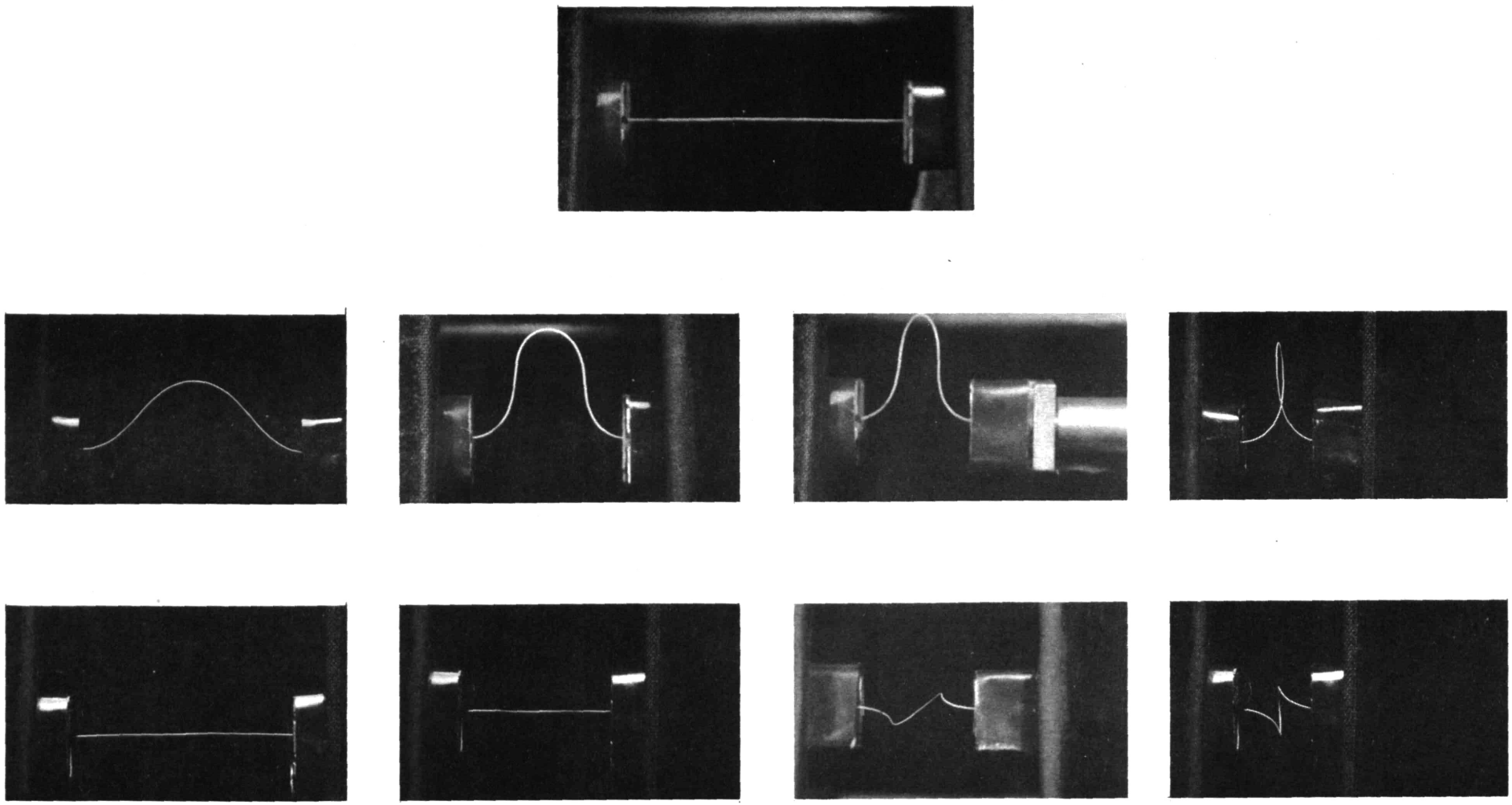

Three Dimensional Buckling

Figure 23

This occurs when the jaw spacing is one half the initial filament length. This limit of two-dimensional stability is suggested for dynamic buckling also, and is partially born out by Figure 18 where the right hand wave is seen to become three-dimensional, and coil up, at about the same time that the maximum tangents become vertical.

The effects of acceleration on filament motion have thus been analyzed analytically and verified experimentally to a certain degree. It was not possible during the course of this study, to obtain the number of monofilaments of different materials that would be considered satisfactory from an experimental point of view. It is suggested that future experimental verification should be carried out - once these different material monofilaments become available.

An example of the application of this material on the dynamic buckling of filaments concerns the external filling supply of the Draper Shuttleless Loom. This consists primarily of a yarn cone from which approximately 7 ft. of yarn is intermittently withdrawn at a frequency of ~ 4 cps. The establishment and collapse of the yarn balloon was described in the early part of this section. The remaining portion of the filling supply is the mechanism which accomplishes the intermittent withdrawal. Included in this mechanism is a " yarn brake " which stops the flow of yarn from the package to the loom at one point along the filament path.

The suddenly stopped yarn buckles dynamically in the region immediately upstream of the brake and lateral deformation

proceeds at a certain rate. If the duration of brake application is beyond a certain minimum, the lateral deformation is so extensive that yarn self entanglement may take place. However, yarn deformation can be kept below this level by limitting the braking time to this minimum value. Thus it is seen that knowledge of the phenomenon allows a prediction of this minimum time duration to be made, thus allowing the loom designer to properly design the brake.

VII. EFFECT OF SURROUNDING MATRIX

A. Introduction

This thesis has thus far only dealt with the dynamic motions of filaments in a low resistance medium, namely air. It is now necessary to examine the principle effects that a solid medium has on filament motion. An example of this is the single filament in an assemblage of filaments which suddenly breaks as the entire assemblage is pulled to rupture. The assemblage strength is obviously dependent on the local mechanism of load transfer of the individual filaments. A specific example would be the fibers in a twisted yarn. This is a problem of practical interest and the one mainly dealt with in this section.

Therefore, consider a hypothetical filament embedded in a matrix (the matrix being the other filaments of the assemblage) where the interaction between the filament and the matrix is modeled as, (1) a constant shear stress resistance along the filament length corresponding to a frictional interaction between filaments, and, (2) a linear force variation in the matrix with lateral deformation of the filament.

The filament is initially at rest. The entire matrix including the filament is then given an increasing tensile strain until the filament breaks. Considering only one half of the broken filament, a strain release wave is seen to propagate from the break along the fiber, thus into the matrix. The energy released is modeled as being absorbed through two

mechanisms. The first is an increase in the kinetic energy of the filament itself and the second is a dissipation of thermal shear energy at the interface of the filament and the matrix.

The strain discontinuity (or the strain release wave) propagates along the filament until a point is reached where the accumulated effect of matrix filament shear has decreased the strain discontinuity to zero or in other words until the strain behind the discontinuity equals the original strain, ϵ_f, at which the filament broke in one spot. The position of the break is taken as $x = 0$. The strain wave propagates in the positive x direction. At $x = x_o$ the strain discontinuity goes to zero as indicated above.

At points beyond $x = x_o$ the strain discontinuity is zero; there is no longer any relative motion between filament and matrix. The resistive shear force suddenly increases at $x \geq x_o$ since the static coefficient of friction is operative beyond this point rather than the lesser kinetic coefficient of friction. Thus the remaining filament and matrix act as a " reflection wall " for any remaining filament kinetic energy. The presence of a reflecting wall may cause the filament to buckle laterally.

The problem is divided into two parts. The first being to determine to what distance the strain release wave propagates along the filament before the accumulated effect of longitudinal shear force reduces the strain discontinuity to zero. And, the second being to look at the equations

governing the dynamic buckling that can take place.

B. Propagation of the Strain Release Wave

The position vector for zero initial filament velocity is given as:

$$\vec{R} = (s + \xi)\vec{i} + \eta\vec{j} + \varphi\vec{k}$$

The longitudinal or $\vec{i}$-direction shear is:

$$\frac{\Delta V_s}{\Delta s})_x = -\pi\mu p D_f \vec{i}$$

Where μ is the coefficient of friction between the filament and the matrix; p is the radial interface pressure; and D_f is filament diameter. The equations of motion for the $\vec{j}$ and $\vec{k}$ directions will not be considered for time, $t \leq x_o/a_s$, where time is measured from the instant of filament rupture.

Substitution of $\vec{R}$ into Equation II-4, for negligible gravity and air drag effects, yields for the $\vec{i}$-direction ($s = x$ since the filament is initially at rest):

$$x_o \frac{\Delta^2 \xi}{\Delta x^2} - \epsilon_f b_{10} = \frac{x_o}{a_s^2} \frac{\Delta^2 \xi}{\Delta t^2}, \qquad b_{10} = \frac{\pi\mu p D_f x_o}{EA\epsilon_f} \qquad \text{(VII-1)}$$

where ξ is the displacement of a given point at x relative to that same point on the unstrained filament. The boundary conditions are:

$$\frac{\Delta \xi}{\Delta x}(0,t) = 0, \qquad \xi(x_o,t) = \epsilon_f x_o$$

The initial conditions are:

$$\xi(x,0) = \epsilon_f x, \qquad \frac{\Delta \xi}{\Delta t}(x,0) = 0$$

which is to say that in the equilibrium state ($t < 0$) the filament has constant strain hence displacement varies linearly with x as shown in the dotted line fo Figure 24a.

The solution to this problem for $0 < t < x_o/a_s$ is given as follows:

$$\xi_1(x,t) = \epsilon_f x + \frac{\epsilon_f x_o}{2}\left(\left(\frac{x}{x_o}\right)^2 - 2\left(\frac{x}{x_o} - \frac{a_s t}{x_o}\right) - \left(\frac{a_s t}{x_o}\right)^2\right) u(x-a_s t) \quad \text{(VII-2)}$$

where $u(x-a_s t) = 0, \quad a_s t < x < x_o; \; = 1, \quad 0 < x < a_s t$

The solution for displacement versus x at time, $t_o = \frac{x_o}{a_s}$, is plotted in Figure 24a. The problem is more clearly understood, however, by considering filament strain and velocity as a function of time.

Figure 24b is a plot of filament strain, $\frac{\Delta \xi_1}{\Delta x}$, versus x, for $0 < t < x_o/a_s$, given by Equation VII-3 as:

$$\frac{\Delta \xi_1}{\Delta x} = \epsilon_f(1-u(x-a_s t)) + \frac{\epsilon_f x}{x_o} u(x-a_s t) \quad \text{(VII-3)}$$

The particular time was taken to be $t = 0.4\ t_o$. Thus the strain does not decrease stepwise to zero behind the strain release wave as occurs in the " without matrix " dynamic buckling previously discussed in Section VI. Instead it decreases linearly with x behind the release wave at any given time. When $x = x_o$ the strain behind the wave front is equal to the original strain and the discontinuity disappears as shown in the dotted line for $t = t_o$ in Figure 24b.

Figure 24c gives a plot of filament velocity versus x for $0 < t < x_o/a_s$ for an arbitrarily selected point, $x = 0.4x_o$.

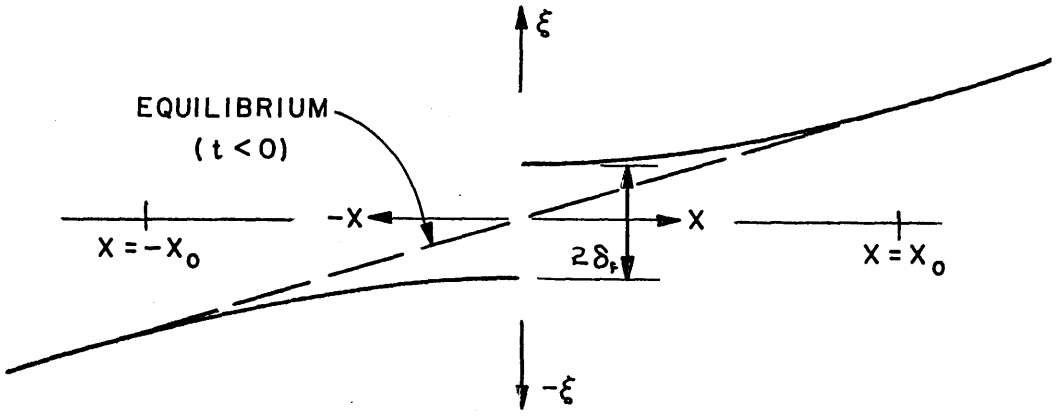

a.

ξ vs X, t = t_0

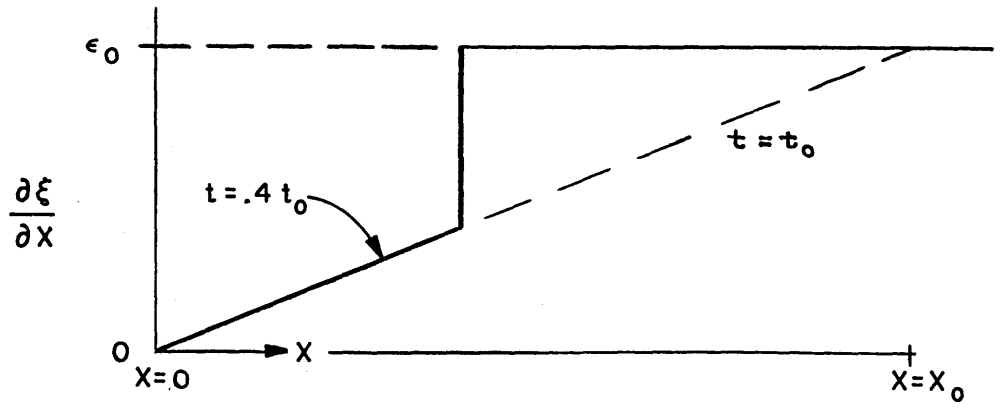

b.

STRAIN vs X, t = .4 t_0

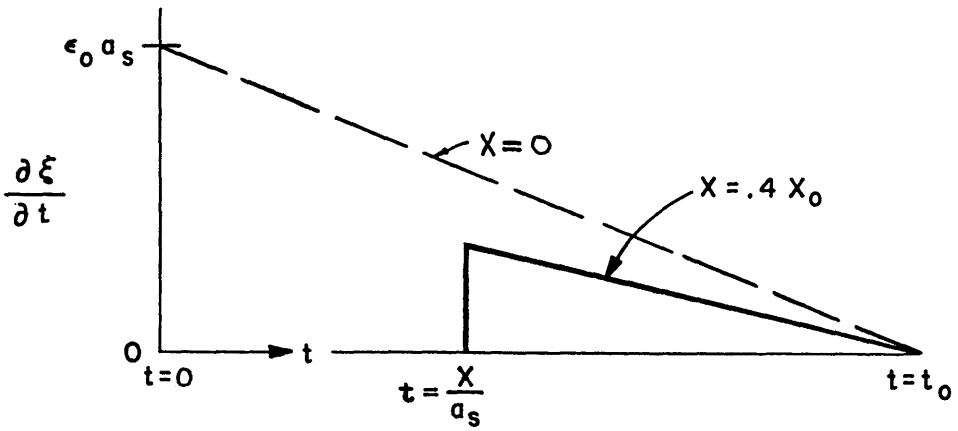

c.

FIG. 24

VELOCITY vs t, X = .4X_0

$$\frac{\Delta \xi}{\Delta t} = \epsilon_f a_s \left(1 - \frac{x}{x_o}\right)\left(1 - \frac{t}{t_o}\right) u(x - a_s t) \qquad \text{(VII-4)}$$

This indicates that the velocity, or kinetic energy, decreases at all $x < a_s t$, for increasing t, and that for $t = t_o = x_o/a_s$, filament velocity is zero throughout.

It is worth pointing out that the influence of friction does not change the strain wave velocity, a_s. This can be seen in Figure 24b by noticing that for $x = a_s t$ (across the strain discontinuity) there exists a finite change in strain (therefore infinite $\frac{\Delta^2 \xi}{\Delta x^2}$) and in Figure 24c a finite velocity change (therefore infinite $\frac{\Delta^2 \xi}{\Delta t^2}$). Thus the term in Equation VII-1, $\epsilon_f b_{10}$, is negligible when considering the discontinuity and therefore its velocity, a_s, remains constant.

The distance of strain wave penetration along the filament, x_o, is found to be:

$$x_o = \frac{E \epsilon_f D_f}{2 \mu p}, \qquad \therefore b_{10} = 2$$

Therefore, the dynamic strain wave penetration is exactly twice the penetration distance required for static equilibrium between accumulated shear force and original tensile strain, or in other words - twice as far as if the break took place " slowly ". Referring to the following figure,

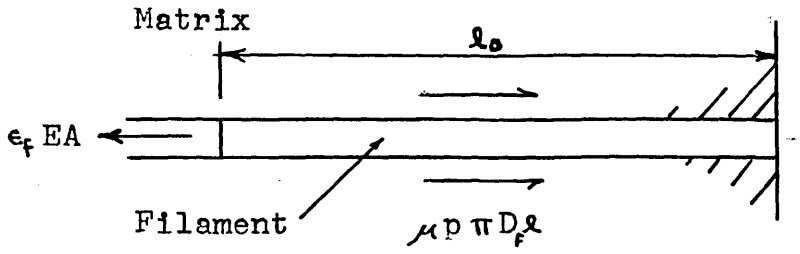

the "static" release penetration distance, ℓ_o, is easily found by equating the filament tension, $T = \epsilon_f EA$ with the total shear force, $\mu p \pi D_f \ell_o$ and solving for ℓ_o. This yields

$$\ell_o = \tfrac{1}{2}\left(\frac{\epsilon_f E D_f}{2\mu p}\right) = \tfrac{1}{2}x_o$$

This means that for time, t, slightly less than t_o, the total shear force exerted by the fiber on the matrix is twice the original load that the filament carried, or twice the load that the rest of the assemblage would have to bear, again, if the break took place " slowly ". This factor of two is, of course, a common factor for impact loading.

The separation distance that occurs at the break is also an important (and easily measurable) parameter defined as:

$$\delta_f = \xi(0,t_o) = \frac{\epsilon_f x_o}{2} = b_{10}\frac{x_o}{4}\epsilon_f \quad \therefore b_{10} = \frac{4\,\delta_f}{x_o \epsilon_f}$$

This dynamic deflection at x = 0 as shown in Figure 24a is predicted as twice the static or " slowly released reflection " that would occur if the break took place " slowly ", as just described. This value of static deflection can be found easily by directly integrating Equation VII-1 for $\frac{\partial^2 \xi}{\partial t^2} = 0$.

In order to verify this solution and to validify the factor of two by which the displacement is multiplied in the dynamic case, we have conducted a set of simple tests. The variable measured is δ_f, or the displacement at x = 0. Figure 25 is a crossplot of this displacement for the static and for the dynamic release situation in the apparatus shown in Figure 26. In these tests a strip of rubber shown is given an initial strain. Two smooth plexiglass plates are

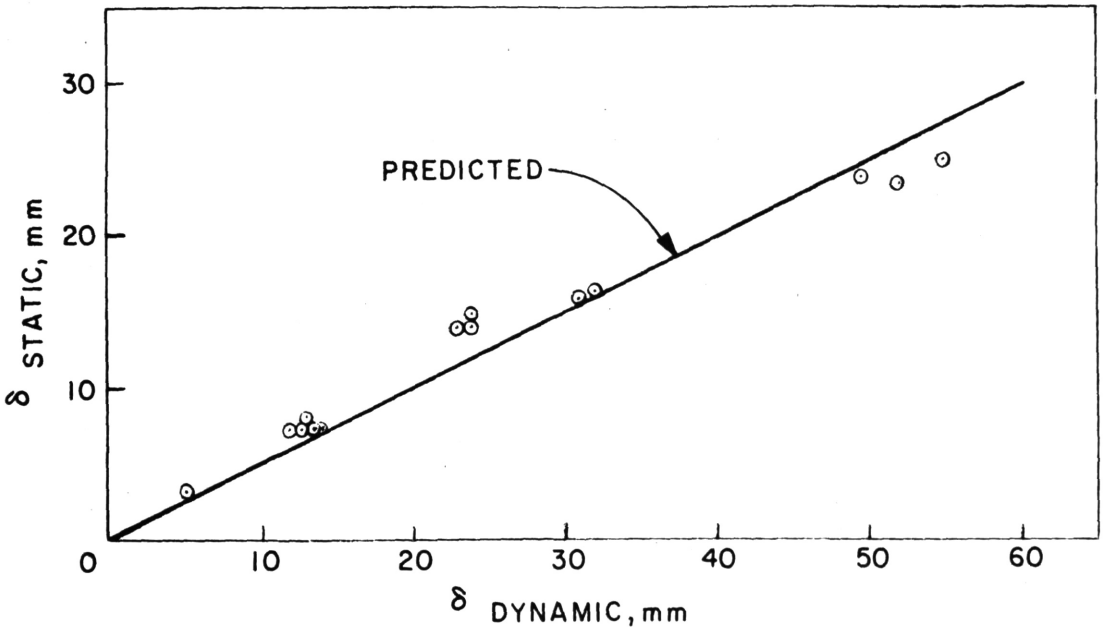

FIG. 25

δ_{STATIC} vs δ DYNAMIC FILAMENT MOTION WITHIN MATRIX

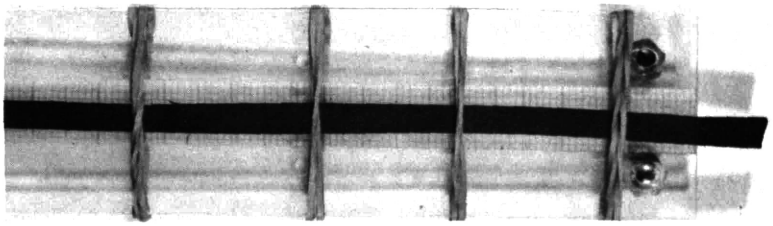

FIG. 26

EXPERIMENTAL APPARATUS FOR FILAMENT MOTION

then used to form a sandwich containing the strip. The strip is then released statically or " slowly " and then dynamically or " quickly ". The deflection at the end of the strip is measured for each type of release, at increasing values of initial strain. Figure 25 illustrates the consistency of the multiple of two that is predicted by the theory.

C. Dynamic Buckling Within the Matrix

When a filament breaks as described above, one of the two parts may have a length less than x_o. If this is true then this part will contain kinetic energy when the strain wave reaches the end of that filament segment. This piece of filament will then travel through the matrix until this energy is dissipated or until it collides with something. If the latter is true the impact force felt during collision may be high enough to buckle the filament laterally into the matrix.

If the filament length is sufficient but the matrix is not continuous as modeled and holds the filament tightly at some point, $x < x_o$, then impact and ensuing buckling also may occur. If it does and if the matrix is of finite height (or radius) the filament may actually penetrate to the surface of the matrix. This is a common occurrence while a piece of yarn is breaking. Fibers which have broken inside the yarn are actually seen to " pop " through the surface. Also during the drafting of fiber webs, although breakage is not necessarily occurring, this same sudden migration takes place upon sudden release of tension as fibers slip by one another.

The three photographs of Figure 27 are examples of the " pop-out " phenomena. The top photograph shows a piece of cotton roving that has been pulled apart - or drafted. Fibers near the surface are seen to pop through the surface while the roving is being pulled apart. They pop out very quickly, with considerable velocity and it seems reasonable that the energy must have been suddenly-released tensile strain energy.

The middle photograph was taken of a test strand comprised of dacron monofilaments twisted together on a special apparatus (29). Several individual monofilaments in the central region of the strand were broken, while the fiber assemblage was under moderate strain. The ruptured filaments are seen to have buckled laterally and popped through the surface. In the bottom photograph, the buckled monofilament was at the exact center of the strand - being identified by its color - and was the only monofilament broken. The yarn was clamped at the extreme right of the picture where the broken filament buckled configuration is slightly evident as two loops protruding through the surface. To the left of these loops the tangled configuration indicates the mode of strain energy disipation.

In order to better understand this type of filament motion, a very preliminary look at the basic equations involved yields a parameter with which it should be possible to categorize different assemblages with respect to the extent of this effect. This parameter could be helpful in any experimental work contemplated.

The basic governing equation for this type of buckling

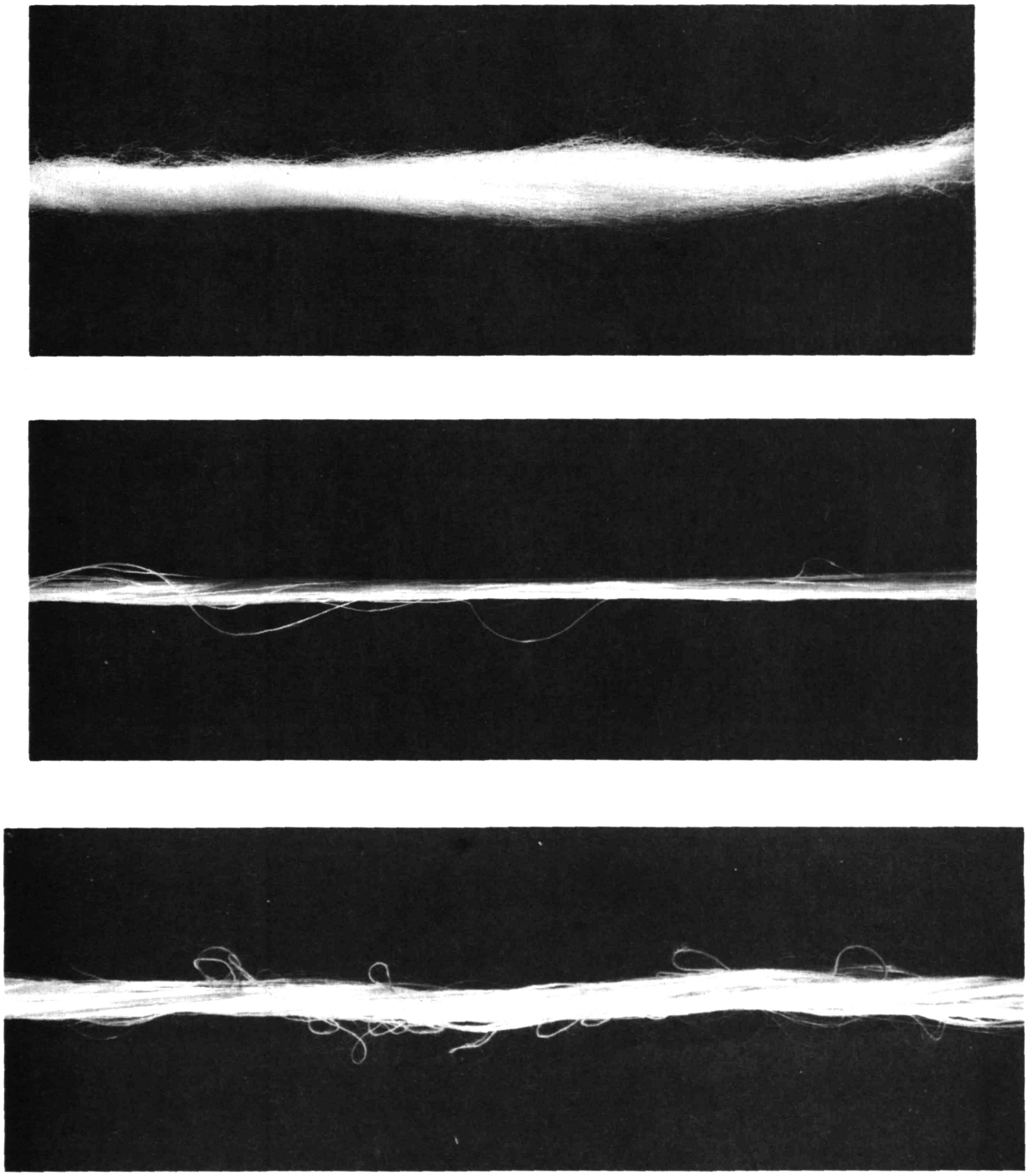

FIG. 27
EXAMPLES OF FILAMENT SURFACE BREAKTHROUGH

is Equation VI-13. However, it is necessary to add a term for the resisting force of the foundation, where the force is considered to vary directly with the filament's lateral displacement into the matrix. The boundary conditions do not change. Therefore, for the $\vec{j}$-direction only:

$$\epsilon \frac{\partial^4 \eta}{\partial x^4} + v a_s \frac{\partial^2 \eta}{\partial x^2} + \frac{\partial^2 \eta}{\partial t^2} + \frac{K}{\rho_f A} = 0 \qquad \text{(VII-5)}$$

Where: K = Matrix Stiffness

v = Filament Impact Velocity

The boundary conditions are:

$$\eta(0,t) = \frac{\partial \eta}{\partial x}(0,t) = \eta(a_s t,t) = \frac{\partial \eta}{\partial x}(a_s t,t) = 0$$

(Note: The x coordinate is now measured from the point of impact; t time from the moment of impact.)

As explained in Section VI, there are no initial conditions to the problem. Also, it is necessary to include the propagation of the strain wave along the filament. This will not be done here, since as explained in Section VI, the model is not valid for large time because of the buckling deformation affecting the equations themselves. It is possible, though, to find an initial deformation mode with lower potential energy than pure axial compression. This mode occurs after the reflected strain wave has traveled a certain distance, $x_o^* = a_s t_o^*$. The first such mode to appear is described by Equation VI-16. The time dependence of amplitude associated with this mode is given by this equation

as:

$$\eta(t) \sim e^{b_{12}(1-b_{13}^2)^{\frac{1}{2}} t/t_o^*} \qquad \text{(VII-6)}$$

where: $b_{12} = \frac{12}{25} \frac{P t_o^*}{(EI \rho_f A)^{1/2}}$, $b_{13} = \frac{25}{12}(\frac{KEI}{P^2})^{\frac{1}{2}}$

P = Impact Compressive Force

This expression makes it very clear that if b_{13} is greater than one, the time dependence is oscillatory with small deflection, while if b_{13} is less than one, then the time dependence becomes exponential and deflections large. Therefore, for filament assemblages it is important that:

$$b_{13} = \frac{25}{12}(\frac{KEI}{P^2})^{\frac{1}{2}} < 1 \qquad \text{(VII-7)}$$

In this expression P is the filament impact force and is, of course, a function of the kinetic energy remaining in the filament at the moment of impact. The criteria chosen to relate these two, is that the velocity of impact is taken as that required of a solid rod in order that the rod have the same kinetic energy as the filament, at impact. This gives a relation between strain, ϵ_f, and ℓ/x_o of:

$$b_{14} = \frac{25}{12} \frac{KI}{\epsilon_f^2 EA^2} > (1-\frac{\ell}{x_o})^2 (1-\frac{\ell}{x_o} + (\frac{\ell}{x_o})^2)) \qquad \text{(VII-8)}$$

This expression is interpreted as follows. If a filament is held at a point, $x = \ell$, which is less than $x_o (x_o = \frac{E \epsilon_f D_f}{2\mu p})$, then impact will take place, followed by buckling. If Equation VII-8 is valid, the lateral deformation will be small - if not, then it will be large.

The above expressions have been developed in order to

obtain a general idea of the effect that a surrounding matrix has on the filament motions discussed previously. However, this subject warrants further, more specific investigation because of the many practical situations that can be represented by this kind of model. These include fiber motion during yarn breakage, fiber motion during drafting and carding, filament motion during cable breakage, etc.

Dynamic snap back such as has been described in this section, is an important mechanism which accounts for load transfer on a local level, within an assemblage of fibrous elements. It is a significant part of the rupture phenomenon in heterogeneous structures such as those encountered in textile products, and in many composite materials.

VIII. DISTINGUISHING PARAMETERS

Certain dimensionless combinations of variables have been found which are helpful in catagorizing the motions of moving filaments and tapes. They are listed here and discussed briefly as an aid in understanding the material of this thesis.

Stiffness Parameter

$$b_1 = \frac{\epsilon}{(c^2-v^2)\ell^2} = \frac{E\,I}{(T-\rho_f A v^2)\ell^2} = \left(\frac{\delta}{\ell}\right)^2$$

The stiffness parameter refers to the relative importance of filament stiffness, EI, to " net filament tension ", $T-\rho_f A v^2$, and is normalized with respect to the system length, ℓ. It is most easily understood as the square of the ratio of boundary length, δ, to system length, ℓ. δ refers to the length of filament adjacent to a boundary which can be considered as a static " beam " - while considering the remaining filament as a vibrating " string ". The effect is considered negligible for $b_1 << 1$.

Coriolis Parameter

$$b_2 = \frac{-2\omega_0 v \ell}{c^2-v^2} = \frac{-2\omega_0 v \rho_f A \ell}{T-\rho_f A v^2}$$

The Coriolis parameter refers to the ratio of the " Coriolis force ", $2\omega_0 v \rho_f A \ell$, to the net filament tension, $T-\rho_f A v^2$. It is twice the angle of rotation of a filament about its axis, measured within the system boundaries at a fixed instant of time. The effect is considered negligible when $b_2 << 1$.

Longitudinal Air Motion Parameter

$$b_3 = \frac{\alpha(v-v_a)\ell}{c^2-v^2} = \frac{r_D \Delta v_a \ell}{T - \rho_f A v^2}$$

The magnitude of b_3 refers to the relative importance of the force from longitudinal air motion, $r_D \Delta v_a \ell$, to the net control tension, $T - \rho_f A v^2$. r_D is the linear air drag parameter. Δv_a is the velocity of the induced $\vec{i}$-direction air motion. The effect is considered negligible when $b_3 << 1$.

Centrifugal Force Parameter

$$b_4 = \frac{-\omega_o^2 \ell^2}{c^2-v^2} = \frac{-\rho_f A \omega_o^2 \ell^2}{T - \rho_f A v^2}$$

This parameter indicates the magnitude of the centrifugal force, $\rho_f A \omega_o^2 \ell^2$, compared again with the net control tension, $T - \rho_f A v^2$. This is the most significant parameter in determining the dynamic aspects of filament motion, since if $b_4 << 1$ then all filament particles can be considered to follow the same path through the system.

Lateral Air Drag Parameter

$$b_5 = \frac{\alpha \omega_o \ell^2}{c^2-v^2} = \frac{r_D \omega_o \ell^2}{T - \rho_f A v^2}$$

The magnitude of this parameter indicates the relative importance of air drag in determining filament oscillation amplitude. It is specifically the ratio of lateral resistance force, $r_D \omega_o \ell^2$, to filament net control tension, $T - \rho_f A v^2$. If $b_5 << 1$ then the system amplitudes, at resonance, can be large.

Gravity Parameter

$$b_6 = \frac{g\ell}{c^2 - v^2} = \frac{\rho_f A g \ell}{T - \rho_f A v^2}$$

This parameter refers to the relative magnitude of gravity force, $\rho_f A g \ell$, or filament weight, to the net effective tension, $T - \rho_f A v^2$. If the weight of the filament is small compared to the net tension, then gravity can be ignored.

"Mach Number"

$$b_7 = \frac{v}{c} = v\sqrt{\frac{\rho_f A}{T}}$$

This ratio of filament velocity, v, to lateral wave phase velocity, c, is the most important measure of the effect that " through-put velocity ", v, has in determining the dynamic oscillations of filaments and tapes. For situations where $v \ll c$ ($b_7 \ll 1$) filament longitudinal motion can be neglected and the filament modeled as fixed or attached to the system boundaries.

Dynamic Buckling Transition Parameters

$$b_8 = \frac{\rho_f A \ell^3 a}{\pi^2 EI}, \qquad b_9 = \left(\frac{E}{\rho_f a \ell}\right)^{\frac{1}{2}}$$

When a filament is subjected to a longitudinal deceleration, a, of sufficient magnitude, the filament will buckle laterally. The parameters, b_8 and b_9, can be used to predict the buckling mode. If they are both small compared to one, the buckling mode is dependent on filament stiffness and buckling waves of predictable length occur. If they are both large the buckling

becomes highly dependent on the initial shape of the filament.

Matrix Strain Parameter

$$b_{10} = \frac{\pi \mu p D_f x_o}{EA \epsilon_f}$$

This parameter refers to the ratio of total dynamic shear force exerted by a matrix on a filament, $\pi \mu p D_f x_o$, to filament tension, $EA\epsilon_f$. If a strained filament is suddenly let free at one end and the filament is of sufficient length, then $b_{10} = 2$.

Tension Parameter

$$b_{11} = \sqrt{\frac{T}{\rho_f A v^2}}$$

The tension parameter, b_{11}, is the square root of the ratio of filament tension, T, to filament momentum flux, $\rho_f A v^2$. If b_{11} is large compared to one, then filament motion is primarily controlled by filament tension. If b_{11} is small compared to one then filament stiffness or air drag act to control filament motion. For constant tension, b_{11} becomes equal to the reciprocal of b_7, the Equivalent Mach Number.

Dynamic Buckling Amplitude Parameter

$$b_{12} = \frac{12}{25} \frac{P t_o^{*}}{(EI \rho_f A)^{1/2}}$$

This ratio of filament impact force, P, to the quantity, $EI\rho_f A$, refers to the rate at which the amplitude of dynamic buckling increases. For b_{12} increasing from zero, the deformation will proceed at progressively higher rates.

Assemblage Parameter

$$b_{12} = \frac{25}{12} \left(\frac{KEI}{P^2}\right)^{\frac{1}{2}}$$

This parameter describes the relative effect of matrix or assemblage stiffness, K, and filament stiffness, EI, to filament impact force, P. If b_{13} is greater than one then the dynamic buckling of a filament within a matrix or assemblage will have small oscillatory amplitude. However, if b_{13} is less than one then the amplitude will be exponential, and large.

Assemblage Parameter for Strain

$$b_{14} = \frac{25}{12} \frac{KI}{\epsilon_f^2 EA^2}$$

This parameter is similar to parameter, b_{13}. However, the arbitrary value of impact force, P, has been estimated as a function of the initial filament strain and the ratio of filament length, ℓ, to strain wave penetration length, x_o.

If $$b_{14} > \left(1 - \frac{\ell}{x_o}\right)^2 \left(1 - \frac{\ell}{x_o} + \left(\frac{\ell}{x_o}\right)^2\right)$$

then the lateral deformation of a single filament after breaking within a matrix of similar filaments will be small and oscillatory. If the statement is not true the lateral deformation will be large.

k_o Solution Parameters

$$b_{15} = \frac{R\cos\theta_R}{2}; \qquad b_{16} = \frac{R\sin\theta_R}{2}$$

These two parameters are functions of parameters b_1 through b_5. They are used to consolidate the presentation of the k_o solution. If air drag is negligible the angle θ_R becomes equal to zero and the k_o solution is considerably simplified since $b_{15} = R$ and $b_{16} = 0$.

Filament Rotation Parameter

$$b_{17} = \frac{-b_2}{2} = \frac{\pi}{2} b_7 b_{19} = \frac{\omega_o v \ell}{c^2 - v^2} = \frac{\omega_o v \rho_f A \ell}{T - \rho_f A v^2}$$

This parameter refers to the rotation of a moving filament about the x-axis, relative to a plane rotating with the filament at angular velocity, ω_o. It is a direct function of parameter b_2 as shown.

Wave Number Parameter

$$b_{18} = \frac{\omega_o \ell / c}{1 - v^2/c^2} = \frac{\omega_o \ell / c}{1 - b_7^2}$$

This parameter is a measure of the product of corrected wave number, $\frac{\omega_o / c}{1 - v^2/c^2}$, and system length, ℓ.

Relative Frequency Parameter

$$b_{19} = 2\frac{\omega_o}{\Omega} = \frac{2\,\omega_o \ell / c}{\pi(1 - v^2/c^2)} = \frac{2}{\pi} b_{18}$$

This parameter is equal to twice the ratio of the forced input frequency, ω_o, to the natural frequency of the k_o solution for zero air drag, Ω. For b_{19} equal to odd integers the system amplitudes are a minimum. For b_{19} equal to even integers, or forced input frequency equal to system natural frequency, resonance occurs and filament amplitudes become

large. This parameter is also a measure of the number of half "balloons" that the filament path contains.

Solution Limit Parameter

$$b_{20} = \frac{\Delta T}{T_o} = \frac{1}{2}\left(\frac{h_o}{\ell}\right)^2 \left(\frac{b_2}{2b_7 \sin b_{19}\frac{\pi}{2}}\right)^2$$

This final parameter is stated as a means to predict the limit of validity of the basic linear equations of moving filaments. b_{20} must be small compared to one for the equations to hold, since the assumption of constant tension is no longer valid if b_{20} is comparable to one.

IX. EXPERIMENTATION

This final section contains a description of the experimental apparatus that was used in obtaining the data and some of the photographs presented in this thesis. Also included here are explanations of the method used to compare the results of the numerical integration of the non-linear equations of filament motion reported by Padfield (4), with the equations of this thesis.

A. Filament Rotation Angle Measurements

The values of filament rotation angle, b_{17}, plotted in Figure 12 were obtained in two ways. First by calculating b_{17} from numerical data given by Padfield (4) and secondly by directly measuring Padfield's space curves. A typical set of these filament space curves is reproduced in Figure 28a. The nomenclature identifying these curves has been changed to that of this thesis.

Points A and B of Figure 28a were chosen as the system boundaries. The value of $b_{17_{meas}}$ was found by measuring the amount of filament rotation about the x-axis between points A and B.

The values of calculated filament angle, $b_{17_{calc}}$, were obtained from Padfield's original data using the definition of b_{17} of this thesis:

$$b_{17} = \frac{\pi}{2} b_7 b_{19}$$

where b_7 is the ratio of filament velocity, v, to lateral

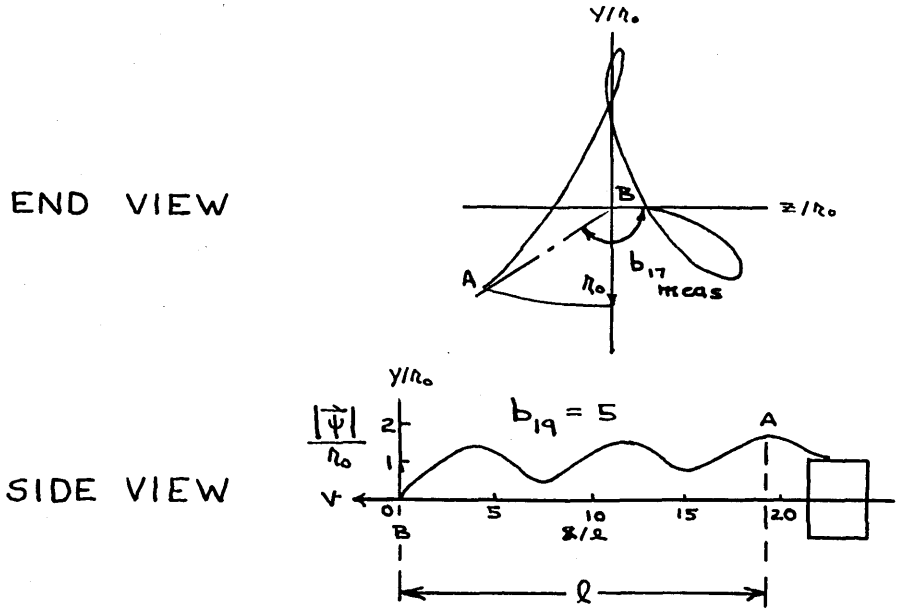

FIG. 28a

TYPICAL FILAMENT SPACE CURVE OF REFERENCE 4

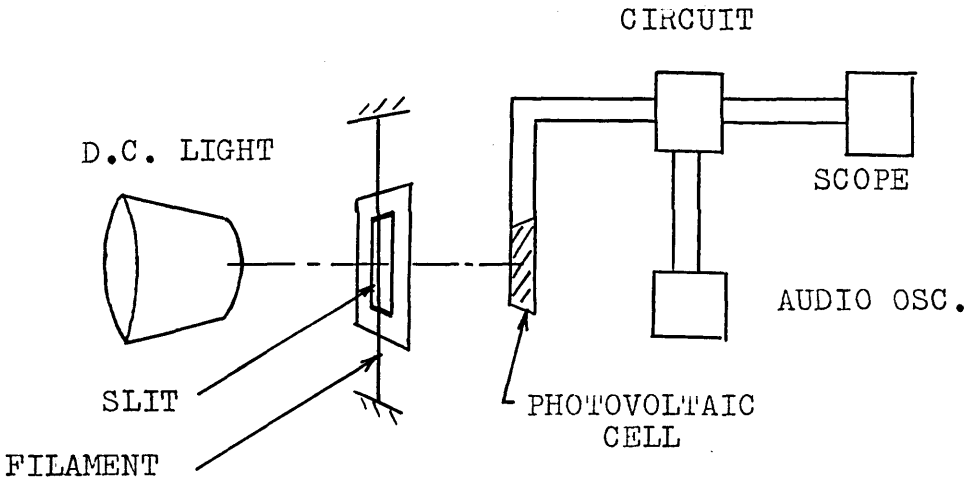

FIG. 28b

SCHEMATIC OF FREQUENCY MEASUREMENT APPARATUS

wave velocity, c, and where b_{19} is directly measured from the figures as shown since it represents the number of half balloons.

Referring to Figure 28a, a sample calculation is given as follows:

$$b_{17_{meas}} = 150^{\circ} \quad \text{(From Figure 28a)}$$
$$b_{7} = .342 \quad \text{(Given in Ref. 4)}$$
$$b_{19} = 5 \quad \text{(From Figure 28a)}$$
$$b_{17_{calc}} = (90^{\circ})(.342)(5) = 154^{\circ}$$

The agreement between the two values of b_{17} is seen to be very good for this case.

B. Boundary Region Frequency Measurements

The frequency measurement apparatus shown in Figure 15 was used to measure the natural frequency of 27 mil nylon monofilaments, of lengths varying from 1.5 inches to 18 inches. The range of tension varied from 200 grams to 1200 grams. The apparatus functions as follows. A filament is positioned between a high intensity d.c. light source and a photovoltaic cell. The cell is behind a metal sheet with a quarter inch by ten mil slit. As the filament vibrates laterally at its natural frequency, excited by the random room vibration, it creates an a.c. voltage in the cell by blocking out light. This voltage is fed through a differentiating circuit and into an oscilloscope. The signal is too small to be read directly, but by adding a voltage of known frequency, from an audio oscillator, the oscillator signal can be tuned

to the filament frequency by watching the oscilloscope. The value of frequency is then read from the oscillator. (Figure 28a)

C. Balloon Length Measurements

The values of b_{19} plotted in Figure 16c, were also obtained from the numerical data of Reference 4, discussed above. b_{19} is measured as shown in Figure 28 and then calculated from Equation V-36,

$$b_{19} = \frac{2\ell}{\pi r_o}\left(\frac{1}{1-\frac{1}{b_{11}^2}}\right)\frac{1}{b_{11}} \qquad \text{(V-36)}$$

For an overend unwinding cone, as in this case, b_{11} is equal to the reciprocal of b_7. Therefore, Equation V-36 becomes:

$$b_{19} = \frac{2\ell}{\pi r_o}\left(\frac{1}{1-b_7^2}\right)b_7$$

The values of b_{19} calculated from this equation with the data accompanying each figure of Reference 4 are those used in the cross plot of Figure 16c.

The balloon measurements plotted in Figure 16b were made using the yarn ejector shown in Figure 29a. This ejector consists of an air turbine which drives a set of gears, with which yarn in turn can be driven at speeds up to 300 ft/sec. These gears were used to withdraw yarn overend from a yarn cone. The distances from the yarn take off point to the yarn nodes, or points of minimum lateral displacement, were measured. The yarn path between two such nodes is called one balloon. Each additional balloon is equivalent to an increase

of two in the magnitude of b_{19}. Figure 16b is a plot of the number of half-balloons, b_{19}, as a function of x.

This yarn ejector was also used to obtain the photographs of Figures 4 and 29b, c, d, e, f. Cotton yarn was forced to "flow" (from left to right in the figures) by this apparatus. These figures are interesting because they depict yarn flow which is being governed by yarn momentum rather than yarn tension, as is usually the case. The analogies drawn between this type of filament motion and the flow of fluids, in the captions of these figures, are only to draw attention to this similarity. The photographs were taken in a semi-dark room with the aid of one flash from a Strobotac Unit. The overall motion is evidenced in the envelope of the yarn configurations, while one specific configuration is in focus.

D. Dynamic Buckling Photographs

The photographs of Figure 18 were taken with the aid of Professor Eggerton of the Electrical Engineering Department of M.I.T., and the equipment of his laboratory. The following procedure was used. An 8.5 mil nylon monofilament, 18 inches long, was stretched between two supports under strain. The monofilament was then broken at one end with a rifle bullet. Almost simultaneously a single light flash from a flash unit, triggered by the shock wave of the exploding rifle, exposed the negative in a camera focused on the other end of the filament. The laboratory lights were kept low during the experiment in order not to over-expose the negative. The six photographs of Figure 18 were obtained by progressively

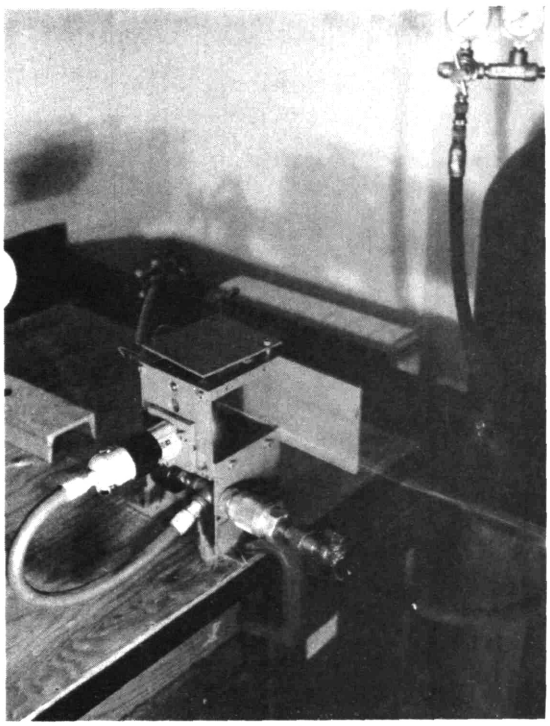

AIR TURBINE DRIVEN
GEAR YARN EJECTOR
(a)

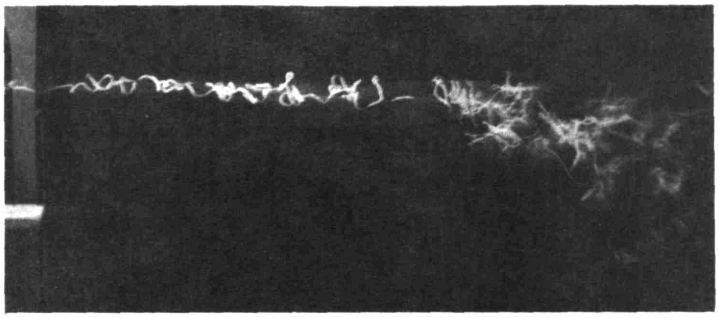

AIR DRAG AND GRAVITY EFFECT
$b_7 > 1$
(b)

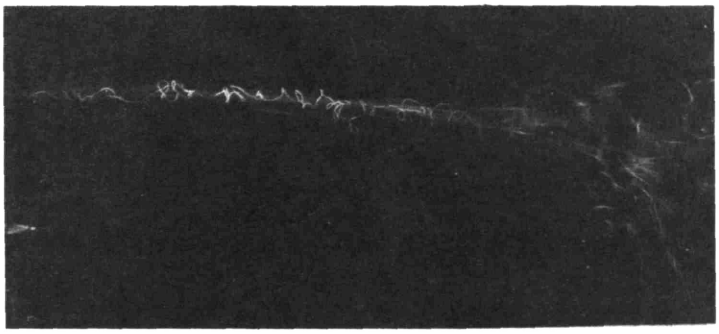

AIR DRAG AND GRAVITY EFFECT
$b_7 > 1$
(c)

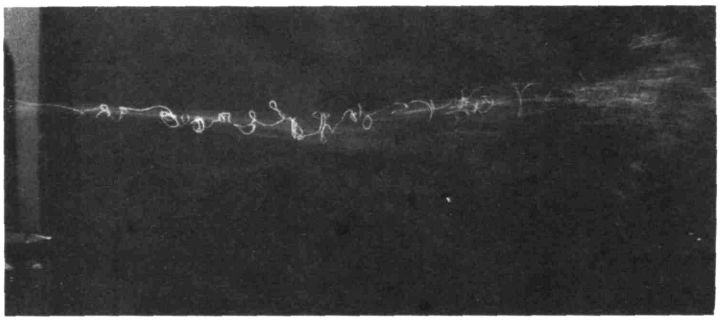

GENERATION OF "LIFT"
(d)

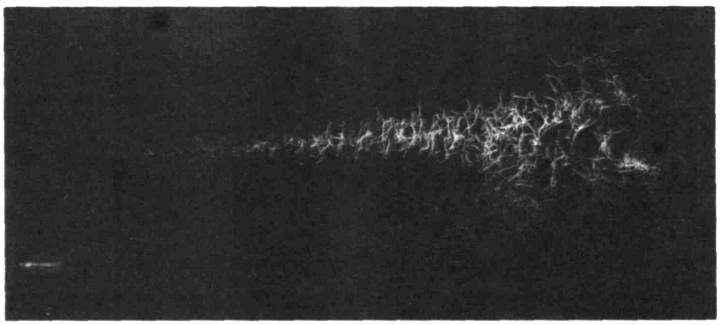

"VENTURI EFFECT"
(e)

FIG. 19
-125-

increasing the time increment between the rifle explosion and the light flash, with an electronic delay. Thus the six photographs do not show the continuous buckling of the same monofilament but rather progressively later stages in the buckling of six identical monofilaments.

E. Dynamic Buckling Wave Length Measurements

The deformation wave lengths reported in Figures 21 and 22 were measured from dynamically buckled samples of copper wire and nylon monofilament. The samples were dynamically buckled while held by the jaws of an Instron Testing Machine, by cutting one end of the sample. The average wave length of the deformation at the other end of the sample was measured, as a function of the initial tension level in the sample prior to cutting. The abscissa of these two figures, v, (Estimated Impact Velocity) was then calculated from this initial tension level and from the estimated dynamic modulus of the material, as explained on Pages 93 and 94 where the figures are discussed in detail. These wave lengths were difficult to measure because it was hard to define exactly what a complete wave was. However, reproducible data was obtained for the copper wire by measuring only the length of the wave immediately adjoining the jaw. While consistent data was obtained for the nylon monofilament by averaging the measured wave lengths of the entire deformed sample.

F. Experimental Apparatus for Filament Motion

The apparatus shown in Figure 26 consists of a sandwich

formed from two $\frac{1}{8}$ inch by $1\frac{1}{2}$ inch plexiglass plates and a $\frac{1}{8}$ inch by $\frac{3}{16}$ inch rubber strip. The elastic bands surrounding the sandwich force the plexiglass plates to exert a pressure on the rubber strip. The data of Figure 25, were obtained by repeating the following procedure. The top plexiglass is raised out of contact with the rubber strip and the strip is then given an initial strain. The top plate is released and the sandwich is formed. The strip is then released statically or "slowly" and then dynamically or "quickly". The deflection at the end of the strip is measured for each type of release, at increasing values of initial strain. Figure 25 illustrates the consistency of the multiple of two that is predicted by the theory.

X. SUMMARY AND CONCLUSIONS

The material of this thesis is the result of an attempt to formulate a general analytical approach to the phenomena of moving filaments and tapes. This material has been presented as equations, which can be used to predict the paths through space of actual filaments and tapes that are subjected to forced displacement oscillations. In order that the predictions of these equations be accurate, the effect of filament bending stiffness, filament tension, gravity and air drag were included in the analysis.

The concept of a filament position vector, R, was used to identify in a general manner the position or path of the filament as a function of time and the spacial coordinates. A general vector differential equation was then derived in terms of this position vector.

This general vector differential equation has been examined extensively for the case of linear filament motion. The term linear filament motion refers to filament motion which is essentially straight line travel between two points with the addition of small perturbations in the two lateral directions. The solutions of these equations are applicable to many practical problems of monofilament, multifilament and staple yarn processing situations such as the spinning balloon, the overend unwinding balloon and the yarn space curves near the traversing mechanisms of winding machinery. They can also be used to predict the space paths of thin tapes, where air drag becomes important, and heavy metal cable, where stiffness becomes important.

The concept of a stiffness boundary region was developed, which can be utilized to predict easily the extent that filament motion will be a function of stiffness. The parameters of the equations which describe filament motion for zero stiffness have been modified to include the length of this boundary region.

The effect of acceleration and deceleration in the direction of filament overall travel has also been examined. Equations are given which can be used to predict the time dependence and mode shapes of both the stable oscillations of an accelerating finite length filament and the unstable deformations of a decelerating or dynamically buckling infinitely long filament. It is possible to use these equations to predict the extent of the lateral deformation that occurs when a moving filament is suddenly stopped at one point along its path. This prediction includes both the mode of deformation and the rate of deformation.

The effect that a surrounding matrix of solid material can have on the dynamics of filament rupture has also been examined. Equations of motion for this phenomenon allow a prediction to be made as to the minimum fiber rupture length that is observed in a yarn that has been strained to its breaking point. They also provide, to a limited extent, a quantitative picture of the internal dynamics of a breaking yarn. The internal dynamics of a breaking yarn is important in determining yarn strength efficiency.

The equations of this thesis which predict filament

paths and strain distributions have been experimentally justified to the point where they can be considered at least qualitatively correct. This includes comparison with previously published experimental and numerical data, comparison with actual experimentation undertaken expressly for this thesis, and the use of photographs, including high speed photographs.

A set of twenty non-dimensional distinguishing parameters have been developed which help to catagorize the many variables which govern filament motion. These parameters allow predictions to be made as to the relative magnitudes of filament stiffness, air drag, gravity, etc. They can also be used to predict identifying quantities such as the number of filament balloons, the magnitude of the filament rotation angle, the length of the boundary region, etc. They are also considered to be logical correlation parameters for experimental or numerical data.

In conclusion, this thesis is considered to have adequately covered the range of possible linear solutions to the differential equations developed and to have qualitatively verified these solutions. The most important continuation of this work would be a comprehensive experimental investigation of several situations, typical of actual textile processing machinery, using the parameters and equations of this thesis as guideposts. This material would then be of utmost value in the design stage of any machinery which handles high speed moving filaments, because it would allow the designer to

predict the filament strain, tension, and amplitude caused by machine-material interaction.

Examples of specific areas of applicability include the early stages of polymer monofilament or glass monofilament production. The effect of variable tension or strain caused by forced filament oscillation as a result of a machine-material interaction, will increase output variability if the material is sufficiently weak or soft. Another example concerns the space limitations for filament processing machinery. Space limitations can become critical and the filament processing machinery designer must be able to design for minimum filament oscillation amplitudes. He must also be aware of the variations in filament behavior as production speeds approach certain limiting values such as occurs when the " effective tension ", $T - \rho_f A v^2$, becomes small.

The designer of mechanisms that interlace, or intertwine thread or yarn should be able to predict the perturbations from a straight line path that a filament will have as a result of dynamic effects. The sewing machine rotary stitching mechanism is an example of a mechanically optimized mechanism which has become speed-limited by the material that passes through it as a result of machine-material interactions. By altering the mechanism thread guide path to include the effects of thread inertia, it should be possible to reduce thread oscillation and strain and tension levels and thus increase machine speed.

An example of undesirable interaction between adjacent yarns occurs during " beaming " or the operation of loom beam

preparation. Actual entanglement may take place if yarn lateral oscillation is sufficient to allow contact of two or more adjacent yarns.

During the process of stretch-breaking of polymeric monofilaments the snapback and dynamic buckling that takes place is an important production variable. This is also true in the carding and drafting of staple fiber. The snapback and dynamic buckling that occurs as one fiber breaks in an assemblage of fibers (yarn) is another example of a dynamic effect that can be understood and included in a design procedure - in this case the design of a yarn. The permanent deformation that occurs to some types of recording tape in the immediate region of a break, can cause a permanent loss of the information stored in that region.

These examples illustrate the areas of applicability of this thesis. The conclusion is made that there exists within the context of textile mechanical processing alone, a multitude of problems requiring an understanding of the phenomena of moving filaments. It is felt that this thesis constitutes a general approach to these problems and that the simplified equations that have been developed are directly applicable to these problems.

XI. APPENDICES

A. Appendix 1.

If a filament oscillates laterally with frequency, ω_o, then the value of the linear drag coefficient, r_D, can be approximated for the case where the nonlinear drag coefficient, C_D, is constant, by equating energy loss as follows:

Let: $$\eta(s,t) = \eta(s)\sin\omega_o t$$

The energy loss per cycle per unit filament length, for constant r_D is:

$$2\int_{-\pi/2\omega_o}^{\pi/2\omega_o} r_D\left(\frac{\Delta\eta}{\Delta t}\right)^2 dt = 2\int_{-\pi/2\omega_o}^{\pi/2\omega_o} r_D\left(\eta(s)\omega_o\cos\omega_o t\right)^2 dt = \pi r_D \eta^2(s)\omega_o$$

The energy loss per cycle per unit filament length, for constant C_D is:

$$2\int_{-\pi/2\omega_o}^{\pi/2\omega_o} C_D\frac{\rho_a}{2}D_f\left(\frac{\Delta\eta}{\Delta t}\right)^3 dt = 2\int_{-\pi/2\omega_o}^{\pi/2\omega_o} C_D\frac{\rho_a}{2}D_f\left(\eta(s)\omega_o\cos\omega_o t\right)^3 dt = \frac{4}{3\pi}\rho_a C_D D_f \eta^3(s)\omega_o^2$$

Equating these two values of energy loss and solving for r_D yields:

$$r_D = \frac{4}{3\pi}C_D\rho_a D_f \omega_o \eta(s)$$

By noticing that the maximum lateral drag force per unit filament length is;

$$\frac{\Delta D_{D\,max}}{\Delta s} = C_D\frac{1}{2}\rho_a(\omega_o\eta(s))\,D_f$$

the equation for r_D can be simplified to:

$$r_D = \frac{8}{3\pi}\frac{\Delta D_{D\,max}}{\Delta s}\;\frac{1}{\omega_o\eta(s)}$$

This can be expressed as:

$$r_D = .85 \frac{\text{Maximum Drag Force per Unit Filament Length}}{\text{Maximum Filament Normal Air Velocity}}$$

The above equation is included in the discussion of air drag forces in Section II-C.

B. Appendix 2

By equating the maximum amplitudes of Equations IV-7 and IV-11 and solving for the filament cross-sectional area moment of inertia diameter, I, it is possible to calculate both a typical monofilament diameter and a typical multifilament diameter. These diameters represent filaments for which the effects of bending stiffness and longitudinal air motion have the same order of magnitude. This is done as follows.

Let: $$\eta_{\max_{IV-7}} = \frac{-b_6}{b_3} = \eta_{\max_{IV-11}} = \frac{-b_6}{384 b_1}$$

therefore $$b_1 = \frac{E I}{(T - \rho_f A v^2)\ell^2} = \frac{b_3}{384} = \frac{r_D (v - v_a)\ell}{384(T - \rho_f A v^2)}$$

Solving for I yields:

$$I = \frac{r_D (v - v_a)\ell^3}{384(E)}$$

Substituting the following typical values,

$$r_D = 200 \text{ lb. sec/ft}$$

$$v - v_a = 50 \text{ ft/sec}$$

$$\ell = 1 \text{ ft}$$

$$E = 10^6 \text{ p.s.i.}$$

yields a value for monofilament diameter of:

$$D_f = 10 \text{ mil}$$

and a value for multifilament yarn diameter of:

$$D_f = 100 \text{ mil}$$

where the multifilament yarn is considered composed of 100 monofilaments and where frictional interaction between monofilaments is neglected.

XII. REFERENCES

1. Webster, A.G., Partial Differential Equations of Mathematical Physics, Dover Publications, 1955.
2. Anderson, W., The Dynamic Buckling of Filaments, M.I.T., M.S. Thesis, February, 1964.
3. DeBarr, A.E., Catling, H., Manual of Cotton Spinning, Vol. 5, The Textile Institute and Butterworth & Co. 1965.
4. Padfield, D.G., Proceedings of the Royal Society, 1958, 382.
5. Rayleigh, J.W.S., The Theory of Sound, Vol. 1, Dover Publications, 1945.
6. Rohsenow, W.M., Choi, H., Heat, Mass, and Momentum Transfer, Prentice-Hall, Inc., 1961.
7. Draper Corp., High Speed Motion Pictures.
8. Bowman, F., Introduction to Bessel Functions, Dover Publications, 1958.
9. Mack, C., Smart, E.J.L., Journal of the Textile Institute, Vol. 45, 1954, T348.
10. Padfield, D.G., Journal of the Textile Institute, Vol. 46, 1955, T71.
11. Hannah, M., Journal of the Textile Institute, Vol. 43, 1952, T519.
12. Padfield, D.G., Journal of the Textile Institute, Vol. 47, 1956, T301.
13. Meier, J.H., Journal of Aeronautical Science, Vol. 12, 1945, 433.

14. Cristescu, N., Archiwum Mechaniki Stosowanej, Vol. 14, 1, 1963, 47.

15. Swope, R.D., Ames, W.F., Journal of the Franklin Institute, Vol. 275, 1, 1963, 36.

16. Booth, K.H.V., British Journal of Applied Physics, Vol. 8, 1957, 142.

17. Jasani, M.M., Kulkarni, M.G., "Some Aspects of Winding on Barber-Colman Experimental Spooler", The Bombay Textile Research Assoc., 1961.

18. Jasani, M.M., Kulkarni, M.G., "Effect of Winding Conditions on Unwinding Tension and Vital Yarn Properties....", Bombay Textile Research Assoc., 1962.

19. Sack, R.A., British Journal of Applied Physics, Vol. 5, 1954, 225.

20. Brunnschweiler, D., The Textile Manufacturer, Vol. 6, 1957, 271.

21. Brunnschweiler, D., Textile Recorder, "Yarn Tension Control in Winding", Parts I, II, III, & IV, May 1959.

22. Mack, C., British Journal of Applied Physics, Vol. 4, 1953, 145.

23. Mack, C., Journal of the Textile Institute, Vol. 44, 1953, T483.

24. Crank, J., Textile Research Journal, Vol. 23, 4, 1953, 266.

25. DeBarr, A.E., Journal of the Textile Institute, Vol. 51, 1960, T17.

26. Mack, C., Journal of the Textile Institute, Vol. 54, 3, 1963, T106.

27. Lindsay, R.B., Mechanical Radiation, McGraw-Hill Book Co., 1960.

28. Skutsch, R., Ann. Phys. Chem., 61, 1897, 190.

29. Monago, C., Unpublished Masters Thesis, Department of Mechanical Engineering, M.I.T.

30. Private Communication from Lesona Corporation.

31. Private Communication from Draper Corporation.